University of Alberta

Developing a Predictive Model of Near – Neutral pH Stress Corrosion Cracking of Underground Pipelines

by

Brett Matthew Conrad

A thesis submitted to the Faculty of Graduate Studies and Research
in partial fulfillment of the requirements for the degree of

Master of Science

in

Materials Engineering

Chemical & Materials Engineering

Spring 2014
Edmonton, Alberta

Abstract

Near neutral pH Stress Corrosion Cracking (NNpHSCC) on underground oil and gas pipelines is an issue facing industry today. Determining where NNpHSCC is likely to occur and grow is an important aspect to developing an Integrity Management Program. This work focused on developing a predictive model to capture the mechanisms involved with NNpHSCC growth utilizing actual field data. In order to better fit the field findings with the limited laboratory runs, different Hydrogen Enhancement Factors (HEF) were applied depending on the conditions of a given loading cycle. The predictive model generated results which demonstrated to distinct portions of NNpHSCC growth: a dissolution controlled phase and a mechanically activated phase. The output of the model was then compared to the field findings, with varied success. Further improvement and calibrations are required along with the gathering of additional field and laboratory data to fine-tune the field validation of the predictive model.

Acknowledgements

The work presented in this thesis would not be possible without the supervision, support, guidance and patience of Dr. Weixing Chen. His ability to explain complex concepts and pass along a passion for Materials Science made the challenging work very enjoyable and rewarding, and for that, I would like to say thank you.

I would also like to thank Dr. Reg Eadie and Dr. Hao Zhang for their thoughtful feedback and invaluable insight during review meetings and weekly conversations. I also wish to thank TransCanada Pipelines Ltd. and Spectra Energy Ltd. for their financial support, as well as Richard Kania from TCPL and Greg Van Boven from SEL for their unique perspective only gained through years of field experience, which greatly helped in the collection of the data vital to this work.

The kind help of Jack Gibeau, Marion Pritchard, and Lily Laser from the University of Alberta is also greatly appreciated.

Brett Conrad

January 2014

Table of Contents

List of Tables

Table of Figures

1.0 Introduction

Pipelines are critical components to North America's oil and gas industry. There are currently thousands of kilometers of underground pipeline making the effective integrity management of these assets both time-consuming and expensive. In order to compensate for the lack of information, it becomes imperative that the transmission companies use the available data effectively. One of the integrity issues with these gas lines is the occurrence of external Stress Corrosion Cracking (SCC). The development of a predictive model for Near-Neutral pH SCC (NNpHSCC) would help pipeline companies utilize the current data available to them as well as identify data that may be beneficial to acquire with the funds allocated for integrity management programs. (1)

The work contained within this paper documents the approach taken in an attempt to analyze actual compressor discharge pressure data and quantitatively assign relevance to each cycle with regards to Corrosion Fatigue (CF).

2.0 Literature Review

2.1 Environmentally Assisted Cracking

Environmentally assisted cracking (EAC), also known as environmentally induced cracking, is the brittle fracture of a normally ductile material under a tensile stress in the presence of a corrosive environment (2). The tensile stress is often below the yield stress and is often difficult to predict, which makes it an expensive issue for a wide range of industries. EAC is a major issue in the petroleum industry including offshore oil rigs, underground pipelines, and refineries (3). There are three differing kinds of EAC: Stress Corrosion Cracking (SCC), Corrosion Fatigue (CF) cracking, and Hydrogen Induced Cracking (HIC). These three forms can often occur at the same time as well, making the analysis and prediction of EAC that much more difficult.

2.1.1 Stress Corrosion Cracking (3)

The term SCC has in the past been used to refer to all kinds of EAC; however, today the term's meaning has been restricted to describe a situation in which the crack propagation is assisted, and in some cases driven by, anodic dissolution at the crack tip.

In order for the crack to grow, the dissolution rate at the crack tip must be significantly higher than the crack wall dissolution rate. If the opposite is true, the narrow crack-like feature will begin to widen and turn into a general corrosion pit. This mechanism can be shown in Figure 1.

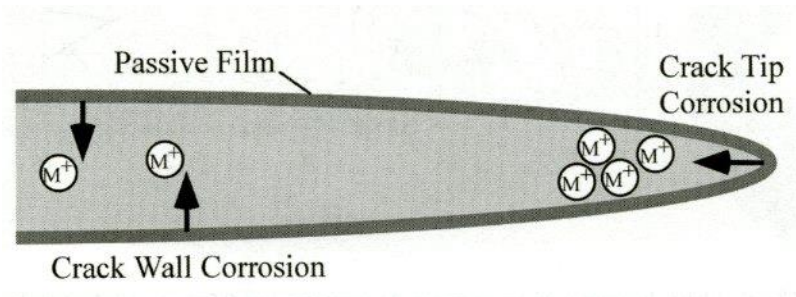

Figure 1 -- Illustration of Anodic SCC (3)

The environmental conditions involved with SCC are complex. Temperature, solution conditions such as pH, oxidizers, aggressive ions, and inhibitors or passivators all play important roles in determining whether or not SCC will be present. The polarization behavior of the material is also important as it has been shown that SCC susceptibility often falls in the regions shown below on the polarization curve (2).

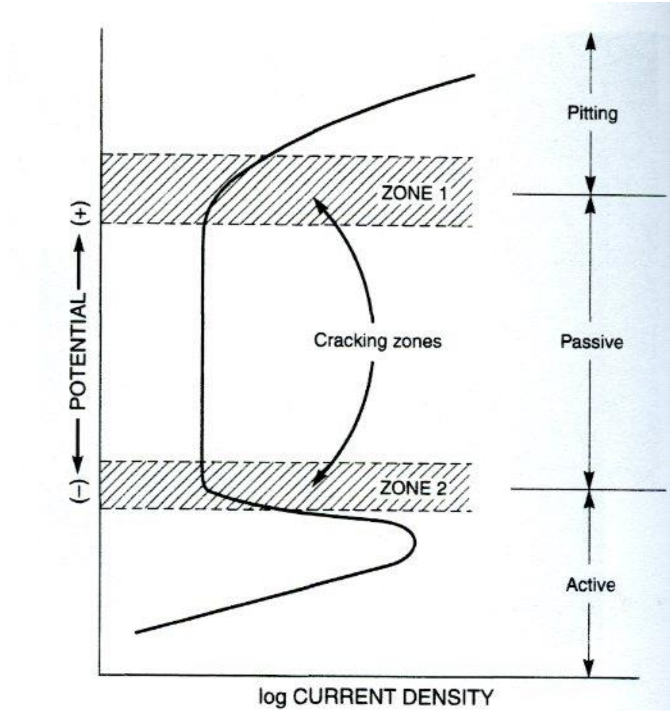

Figure 2 -- Anodic Polarization Curve Showing Regions of SCC Cracking (2)

The polarization curve describes a materials' tendency to passivate under certain electrochemical potentials and current densities. As can be seen above, the susceptibility of SCC occurs in the transition region between the passive and active regions, as well as the transition between passive and transpassive regions. These transition regions are useful for determining the initiation tendencies of SCC; however, the diagrams do not take into account any crevice corrosion behavior, which may be experienced at the crack tip during SCC. Due to this, the polarization curve does not speak to the crack propagation behavior (3).

SCC often occurs when the material/service environment combination causes a passive layer to form. When this is the case the passive layer, which is often a brittle ceramic, fractures at the crack tip due to the stress intensity associated with it. This exposes the bare material to the environment, allowing corrosion to continue in the crack growth direction undeterred. This mechanism is known as a discontinuous film rupture model. There is another model where the crack tip does not repassivate, but rather continues to actively corrode. The discontinuous model is shown in Figure 3.

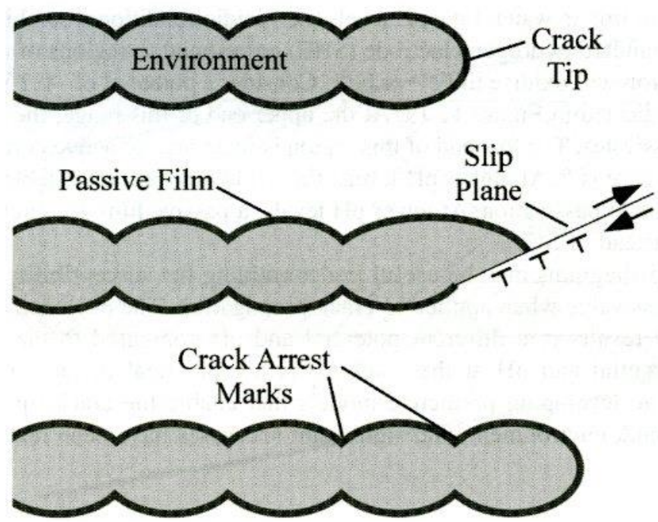

Figure 3 -- Film Rupture Model with Discontinuous Crack Growth (3)

Another issue that may occur, depending on the material and environment, is corrosion product wedging. When the passive layer is formed, the corrosion product may have a larger volume than the base material. This causes the crack to become filled with corrosion product, placing the crack under compressive stress.

The influence of a passive layer on the occurrence of SCC often creates situations in which general corrosion is not present, making SCC detection difficult.

2.1.2 Hydrogen Embrittlement

Hydrogen embrittlement (HE) occurs when atomic hydrogen enters the lattice of an alloy and reduces its ductility and toughness (3). Atomic hydrogen can easily diffuse into alloys and reside in interstitial sites as well as grain boundaries, due to its small size. The diffusion of hydrogen can also occur at room temperature, making this issue a large concern for a wide range of applications.

While there are several mechanisms proposed concerning the mechanism of hydrogen embrittlement, the primary cause involves the presence of atomic hydrogen in the lattice, which reduces cohesive strength of the individual bonds.

The fundamental theory behind HE assisting in cracking and generating Hydrogen Induced Cracking (HIC), can be seen in the critical stress calculation below (3):

$$\sigma_f = \left(\frac{2E(\gamma_s + \gamma_P)}{\pi a}\right)^{1/2}$$

Where E is the elastic modulus of a material, γ_s is the surface energy, γ_p is the energy for plastic deformation, and a is the defect length. The presence of hydrogen decreases the atomic bonding strength, thereby decreasing the energy needed to generate surfaces. The hydrogen also decreases the plastic deformation energy, as the decrease in bond strength allows dislocations to move easier past each other.

The presence of micro-sized HIC cracks ahead of the main crack tip can coalesce with the main crack and cause a previously blunted crack to re-sharpen.

2.1.2.1 Sources of Hydrogen

There are two different methods at which hydrogen reaches and affects the crack tip. They are often referred to as Internal Hydrogen Assisted Cracking (IHAC), and Hydrogen Environment Assisted Cracking (HEAC) (3). It has been reported that the stretching of the lattice due to elastic strain allows for more room for the hydrogen atom to diffuse (3); however, this increase in lattice space also allows hydrogen to diffuse out of the high stress area associated with a crack tip. Once an area has been embrittled, small micro-cracks can form ahead of the crack tip and eventually coalesce, joining up with the main crack and propagating the crack tip.

In IHAC, atomic hydrogen that has been absorbed into the material diffuses to the crack tip. The diffusion of hydrogen is dependent on temperature, and follows an Arrhenius Law as depicted below (4).

$$D = D_0 e^{-Q/RT}$$

As shown above, as temperature increases, so does the diffusivity of hydrogen into a given material. This type of dependence would lead one to believe that as temperature increases, so does the susceptibility to HE; however, the severity of IHAC appears to reach a maximum in between 50-100°C (3). This may be due to the fact that as the temperature increases, a materials relative toughness increases as well as its resistance to HE.

A source of hydrogen can also be present outside of the material itself, which is the case in HEAC. Hydrogen enters the material through the crack tip itself. The source of this hydrogen can be many things, including H_2 gas, water, or some corrosion products. The rate at which the hydrogen dissociates into the atomic form depends on several different factors such as temperature, corrosion deposits, etc., and may vary significantly between individual circumstances.

2.1.2.2 Effect of Loading Conditions (3)

While it is easiest to look at HE under a constant load in a lab, in-service conditions rarely have a constant load applied to a structure. The variability in loading cycles as well as the overall loading history of a component influences the susceptibility to HE.

An increasing stress not only stretches the lattice, increasing hydrogen diffusion, but also produces a larger plastic zone, which may trap the hydrogen. This fact would point to a fast loading rate to produce more HE; however, the steps involved with the dissociation and diffusion of hydrogen are limited by kinetics. These two competing factors make the loading dependency of HE variable, depending on both the service environment and material.

There is a scenario in which very small fluctuations have been reported to cause HEAC. This loading pattern is known as *ripple loading* (3). Depending on the viewpoint and definitions of the various forms of EAC, some people classify these occurrences as HE; however, for the sake of this project, ripple loading will fall under corrosion fatigue.

2.1.2.3 Effect of Yield Strength (3)

It has been well established and accepted that high strength metals often have a higher susceptibility to HE. Figure 4 shows the relationship between HEAC threshold stress and the yield strength of various low-alloy steels (3).

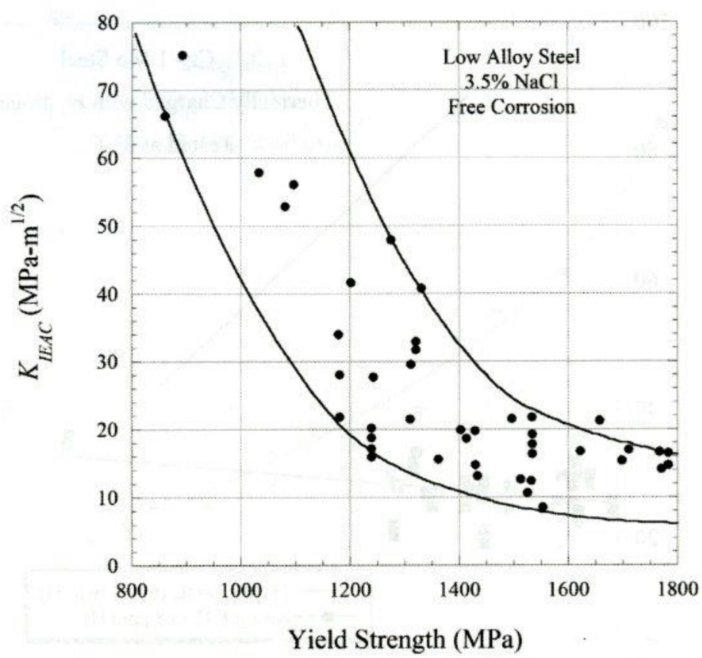

Figure 4 -- Yield strength dependence on the HEAC threshold (3)

One possible explanation for this increase in HEAC severity is that when a plastic zone is created, the stresses involved are much higher in high strength materials, due to a larger yield stress. This reasoning is difficult to prove however, as isolating yield strength from other metallurgical factors is nearly impossible.

2.1.3 Low Temperature Creep

Creep is the time-dependent plastic deformation of a material under a constant stress below the yield strength of the material. Traditionally, this phenomenon occurs at a relatively high temperature with regards to their melting point (usually at temperatures greater than $0.4T_{melt}$ in metals) (5). This is primarily due to the fact that above this temperature, mobile dislocations that are hindered by obstacles can climb over the obstacles through atom-vacancy exchange mechanism and move continuously to cause plastic deformation (5) .

Underground natural gas transmission lines do not operate at temperatures in the range of $0.4T_{melt}$. The low temperature creep for structural materials like steel is a consequence of time-dependent dislocation glide. It occurs due to the motion of existing mobile dislocations pre-generated by plastic deformation. With few exceptions, the creep strain-rate is the highest at the start of the creep upon loading since this corresponds to the highest density and velocity of mobile dislocations. As creep deformation proceeds, mobile dislocations are progressively trapped, so that fewer mobile dislocations are available for deformation and the dislocation velocity is reduced as a result of work-hardening due to dislocation trapping (which reduces, in turn, the effective stress for dislocation motion). Eventually, the creep rate is reduced to zero as the mobile dislocations are exhausted.

A structure, like steel pipelines, is usually applied with a stress below the yield strength, and the low temperature creep if generated is usually very limited. However, when cracks are developed in the structure, the crack tip is often loaded to a stress above the yield strength and substantial plastic deformation and thus mobile dislocations can be generated. Time-dependent plastic deformation due to the motion of existing mobile dislocation can be observed even if the applied stress is not increased. This low temperature creep often blunts the tip of crack and reduces the mechanical driving force for crack growth.

2.1.4 Corrosion Fatigue Cracking (3)

Corrosion fatigue cracking (CFC) is similar to SCC in that both involve corrosion inducing brittle fracture in a normally ductile material (2). The one main difference between CFC and SCC is that the loading in CFC is not constant, as it is in SCC. In order to fully break down this type of EAC, fatigue loading and the associated crack growth must first be considered.

2.1.4.1 Fatigue (3)

Fatigue is the failure, at relatively low stress levels, of structures that are subjected to fluctuating and cyclic stresses (5). In the early 1960's, Paris et al. (6) (7) demonstrated that fatigue crack propagation can be modeled by using fracture mechanics principles.

In order to characterize and quantify various cracks and their respective loading conditions, a stress intensity factor was developed. This stress intensity factor is a variable which characterizes a loading condition's driving force for brittle failure, as well as a materials inherent resistance to such a failure. Under certain conditions, the stress-intensity factor can also be used to characterize fatigue crack growth. Instead of using simply just the amplitude of the stress-intensity factor, the difference (ΔK) is used. The growth rate, defined as crack growth per loading cycle, da/dN, then becomes a function of ΔK and the R-ratio, which is the ratio of the minimum stress intensity factor over the maximum stress-intensity factor. This can be seen in the equation below, and is the basis for the Paris' Law, which is explained later in this work (3).

$$\frac{da}{dN} = f_1(\Delta K, R)$$

When looking at fatigue in metals in air, empirical studies have been done in an attempt to model fatigue crack growth based on this relationship. Plotting a typical fatigue behavior of metals on a log-log scale of crack growth rate versus ΔK gives us the plot seen in Figure 5.

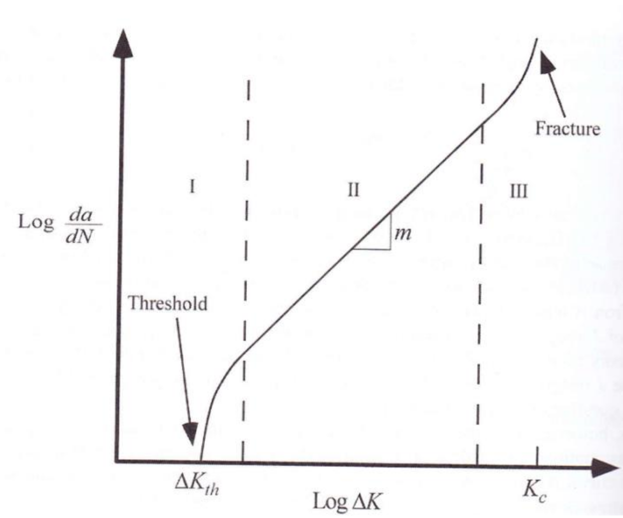

Figure 5 -- Typical Fatigue Crack Growth Behavior in Metals (3)

As can be seen in Figure 5, the second period of crack growth is the easiest to model. The linear region of the log-log plot can be described by a power law known as the Paris Law:

$$\frac{da}{dN} = C\Delta K^m$$

Where over time, it has been shown that the exponent *m* can range from values of 2 to 4 (3). According to the equation, the fatigue crack growth rate depends only on ΔK, and is insensitive to the R ratio and therefore the magnitude of the stresses involved (i.e. K_{max}).

ΔK_{th} is the fatigue threshold stress-intensity factor, which is the lowest difference between the maximum and minimum load which is required to initiate fatigue crack growth. While it may appear that this value is constant, ΔK_{th} consists of an intrinsic component related to material properties, and extrinsic component that is a function of the loading conditions, such as R ratio.

2.1.4.2 Cycle Counting

While fatigue analysis is complicated when looking at regular cycles, it becomes considerably more complicated when trying to analyze real-life cycles. The American Society of Testing and Materials (ASTM) has derived several different methods for counting cycles for the purpose of fatigue analysis (8). These methods include Level-Crossing counting, Peak counting, Simple-Range counting, and Rain Flow Counting (RFC). Level-Crossing counting counts the number of occurrences of a positive slope crossing a preset stress level. Peak counting can be classified as a typical counting method, where every relative maxima or minima are counted. Simple-Range counting counts the range between reversals and counts them as cycles depending on whether they are followed by positive or negative reversals. Ranges are only counted if they are greater than a preset amount.

In RFC, the loading profile is reduced to loading and unloading portions. Then, these portions are rotated 90 degrees and ‘raindrops’ are placed down the loading profile to determine which cycles are counted for the fatigue analysis. Only the largest relative cycles are counted. This process can be seen in the figure below:

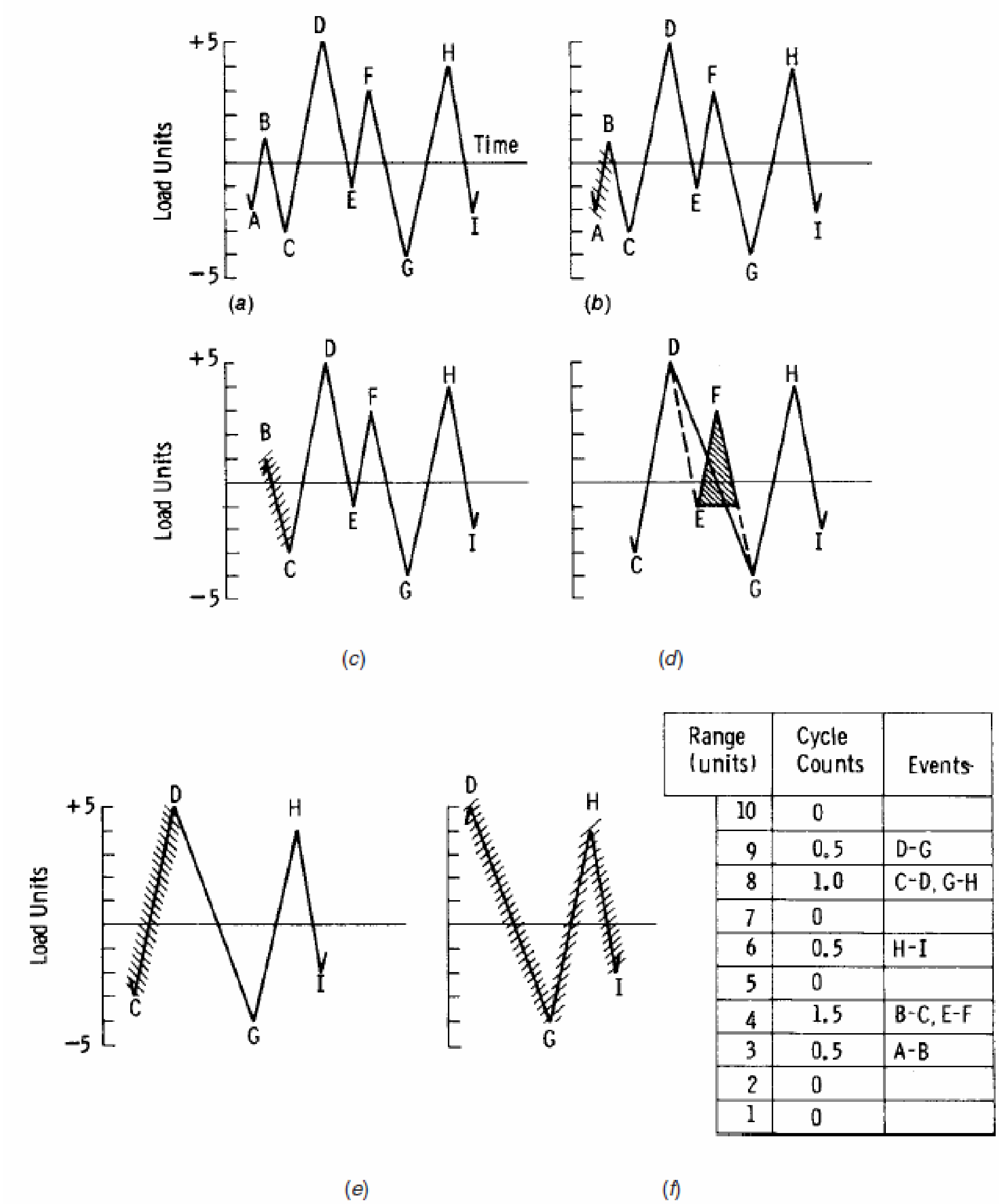

Range (units)	Cycle Counts	Events
10	0	
9	0.5	D-G
8	1.0	C-D, G-H
7	0	
6	0.5	H-I
5	0	
4	1.5	B-C, E-F
3	0.5	A-B
2	0	
1	0	

Figure 6 – Rain Flow Counting Example (8)

In the above example, it can be seen that the smaller intermediate cycles are removed. This is a unique way to remove artificial cycles which may present in the data, and has shown value in other industries. RFC has been applied to pipelines in the past when considering the loading spectrum of pipelines; these analyses have been only considering mechanical factors when looking at fatigue cracking, not taking into consideration additional environmental factors which may be present when discussing EAC.

2.1.4.3 Addition of the Environment to Fatigue Cracking (Corrosion Fatigue) (3)

Corrosion fatigue occurs when crack growth under cyclic loading is accelerated due to the presence of a corrosive environment. Corrosion Fatigue Cracking (CFC) can occur under relatively low changes in loads (lower than the traditional threshold ΔK). There are three different types or approaches to CFC: cycle dependent, time dependent, and a combination of the two (3).

Cycle dependent CFC is where the crack growth is independent of frequency, and only accelerates as the number of cycles increase. It is often modeled by taking the fatigue growth rate in an inert environment, and applying a multiplying factor based on the aggressive service environment, as seen below (3).

$$\left(\frac{da}{dN}\right)_{aggressive} = \Phi\left(\frac{da}{dN}\right)_{inert}$$

The acceleration factor used to compensate for the aggressive environment can be constant or variable based on the loading conditions, such as ΔK. The cyclic dependency occurs most often in situations where the environment does not promote a high dissolution rate under static loading conditions.

Time dependent CFC is modeled by using a superposition model combining the inert fatigue crack growth rate with the environmental crack growth rate, shown below (3).

$$\left(\frac{da}{dN}\right)_{aggressive} = \left(\frac{da}{dN}\right)_{inert} + \frac{1}{f}\left(\frac{da}{dt}\right)_{EAC}$$

The majority of material/environment combinations result in a combination of cycle and time dependent behaviors. The generalized CFC equation incorporating both aspects of corrosion fatigue is shown below (3).

$$\left(\frac{da}{dN}\right)_{aggressive} = \Phi\left(\frac{da}{dN}\right)_{inert} + \frac{1}{f}\left(\frac{da}{dt}\right)_{EAC}$$

As this equation shows, at high frequencies the crack growth contribution from the time dependent CFC is negligible, as the reacting species has less time to interact with the crack tip. Similarly, at low frequencies the cyclic dependency of CFC diminishes as the EAC crack growth rate becomes enhanced due to the increased time the reacting species have to interact with the crack tip. The effect of frequencies on the different types of corrosion fatigue is shown in Figure 7**.**

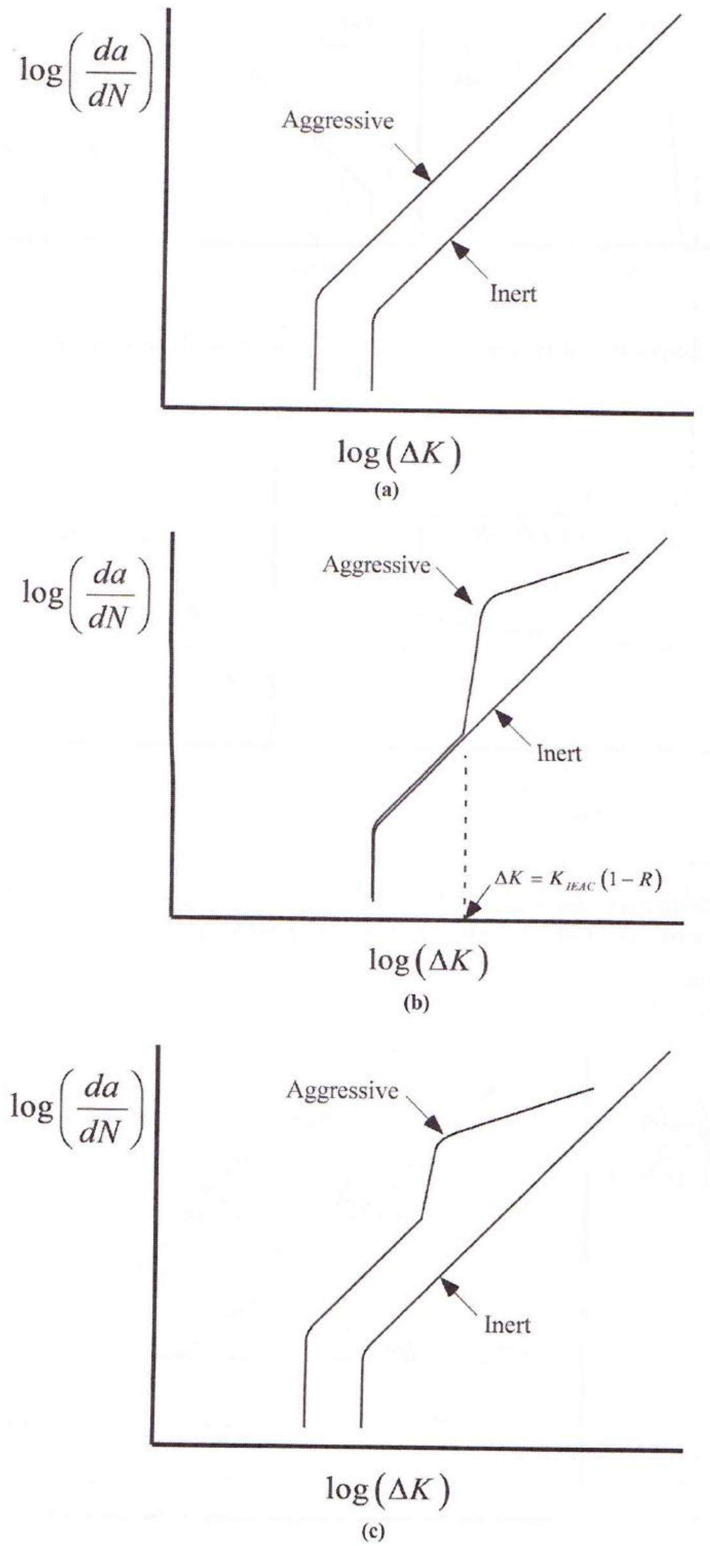

Figure 7 - Types of CF: (a) cycle-dependent CF, (b) time-dependent CF, and (c) cycle- and time-dependent CF (3).

In the same vein of thought as above, the waveform will have an effect on the CFC rate as well. While a square waveform may have more crack growth contribution from the time dependent crack growth due to the longer exposure time at a high load, there is a competing effect in many cases where the increasing load is actually more damaging from a corrosion fatigue point of view. In these cases, a saw-tooth or sine loading scheme may be more damaging than a square waveform. These competing effects make the analysis and prediction of corrosion fatigue extremely difficult to perform on changing environments and loading conditions (3).

The mechanisms proposed to explain CF have focused on the mechanisms that are used to explain the other types of EAC which occur under static loading. These include hydrogen embrittlement, film rupture, and anodic dissolution. In order to account for the fatigue aspect of CF, certain cyclic loading considerations such as the interaction with the plastic zone with the rest of the material during unloading are included.

Wedging of corrosion products is also an issue with CF; however, instead of the effect of wedging being under debate when considering static loading, the effect on fatigue loading is well understood. The effective ΔK for fatigue decreases when corrosion products are present because the compressive stress due to the increased volume of the corrosion product increases the minimum stress experienced. This is illustrated in Figure 8.

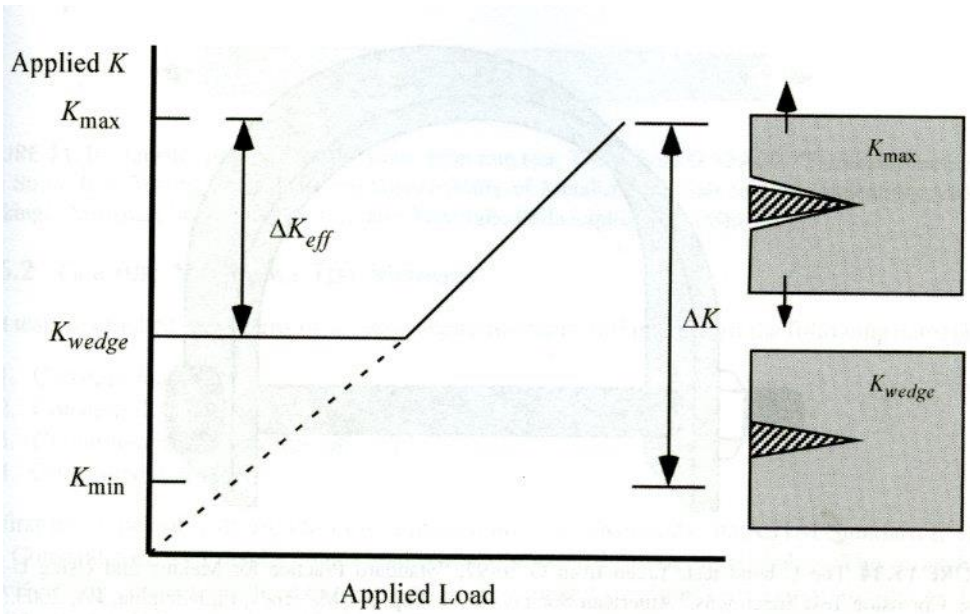

Figure 8 -- Effect of corrosion product wedging on the effective cyclic stress intensity. (3)

2.2 SCC on Pipelines

In general, as was previously stated, SCC requires three conditions in order to initiate: a susceptible material, an aggressive environment, and a tensile stress. In pipelines these conditions are present from a variety of sources, as seen in Figure 9. Each of these conditions will be explored in more detail; however, it is important to recognize that there are two different types of SCC that have appeared on pipelines.

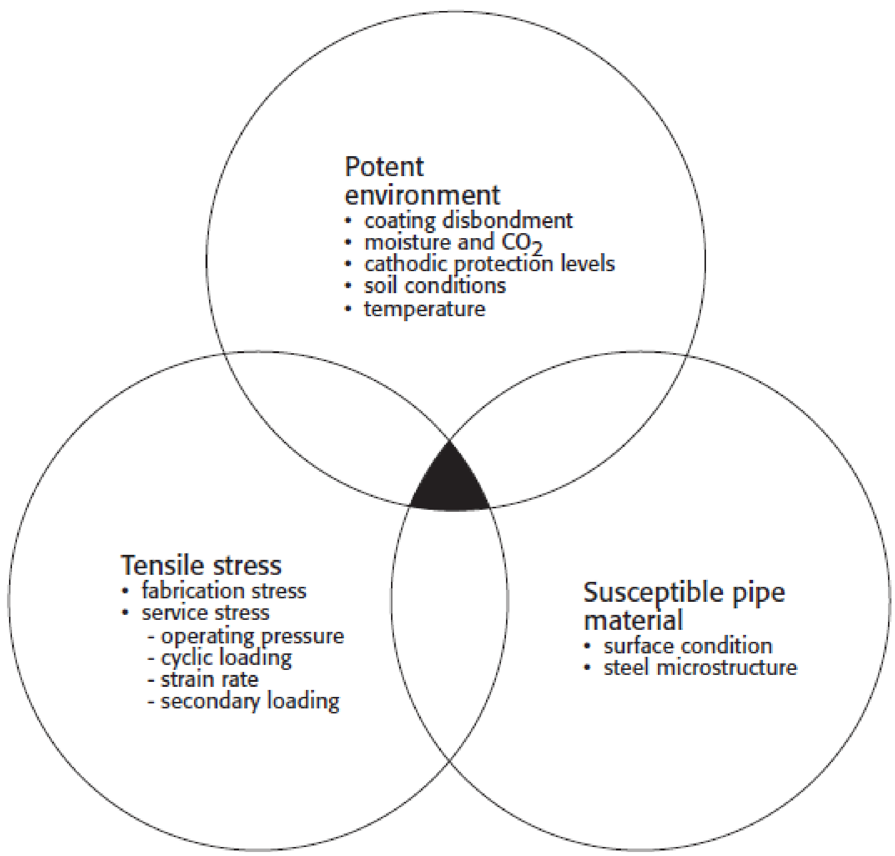

Figure 9 -- Combination of Conditions for SCC on Pipelines (9)

2.2.1 High pH SCC

High pH SCC is also known as Classical SCC. It was found on pipelines in the 1950's and a fair amount of research has been done on this type of cracking. High pH SCC can occur on pipelines in a small range of cathodic potentials where there is a carbonate/bicarbonate solution with a pH between 8.5 and 11. The environment itself must reach the pipe surface through a disbondment or holiday in order for corrosion to form. While steel can form a passive layer under these conditions, which would otherwise stop SCC, a tensile strain can break the brittle oxide layer, allowing SCC to occur. The dependency of High pH SCC on this tensile strain results in strain rate and total strain being important factors in the occurrence of this type of SCC.

Classical SCC cracks are often intergranular in nature and are very tight and narrow. A typical Classical SCC crack is shown in Figure 10. This type of crack morphology is due to the fact that grain boundaries are slightly more anodic relative to the grains themselves. This creates a preferential dissolution along the grain boundaries as the SCC cracks grow.

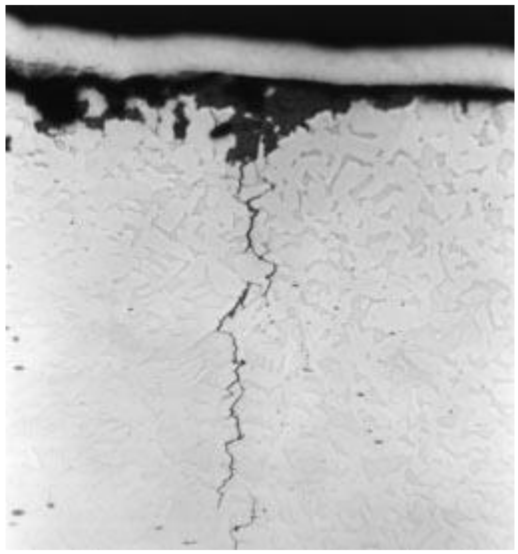

Figure 10 -- Metallographic Section of High pH SCC (Magnified 250x) (9)

2.2.2 Near Neutral pH SCC

There has been considerably less research concerning Near-neutral pH SCC (NNpHSCC), as it was only first seen and identified in the 1980's. There may have been some instances of NNpHSCC in the mid 1970's; however, it was not identified as such at the time. As the name suggests, NNpHSCC usually occurs in a localized environment where the pH is between 5.5 and 7.5. These low pH values indicate regions where designed CP system can no longer provide current to the pipe (10), which will be explained in the following sections. While the initiation mechanism of this type of cracking is not known, there are several conditions that may contribute to its occurrence. The presence of hydrogen may allow cracks to grow from existing corrosion pits due to the HE mechanisms previously mentioned. Carbon dioxide appears to facilitate the near neutral pH due to the formation of carbonic acid when it reacts with water.

The term of NNpHSCC is a term given by the oil and gas industry, due to the appearance of the cracks being very similar to those of High pH SCC. SCC requires a constant stress; however, laboratory experiments have not been able to initiate NNpHSCC under a constant stress (11). It appears that a synergistic effect of both corrosion fatigue and hydrogen embrittlement is required in order to initiate and grow cracks on pipeline steel in a near-neutral environment. (11)

NNpHSCC cracks often have transgranular morphology, moving through grains as opposed to along grain boundaries (see Figure 11). The crack walls corrode more, making the cracks appear much wider; however, as they grow the cracks inevitably become narrower. (9)

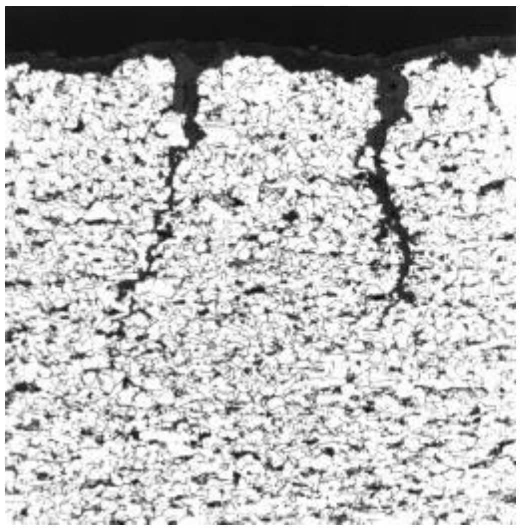

Figure 11 -- Metallographic Image of Near-neutral pH SCC (250x Magnification) (9)

The main focus of this thesis work is focused on the modeling of Near Neutral pH mechanisms of SCC, not the High pH variant.

2.2.1 Environment

The environmental considerations when looking at SCC on pipelines may be the most complex and involved condition. Before one can begin to look at the soil and electrochemical situations that lead to SCC, whether or not this environment can interact with the pipeline itself needs to be examined. This leads to a discussion on pipeline coatings.

2.2.1.1 Pipeline Coatings

Since the 1940's, pipelines have been coated with different materials and methods. Originally, pipelines were coated with tar and asphalt which was applied in the field.

Mechanically, these coatings are often brittle and may disbond fairly easily; however, it has been found in the field that coal tar coatings are slightly more malleable than asphalt. When disbondment occurs the coating often becomes saturated with moisture, allowing some of the cathodic protection current to conduct to the pipe surface, protecting a given section of the disbonded area. SCC becomes an issue with these coatings only in cases where the soil has a high resistivity, limiting the penetration of CP and leaving portions of the pipe unprotected.

In the mid 1950's, while some tar and asphalt coatings were still being used, polyethylene (PE) tape was starting to be applied in the pipe mills, primarily on smaller diameter pipes. It wasn't until the 1960's that the polyethylene tape started to be applied in the field. This type of coating was most popular on Canadian pipelines until the 1970's and 80's. There are several issues with PE tape that causes disbondment in the coating. The first issue is the occurrence of tenting, which occurs when the tape is separated from the pipe surface at the seam weld. This type of disbondment can be seen in Figure 12. Disbondment may also occur with the overlap between wraps. Similarly to asphalt and tar coatings, when tape coatings disbond, they allow moisture to enter the disbondment and come into contact with the pipe surface. The presence of water is never a good thing; however, it poses more of an issue with tape coatings though, as the polyethylene does not conduct electricity as well as the tar and asphalt when wet. This impedes the ability of CP to protect the pipe surface deep into the disbonded area. From these conditions existing under PE tape coatings, it is no surprise that the Canadian Energy Pipeline Association (CEPA) estimates that the number of SCC occurrences is four times higher on tape coated lines than on tar and asphalt coated lines.

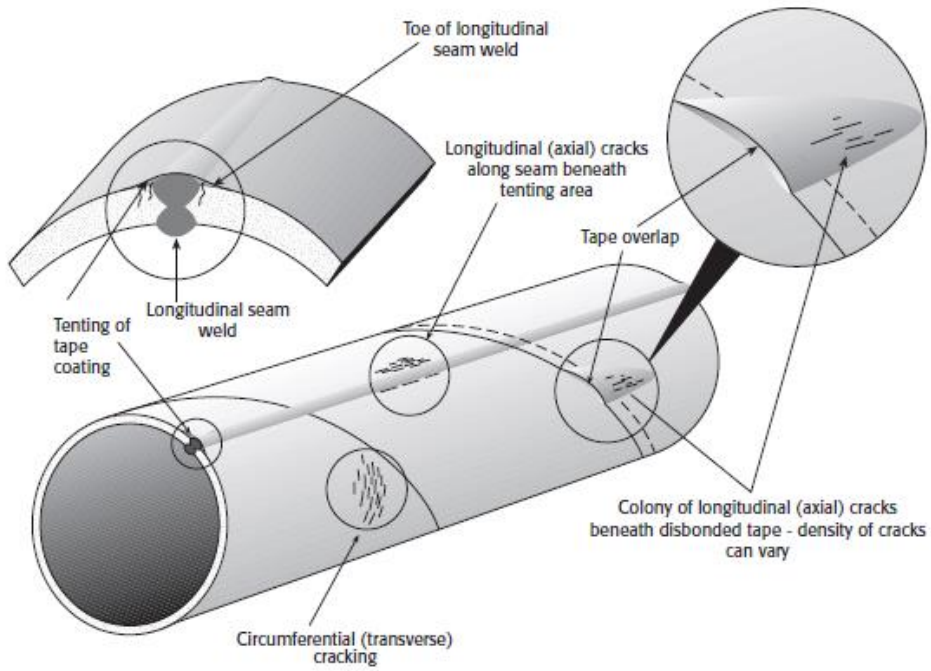

Figure 12 -- Areas of SCC Formation under PE tape coatings (9)

Historically, most of the SCC issues have occurred on pipelines coated with polyethylene tape; however, the application processes of polyethylene tape have improved significantly since their inception. Now they are applied with better mastic, which reduces the occurrences of disbondments. When the coating does disbond, it separates from the mastic instead of the pipe surface. This leaves the mastic protecting the pipeline, increasing in the effectiveness of polyethylene tape.

While polyethylene tape does appear to have the highest risk with regards to the occurrence of SCC, there has been SCC found on asphalt and coal tar coated lines. While the severity of SCC on coal tar lines has been relatively low, there has been a case of a NNpHSCC failure on an asphalt coated line (12). Even with the new findings on asphalt and coal tar lines, the risk of SCC remains considerably higher on tape coated pipelines.

Fusion bonded epoxy (FBE) coatings were developed in the 1970's. The NEB reported that to the date of their 1996 inquiry, no SCC problems were detected on lines that were coated with FBE, some of which had been in service for 20 years (9). The reason that these coatings appear to be resistant to SCC is because not only does the FBE rarely disbond, but when it does disbond, it acts like the tar and asphalt coatings when wet. The FBE conducts the CP and protects the pipe surface under the disbondment.

2.2.1.2 Soil / Topography Conditions

The performance of certain coatings has been thought to vary depending on the soil type, including rocks causing damage to the coating as well as different soils having different affinities for water (9). The density and cohesiveness of certain soils may also have an effect on soil stresses, which can lead to an increase in coating disbondment (13).

Soil analysis is a complex science with multiple characteristics that need to be considered, including: Soil Type, Texture, Oxygen Content, Resistivity, Moisture, pH, Total Acidity, Cation Exchange Capacity, Redox Potential, Chloride & Sulphide content, Carbonates and Bacteria. (14)

Soil type is composed of how the soil is deposited, percentage of parent material versus percentages of sands, silts, clays, and the amount of coarse fragments (coarse fragments are considered to be larger than two mm in diameter). The way soils are deposited and their dominant texture can affect drainage (which affects both liquid and gas movement) and retention of moisture. (14)

Oxygen is necessary for the majority of underground corrosion of steel to occur. Specifically, oxygen concentration cells are required for accelerated corrosion to happen. If accelerated corrosion occurs to quickly, it will overtake the SCC growth rate and will effectively eliminate the stress concentration present. The issue becomes when the corrosion growth rate reaches just the right level to allow for crack tip oxidation. Seasonal precipitation, fluctuating water tables or pipelines which traverse areas with different drainage characteristics all affect the development of oxygen concentration cells. Another factor which may not be considered is when a pipe is backfilled after construction; the backfill material may be different than the native soil, which would create potential drainage issues and development of the oxygen concentration cell. (14)

While oxygen is often a major component of corrosion, in anaerobic conditions sulphate reducing bacteria (SRB) reduces the sulphates in the soil and converts them into sulphides. Sulphides are detrimental to pipeline steel because they inhibit the formation of molecular hydrogen from atomic hydrogen. This increases the possibility of HE, which can not only increase the crack growth rate, but also the chance that a crack will initiate from an already present corrosion pit.

Considering that corrosion is an electrochemical process, a soil's resistivity would obviously be an active player in the corrosion rate. The resistivity is a function of the retention of moisture, which interstitial fluids and dissolved solids are also present. The following figure depicts soil resistivities and their relative corrosiveness. Again, a 'butter zone' of corrosion is required in order for SCC to form.

Table 1 -- Resistivity Guidelines for Soil Corrosivity (14)

Resistivity (ohm-cm)	Degree of Corrosivity
< 500	Very Corrosive
500 - 1,000	Corrosive
1,000 - 2,000	Moderately Corrosive
2,000 - 10,000	Mildly Corrosive
> 10,000	Progressively Less Corrosive

It was found that soil resistivity is only good as an indication of corrosiveness. Escalante (15) found that in soils with a resistivity greater than 2000 ohm-cm, soil resistivity became unreliable as an indicator of corrosiveness. Robinson (16) stated that a pipeline located in soils that have a large variation in resistivity will often be more corrosive than soils that have a small variation in resistivity, even if this resistivity would be more corrosive according to Table 1.

As was previously stated, soil drainage does appear to have a significant impact on Near-neutral pH SCC. Corrosion requires an electrolyte to proceed, so in poorly drained or imperfectly drained soils SCC is more of an issue. The drainage also determines whether the environment with be aerobic (oxidizing) or anaerobic (reducing). The soil potential (whether it be oxidizing or reducing) can also be referred to as its redox potential. While there has been some work using redox potential which shows some correlation between a reducing environment and Near-neutral pH SCC, it fails to explain some occurrences of SCC in apparently aerobic conditions (17).

The soil topography is obviously closely linked to the drainage. Not only do depressions in the ground allow for imperfect drainage, but when the topography causes groundwater to flow across and along the pipe, the formation of Near-neutral pH SCC is favourable. The flowing water allows for the environment to refresh, constantly supplying the localized area with carbon dioxide, keeping the pH around the critical 6.5.

The influence of temperature and CO_2 poses an interesting situation when talking about near-neutral pH SCC. Natural gas lines have temperatures as high as 40°C near the compressor stations cool down as it flows down the line (9). It has been well established that the frequency and severity of High pH SCC increases as temperature increases; this is not the case with near-neutral pH SCC. While the kinetics of both diffusion and electrochemical reactions increases as temperature rises, the solubility of CO_2 decreases. In order for hydrogen to play an active part in cracking, a near neutral pH is required, which in turn requires a significant amount of CO_2. The competing factors make the temperature dependency of near-neutral pH SCC appear erratic. This lack of dependency has been confirmed in both laboratory and field conditions (10) (13). The presence of CO_2 is very important as the cathodic reaction within the environment changes from an oxygen reduction reaction to a hydrogen reduction reaction (18). The CO_2 also combines with the water to create carbonic acid which decreases the pH. These two effects generate more molecular hydrogen, which may in turn break down into atomic hydrogen which increases the susceptibility of cracking.

The final environmental condition to be considered is the level of CP. CP is used in conjunction with various coatings to help protect the pipeline. With CP, current is applied onto the pipe surface, pushing the specific alloy into the 'immune' region of the respective Pourbaix diagram (see Figure 13).

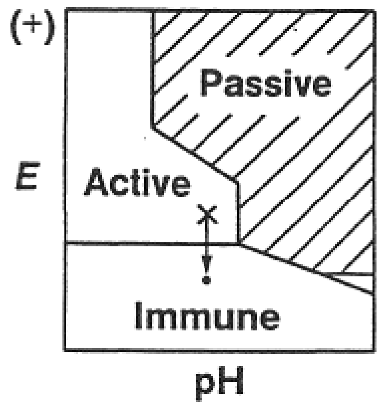

Figure 13 -- Effect of Cathodic Protection Represented on Pourbaix Diagram (19)

CP can be implemented via two ways: an impressed current method and a sacrificial anode method. With the impressed current system, the current is taken from a nearby power-line. The current is converted from AC to DC when it passes through a rectifier. If the current applied to the pipeline was AC, the protection would not be adequate. The sacrificial anode system uses a galvanic connection to provide a current to the pipeline. An anode made out of a relatively more electrochemically active material is placed in a semi-permeable sac and electrically connected to the pipeline. The galvanic action allows the current to flow from the environment onto the pipeline, the exact opposite direction of current flow present in normal corrosion. The current is distributed through multiple electrodes carefully placed within the soil. How the electrodes are configured depends on several factors such as the geometry of the pipeline in the area as well as the resistivity of the soil. An impressed current system is shown below.

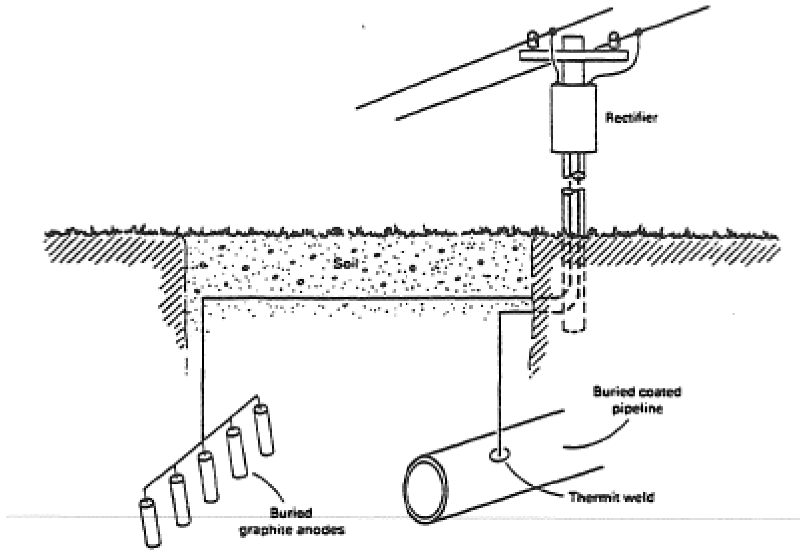

Figure 14 -- Schematic of an Impressed Current Cathodic Protection System (19)

It has been established that Near-neutral pH SCC often occurs where there is an inadequate level of CP (9). While it is required by law to protect buried pipelines with both coatings and CP, a disbondment in coatings can cause the level of CP to drop off to these crucial inadequate levels (20) (18). As was previously stated, this is more of an issue with tape coated lines, due to their shielding nature. The common sense approach to solving this problem would be to increase the amount of CP; however, disbondments on the buried pipe can be as large as a meter (9), which would still limit the ability of CP to protect the pipe surface all the way through the disbondment. An increase in the level of CP may also bake the coatings more which would in turn result in more disbondments occurring. There has been some research on pulsing the CP which has shown that it may increase the depth of protection into the disbondment (9). The complete loss of CP normally results in generalized corrosion; however, if there is residual CP still on the pipe, cracking becomes more of an issue.

2.2.2 Susceptible Material

While the environment contains many different variables and conditions which affect the severity of SCC found on buried pipelines, if the service material in place does not show susceptibility to SCC, it will not be an issue. With that being said, near-neutral pH SCC has been discovered on a wide range of pipeline diameters and steels (9) (10).

There does not appear to be a direct correlation between the manufacturing process and the steel's susceptibility to SCC. The main characteristics that affect the SCC susceptibility include the steel's composition, cleanliness, grade, and surface condition. A steel's composition directly affects its corrosion behaviour. It has been found that adding certain elements such as chromium, molybdenum and nickel in amounts ranging from two to six percent can decrease the susceptibility of a material to high pH SCC (9). While the composition affects the general corrosion behaviour, a material's SCC behaviour varies considerably on the microstructural discontinuities as well as surface condition. Not only do corrosion pits and other surface heterogeneities act as stress raisers but they can also affect the coating condition of the pipe, decreasing the smooth surface area for coating adhesion. Due to the increased stress concentration of corrosion pits, micro-cracks have been shown to initiate at these pits located at grain boundaries, pearlitic colonies, and banded phases (21). Once initiated, the cracks may grow either transgranularly or intergranularly depending on the environmental conditions. Even if a crack is initiated at a grain boundary, it is still possible for the crack to grow not in the direction of the boundary itself, depending on the circumstances. It has also been reported that cracks can initiate at inclusions as well. The amount of inclusions in a steel is referred to as its cleanliness. The more non-metallic inclusion, the less 'clean' the steel is and vice versa. These inclusions will have slightly different mechanical properties, possibly creating weakest links or introducing another stress raiser into the microstructure. This stress raiser may come from the preferential corrosion of the inclusion.

The yield strength of the steel may also has an effect on SCC susceptibility. On one hand, if a material has lower yield strength, it is possible to have small (micro-scale) areas in which localized plastic deformation occurs. This deformation has higher internal tensile stresses, which in turns make the region slightly anodic compared to the surrounding material. This is due to the fact that as the lattice is stretched under tensile loading, the distance between the atoms weakens the electromagnetic bond, which makes it easier for the material to give away electrons. The anodic region is more likely to corrode and generate pits, which may lead to the initiation of SCC.

A higher tensile strength does not necessarily reduce a materials susceptibility to SCC. The transgranular crack growth of near neutral pH SCC suggests that the growth is mechanically driven, making hydrogen embrittlement an important factor. As previously mentioned, there appears to be a correlation between an increase in yield strength and the hydrogen embrittlement threshold stress. The optimum combination would be a material that had relatively high yield strength and low hydrogen embrittlement susceptibility.

As with other forms of cracking (e.g. fatigue), hardness can also be an issue when considering SCC susceptibility. An increase in the localized hardness of a material will decrease its toughness, allowing cracks to propagate easier. The hard spot is brittle and is not likely to plastically deform at the crack tip, which would normally blunt the crack, slowing its progression.

Other manufacturing defects, such as Lack of Fusion (LOF) in seam welds and laminations in the pipe body, present other potential stress raisers which can increase a material's SCC susceptibility.

2.2.3 Tensile Stress

In order for SCC to occur, a tensile stress is required. There are several sources of stresses that can be introduced to a pipeline. These sources can be classified based upon what orientation they act on the pipeline. Cracks are generated in a perpendicular orientation to the applied stress; therefore, circumferential or transverse stresses generate cracks which grow in a longitudinal or axial direction, and vice versa.

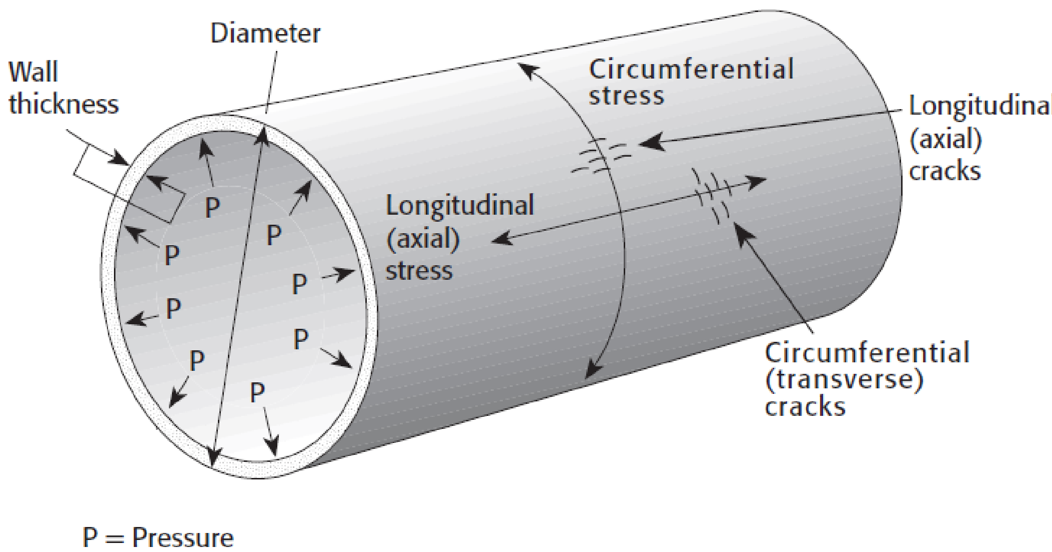

Figure 15 -- Stresses in pipelines (9)

Circumferential stresses may have several sources, including the internal operating pressure, bending and residual stresses created during manufacturing and welding processes, local stresses due to mechanical gouges, corrosion pits and at other stress raisers, secondary stresses that may cause the pipe to go out of round (i.e. soil settlement and landslides), stresses due to temperature variation through the thickness of the pipe wall, and external interference incidents. There are also stresses generated in the longitudinal direction, due to the internal operating pressure, although the longitudinal stress generated by this pressure is between often half the circumferential stress. Land movement, temperature variations, and external interference incidents. The largest stress component of those listed is the circumferential stress due to the internal pressure of the service fluid, and was the primary focus of this modelling effort. (9)

The stress generated by the internal operating pressure, or the 'hoop stress' varies between different pipelines and can be calculated with the Barlow equation, shown below:

$$\sigma_1 = \frac{PD}{2t}$$

Where sigma is the hoop stress, P is the internal pressure, D is the outer diameter of the pipeline, and t is the wall thickness. This equation describes the stress experienced in the circumferential stress due to the internal pressure. It is derived by putting into equilibrium the force of the pressure acting on the pipe and vice versa. This equilibrium can be seen in the relation below (22):

$$2[\sigma_1(t\ dy)] = P(2r\ dy)$$

Where *r* is the radius and *dy* is the incremental length along the pipe. Solving for σ_1 gives us:

$$\sigma_1 = \frac{Pr}{t}$$

Seeing as the radius, *r*, is equivalent to half of the diameter *D/2*, this gives the Barlow equation. If the same process was used to calculate the longitudinal stress generated by the same internal pressure, the following equilibrium is given (22):

$$\sigma_2(2\pi rt) = P(\pi r^2)$$

Solving for σ_2 yields:

$$\sigma_2 = \frac{Pr}{2t}$$

Which as discussed previously, is half of the circumferential stress produced by the internal pressure of the pipe.

The circumferential stress that a pipe experiences is often expressed as the hoop stress as a percentage of the Specified Minimum Yield Strength (SMYS) of the pipe steel, although the actual yield strength of the material can be 10 to 30 percent higher than SMYS. The allowable stress for a specific line is depicted by CSA Z662-11 and depends on the class location and how inhabited a specific area. The highest allowable % SMYS for natural gas is 80%; however, this is most likely lower than 80% of the actual yield strength of the pipe steel. Industry research has shown that no SCC failures have occurred when the operating stress of the pipeline is less than 50% SMYS.

The stress associated with the pressuring up of the service fluid is not constant, due to fluctuations associated with pressure drops along the pipeline, as well as variations within compressor operation. The fluctuations in stress are often more varied in liquid lines than in gas lines, due to the variations and fluid density changes associated with turning pumps on and off (9). The changes in pressure can vary from nearly instantaneous to over several days between loading cycles, making the determination of frequency extremely difficult. This type of varied loading may be considered to be fatigue loading. Studies have shown that fatigue loading is required to initiate SCC cracks (9; 23).

In order for the total stress to reach SMYS, other significant stresses other than the hoop stress need to be involved. When flat steel plate is formed into pipe, residual stresses are introduced into the material. The amount of residual stress depends on the specific manufacturing process. The residual stresses introduced in this fashion can be reduced by performing a high-pressure hydrostatic test. Residual stresses are also generated during welding processes, in which the rapid cooling of the fusion zone creates thermal stresses when post-weld heat treatment (PWHT) is not properly performed. Misalignment of pipes which are welded together may also generate residual stress in the form of a bending moment.

It has been shown that residual stress can increase the effective stress experienced by the line pipe steel to levels greater than 100% SMYS. This type of loading would generate the stress required to initiate SCC.

When discussing the tensile stress associated with SCC, it becomes imperative to talk about not only yielding, but the fracture mechanics involved with crack growth.

2.2.3.1 Fracture Mechanics (3)

When discussing the loading required for SCC initiation and growth, the science of Fracture Mechanics plays a vital role.

The first branch of Fracture Mechanics is Linear Elastic Fracture Mechanics (LEFM). This approach applies to materials which obey Hooke's Law; that is, they act in a linear fashion and do not have excessive plastic deformation. There are other branches of fracture mechanics which are used for materials which act plastically; however, the majority of these approaches are simply extensions of LEFM.

While there have been several different methods to capture the condition at the crack tip (e.g. Griffith Energy Theory, Energy Release Rate Theory), for the purpose of the project at hand, the most pertinent method would be the use of the Stress Intensity Factor (SIF), as previously discussed before. Through the analysis of the crack tip, it was shown that for specific loading conditions and crack configurations, it is possible to describe the loading condition at the crack tip.

There are several different ways to load the crack tip (see Figure 16); however, Mode 1 loading is the condition primarily considered when discussing crack stresses in the pipeline (3).

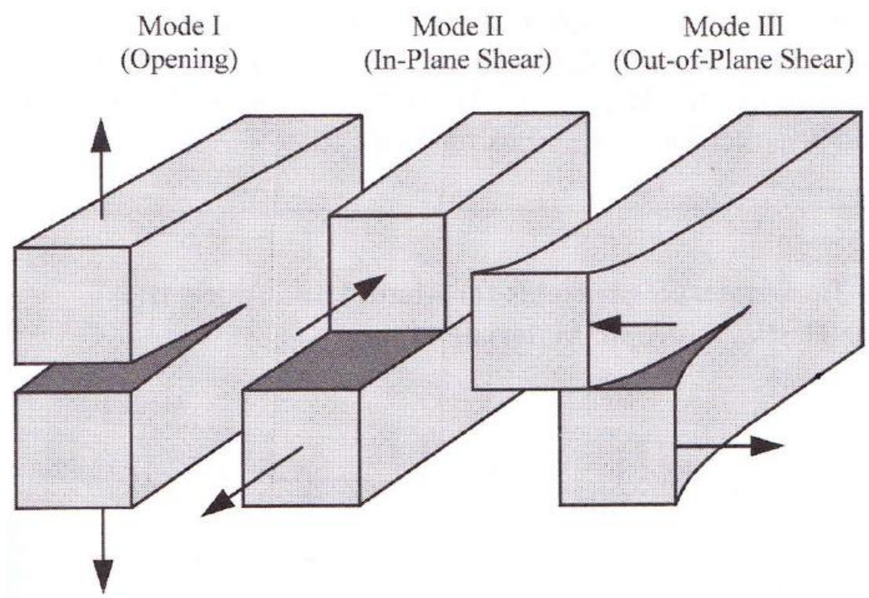

Figure 16 -- Three Modes of Loading which can be applied to a crack (3)

Before the description of how Mode 1 analysis is provided an explanation of the coordinate axis is required for reference. The coordinate axis is illustrated in Figure 17.

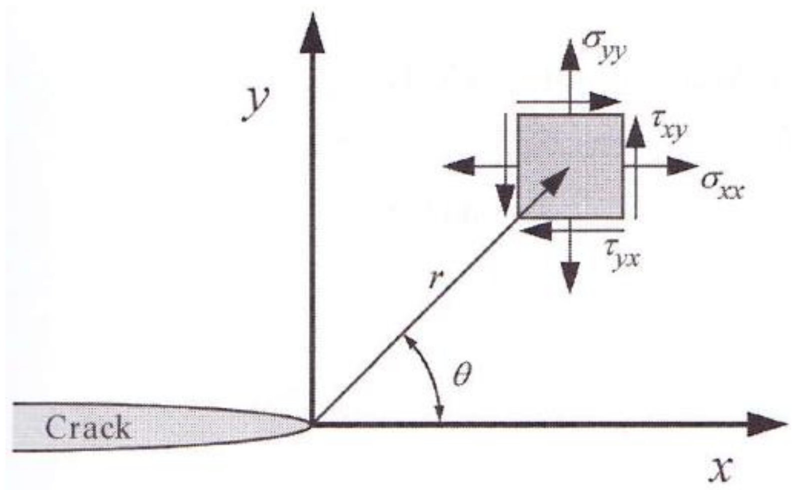

Figure 17 -- Definition of the coordinate axis ahead of a crack tip. The z direction is normal to the page. (3)

The local stress normal to the crack plane decreases as the position moves away from the crack tip. Solved closed-form equations have determined that the stress is proportional to $1/\sqrt{r}$. (3)

In order for the SIF to be useful, there needs to be a relationship between that and the global behaviour of the metal (i.e. macroscopic loading conditions such as hoop stress in a pipeline). From manipulation of the closed form equations describing the crack tip, the relationship between global loading and the crack tip solution can be shown in the LEFM equation below (3):

$$K_I = \sigma\sqrt{\pi a}$$

Where K_1 is the stress intensity factor in Mode 1 loading, sigma is the global stress on the material, and a is the depth of a through crack already present in the material. It should be noted that this equation is only applicable for Mode 1 loading, which can be seen in Figure 16. The opening load on the crack most closely resembles the force applied via the hoop stress due to internal loading of a pipeline.

The derivation of this equation is for cracks located in an infinite plate. Once this method gets applied to actual structures, there are geometric boundaries and limitations which must be considered. In order to account for the boundary conditions, a geometric factor (β or Y, depending on the nomenclature) is applied.

The stresses in the x and y direction can be represented by the equation below. It should be noted that this equation only holds true for the case where Θ = 0 and r = 0. (3)

$$\sigma_{xx} = \sigma_{yy} = \frac{K_I}{\sqrt{2\pi r}}$$

Although pipeline steel is assumed to behave in a linear elastic behaviour, there will still be some localized plastic deformation at the crack tip will occur due to the stress concentration. LEFM of sharp cracks predicts an infinite stress at the crack tip, which is not realistic in the case of pipeline steel. In order to take this crack tip plasticity into account, two different modifications have been applied to the basic SIF equation.

The first approach to considering crack tip plasticity is the Irwin approach. In this approach, the stresses are solved using the equation above. The boundary between plastic and elastic behaviour is predicted to be where the stresses meet the given yield criterion (e.g. in a plane stress condition $\sigma_{yy} = \sigma_{YS}$). Substituting the yield criterion into the left side of equation above and solving for *r* gives a first-order estimate of the plastic zone size (3):

$$r_y = \frac{1}{2\pi}\left(\frac{K_I}{\sigma_{YS}}\right)^2$$

The issue with the first-order estimation is that is assumes an elastic crack-tip solution. When plastic deformation occurs, stresses in the crack plane near the crack tip must be redistributed in order to reach equilibrium. The corrected equation for the plastic zone size is given below (3):

$$r_p = \frac{1}{\pi}\left(\frac{K_I}{\sigma_{YS}}\right)^2$$

As can be seen from comparing the two equations, the second approximation is twice as large as the first. The explanation of elastic crack tip behavior versus plastic crack tip behavior can be seen in Figure 18.

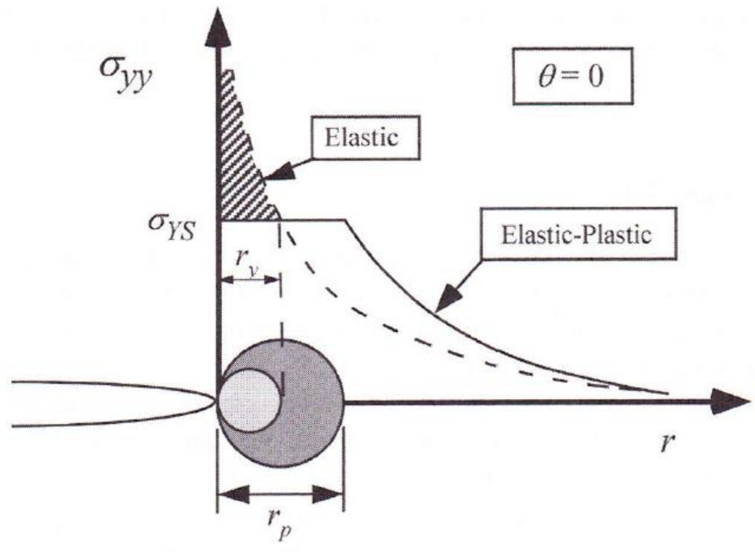

Figure 18 -- First-order and Second-order estimations of the plastic zone size using the Irwin Approach (3)

The area of the plastic size is added onto the crack depth to get an effective crack depth (often shown as a_{eff}). This effective crack depth is used to calculate an effective SIF, as seen below (3):

$$K_{eff} = Y(a_{eff})\sigma\sqrt{\pi a_{eff}}$$

Due to the fact that the geometric factor is dependent on the effective crack depth, an iterative process is required in order to get an accurate effective crack depth and SIF.

The second approach for approximating the plastic zone size is the Strip Yield Model. This model assumes a long, slender plastic one at the crack tip in a non-hardening material in plane stress. The effective SIF equation from this model can be seen below (3):

$$K_{eff} = \sigma_{YS}\sqrt{\pi a}\left[\frac{8}{\pi^2}\ln\sec\left(\frac{\pi\sigma}{2\sigma_{YS}}\right)\right]^{1/2}$$

A comparison of the two models can be seen in Figure 19.

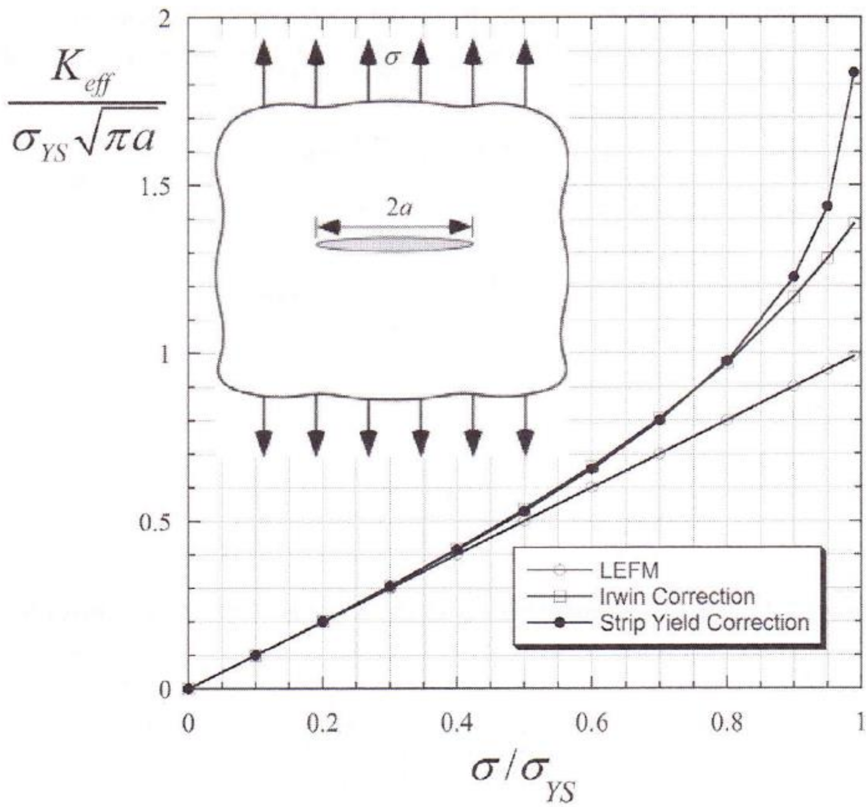

Figure 19 -- Comparison of plastic zone corrections for a through crack in plane strain (3)

There is good agreement between the two models up until the applied stress reaches a point of 0.85 σ_{YS}. The plastic zone shape predicted by the Strip-Yield model is not representative of the plastic zone in metals; however, it does bear some resemblance to polymers. For the purpose of crack analysis of metals, the Irwin approach appears to be more appropriate.

2.2.3.2 Monotonic Loading vs. Fatigue in NNpHSCC

Transgranular cracking (that which is observed when discussing NNpHSCC) requires a simultaneous condition for film formation on the crack walls and an active surface at the crack tip (11). This criterion will only occur under certain conditions, and in order for transgranular cracking to occur, the film at the crack tip must be ruptured, revealing the fresh surface for corrosion to continue. As Chen et al. (11) discuss:

> *When transgranular cracking is observed in a corrosion environment that strongly passivates the materials being exposed, film rupture by localized plastic deformation for a static stress (condition of stress corrosion cracking) becomes*

insignificant and crack growth would be too slow to cause any engineering concerns. Under the circumstances, cyclic loading becomes important, which can enhance the process of film rupture to make the crack to grow at a rate that is of engineering significance. This would be the case of corrosion fatigue.

Although NNpHSCC has been found on pipelines since the 1960's, the fact that it is called SCC may be a bit of a misnomer. It may be called SCC because natural gas transmission lines are operated a near monotonic loading. Attempts to model NNpHSCC using monotonic loading through tests such as slow strain rate tests, with no convincing evidence that SCC cracks can be grown in a Near-neutral environment.

Chen & Sutherby (24) attempted to characterize crack growth behavior in Near-neutral soil environments with respect to various loading and environmental conditions. In their work samples of pipeline steel were pre-cracked and then placed under cyclic loading with stress R ratios (ratio of minimum stress to maximum stress in a loading cycle) ranging from 0.6 to 0.8. The specimens were placed in four different near-neutral pH electrolytes during the loading to simulate trapped water under disbonded coating in the field. The corrosivity of the four electrolytes was tested via a weight-loss coupon test. The chemical composition and corrosivity results can be seen below.

Table 2 -- Composition of Electrolytes used in Experiment (24)

Composition (g/L)	C1	C2	C3	NOVATW
$MgSO_4 \cdot 7H_2O$	0.0274	0.0274	0.0274	—
$CaCl_2$	0.0255	0.0255	0.0255	—
KCl	0.0035	0.0035	0.0035	0.015
$NaHCO_3$	0.0195	0.0195	0.0195	0.437
$CaCO_3$	**0.0061**	**0.0606**	**0.2422**	0.23
$CaSO_4$ $2H_2O$				0.035
pH (purged with 5 pct CO_2 + N_2)	**5.89**	**6.29**	**6.83**	**7.11**

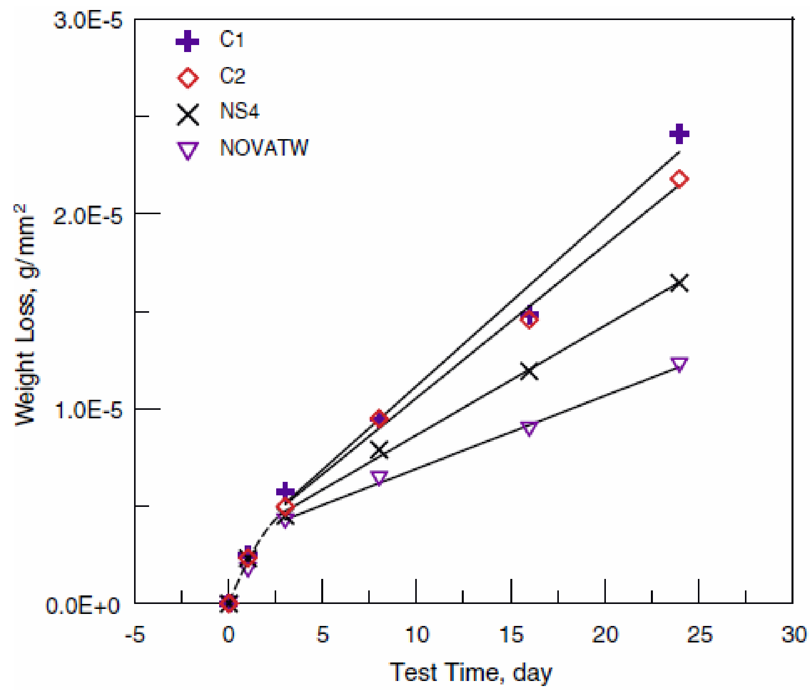

Figure 20 -- Variations in weight loss of X-65 pipeline steel with time when exposed to four different near-neutral pH soil solutions (24)

Due to the fact that the researchers wanted to focus on the loading conditions as well as the environmental conditions, only two electrolytes were chosen. The C2 solution and NOVA Trapped Water (NOVATW) solution were selected due to correlation in the field with regards to composition and pH values. These solutions were used in a variety of tests with variable loading conditions in an attempt to compare the respective crack growth rates. The results can be seen below.

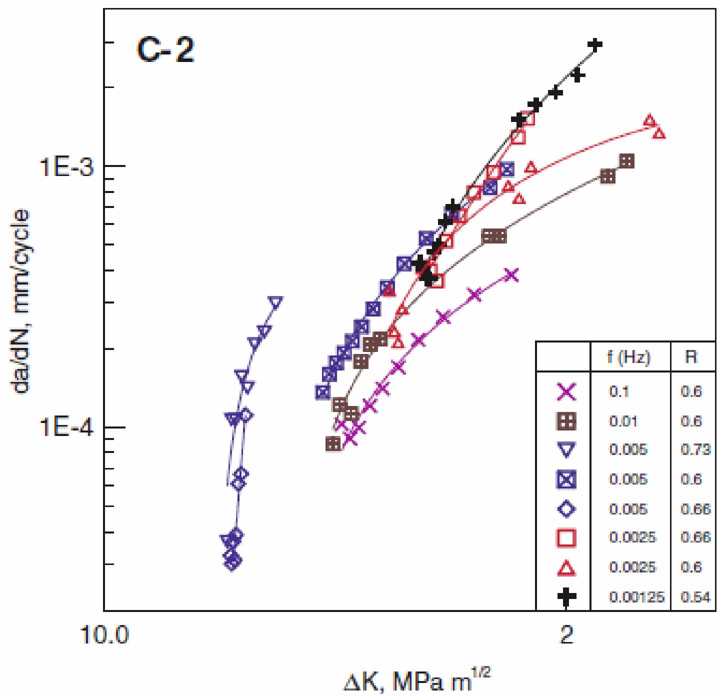

(a)

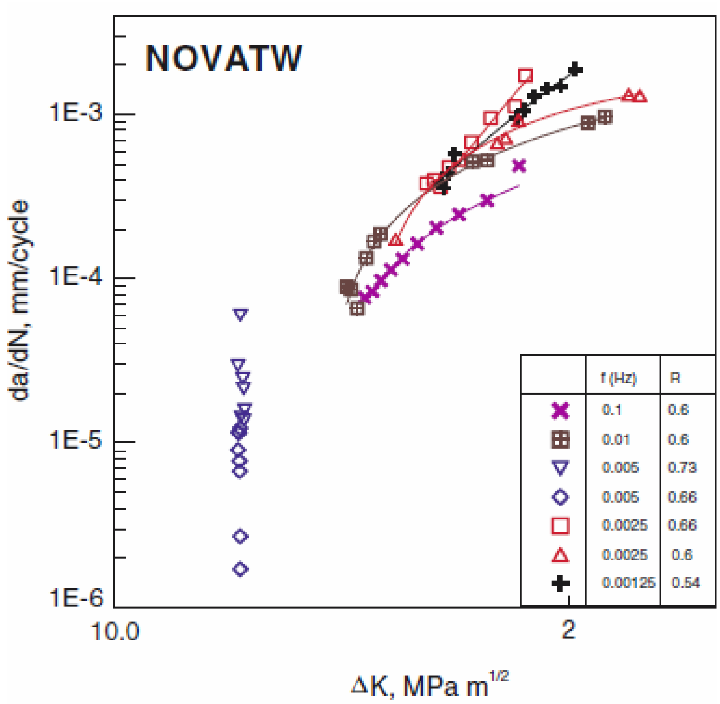

(b)

Figure 21 -- Crack growth rate (da/dN) as a function of ΔK obtained from testing in (a) C-2 solution and (b) NOVATW solution (24)

From Figure 21 it can be seen that although the crack growth rate is dependent on ΔK; however, the loading at a frequency of 0.005 Hz could not be resolved to fit this dependency. In order to resolve this frequency with the rest of the data, a dependency on both ΔK and R ratio is required. The R ratio is based off of both ΔK and K_{max}, as (24):

$$R = 1 - \left(\frac{\Delta K}{K_{max}}\right)$$

In order to resolve the data with the inconsistencies, the crack growth rate was plotted against $(\Delta K^2 K_{max})/f^{0.1}$. The resulting data plots can be seen in Figure 22.

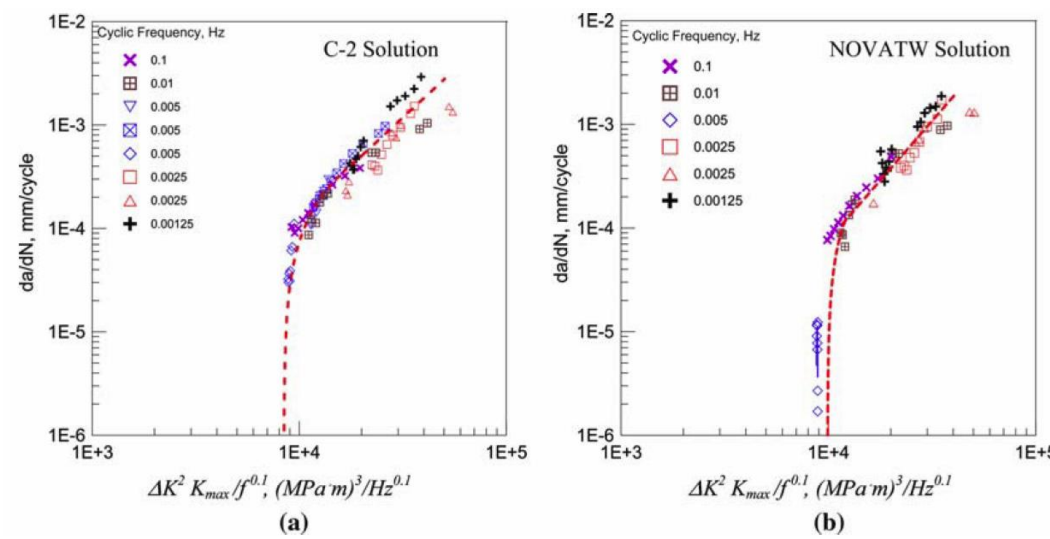

Figure 22 -- Crack growth rate (da/dN) as a function of $\Delta K^2 K_{max}/f^{0.1}$ obtained from testing in (a) C-2 solution and (b) NOVATW solution (24)

When the data is normalized, some "special characteristics" (24) can be seen. The first feature of note is the apparent separation between active crack growth and dormancy. There appears to be a threshold loading condition in the various environments which is a very apparent dividing line between these two potential stages of a crack's life. This threshold loading condition is dependent on ΔK, K_{max}, and frequency, as opposed to simply ΔK, as others have studied before. Chen and Sutherby (24) then took data from other published sources to try and determine if this threshold value was consistent when looking at near-neutral pH environments. The extra data was plotted to determine how individual loading factors affect the dormancy behavior. The results can be seen below in Figure 23.

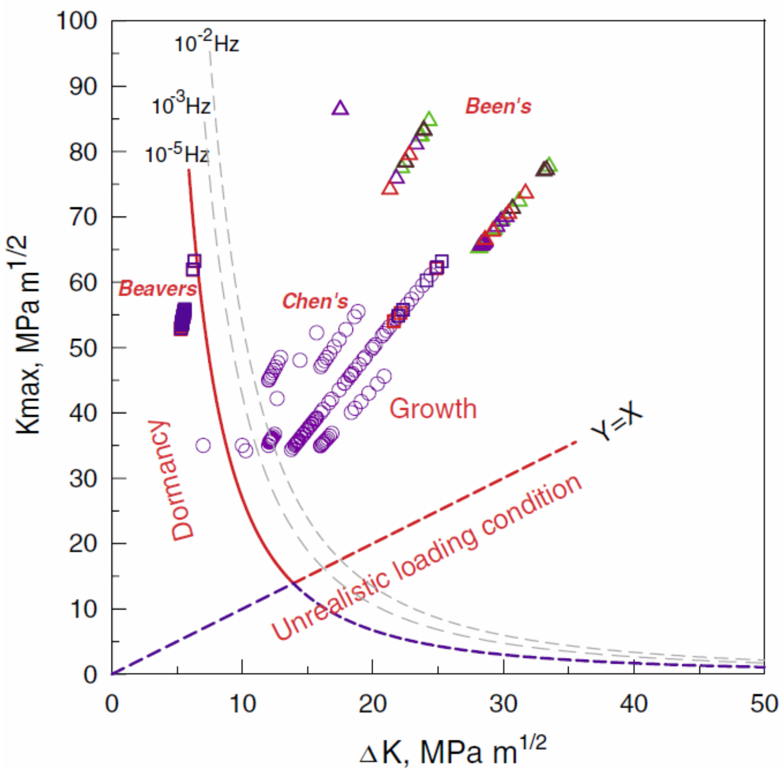

Figure 23 -- Map of crack growth behaviors as affected by ΔK, K_{max} and f (24)

2.3 Modeling of SCC

There have been numerous attempts of modeling SCC growth, with mixed results. The complex interaction of the environment, material properties, and stress make modeling these features very difficult to do. The majority of SCC modeling efforts looks at environmental conditions such as soil type and terrain.

TransCanada Pipelines Ltd. employed J.E. Marr & Associates to develop a predictive model of SCC (9). This model did not distinguish between High-pH SCC and NNpH SCC, and identified various terrain conditions which promoted “significant SCC” on tape coated and asphalt coated lines. The term “significant SCC” comes from CEPA recommended practices. In order for a colony to be significant, it must have a depth equal or greater than 10% of the wall thickness and have a length equal to 75% the length required for a 50% through-wall crack to rupture. The topography which had significant SCC colonies on tape coated and asphalt coated lines are seen in Table 3 and Table 4 respectively.

Table 3 -- Description of Significant Terrain Conditions for Tape Coated Pipe (9)

Soil environment description	Topography	Drainage
Clay bottom creeks and streams (generally <5m in width)		
Lacustrine (clayey to silty, fine textured soils)	inclined level undulating	very poor
Lacustrine (clayey to silty, fine textured soils)	inclined level undulating depressional	poor
Organic soils (> 1m in depth) overlaying glaciofluvial (sandy and/or gravel textured soils)	level depressional	very poor
Organic soils (> 1m in depth) overlaying glaciofluvial (clayey to silty, fine textured soils)	level depressional	very poor
Moraine tills (variable soil texture - sand, gravel, silt and clay with a stone content > 1%)	inclined to level level undulating ridged depressional	very poor poor imperfect to poor
Moraine tills (variable soil texture - sand, gravel, silt and clay with a stone content > 1%)	inclined	poor imperfect to poor

Table 4 -- Description of Significant Terrain Conditions for Asphalt Coated Pipe (9)

Soil environment description	Topography	Drainage
Bedrock and shale limestone (<1 m of soil cover over bedrock or shale limestone)	inclined level undulating ridged	well drained
Glaciofluvial (sandy and/or gravel textured soils)	inclined level undulating ridged	well drained
Moraine tills (sandy soil texture with a stone content > 1%)	inclined level undulating ridged	well drained
Sites which do not beem the <850 mV "off" criteria used in the Close Pipe to Soil Corrosion Survey (exclusive of the three sets of terrain conditions discussed above)		

The first step in developing these predictive models was to gather the preliminary information of the pipeline, which includes coating type, year of construction, grade of material, diameter, etc.

The terrain information was then gathered from aerial photos and soil surveys. The combination of the base pipe information and the soil information was used to develop a database. The database was then compared to the two tables above to classify areas along the pipeline as either susceptible or non-susceptible to SCC. The relative susceptibility was also considered to fine-tune the model.

Concerning the effectiveness of these models, five different CEPA companies provided information to the NEB in 1996 regarding their SCC model correlation digs (9). The companies had performed 1,920 investigative excavations looking for SCC. Forty-five percent of these digs were selected using predictive models, and SCC was found at 44 percent of the digs. When digs were done without input from predictive models, SCC was found at four percent of the digs. The information gathered by the 5 CEPA companies can be seen graphically in Figure 24**.** The disparity between these sets leads to two interesting conclusions: the predictive models based on terrain are capable of identifying potential areas of SCC, and the base of the model, which uses the regular maintenance digs, may not capture enough information regarding the susceptibility of SCC that a line may have.

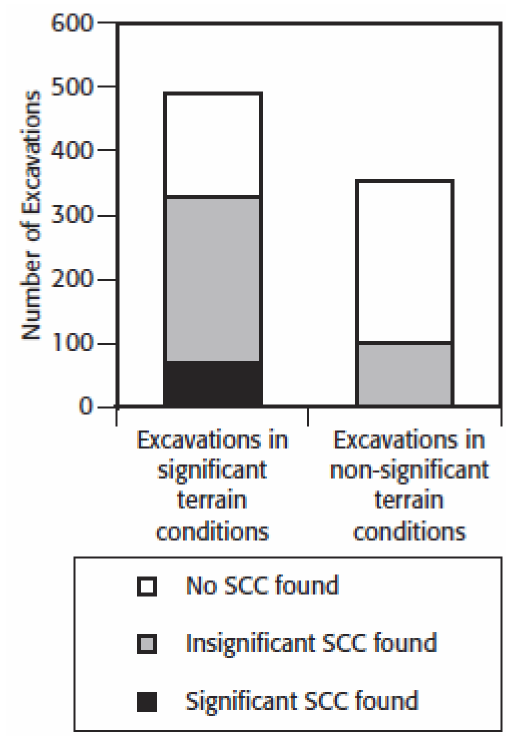

Figure 24 - Effectiveness of Predictive Models Developed by 5 CEPA Member Companies (9)

The models have shown enough promise in order to have the NEB issue a recommendation that if a line is believed to be susceptible to SCC, then companies must develop a model to identify areas to dig.

One of the drawbacks to the existing topography models is the ability to predict the severity of SCC at a location. This is extremely difficult, as there are tens of thousands of kilometers of pipeline and to select a specific section (which is typically 12 m long) to contain significant SCC is statistically improbable. In order to address some of this issue, in-line inspection (ILI) data is used. Although there is currently ILI tools which can detect cracks in natural gas lines (i.e. Electro-Magnetic Acoustic Transducer (EMAT) technology), older ILI technologies, such as Magnetic Flux Leakage (MFL) can be used.

In a case study presented by Kinder Morgan (25), information regarding corrosion features related to NNpHSCC was gathered on a large number of integrity digs. NNpHSCC is not always associated with external corrosion, although on the system in question the most severe colonies were documented with very light corrosion (i.e. <10% WT depth). This corrosion is not typically identified by a MFL inspection tool. Generally, this low level of corrosion is ignored during MFL inspections because the purpose of the inspection is to find severe corrosion which may act as an integrity threat to the pipeline. Identifying light corrosion in the MFL inspection run can highlight potential areas of disbonded coating, and although they are not normally reported, if the operator requests, MFL surveys can be graded at a specific depth less than 15%. This MFL data was combined with existing terrain / soil models to help refine the process. Another aspect which was used with this model was the CP data for specific coating types such as asphalt and coal tar. A CP Closed Interval Survey (CIS) measures the potential drop of a CP system, which usually points to defective coating. When the coating breaks down, the bare metal requires current from the CP system to be protected against corrosion. The more current which is used up, the more bare metal could be exposed. A typical CIS reading which represents potential coating damage can be seen in Figure 25. The area highlighted on the left is a normal reading for CP, whereas the circled area on the right points to coating damage.

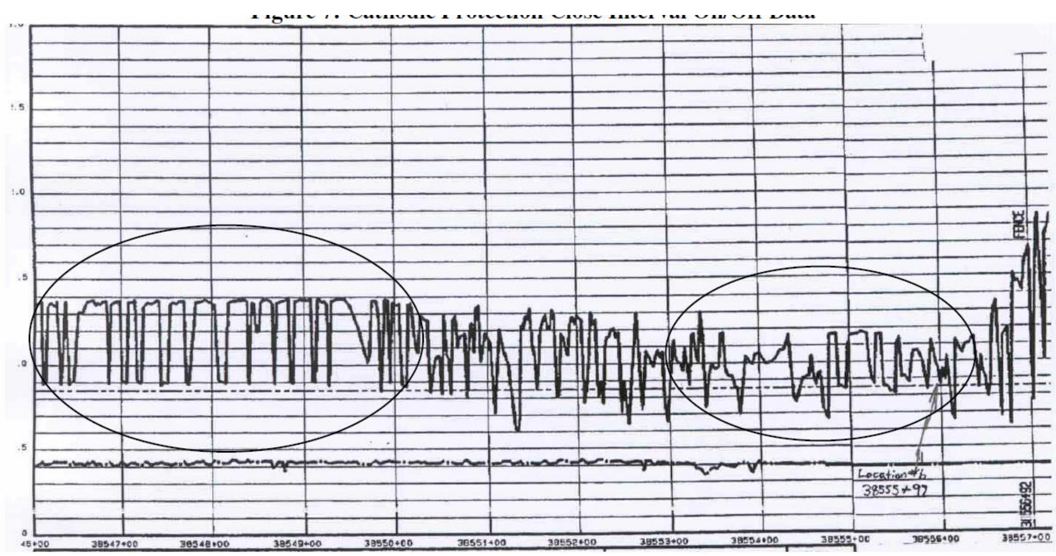

Figure 25 -- Cathodic Protection Close Interval On/Off Data (25)

The model was tested on a pipeline which had experienced a failure due to axially oriented NNpHSCC in 2000. Starting from the failure site, Natural Gas Pipeline Company of America (NGPL) developed a base level for their model. Once the base results were gathered, this model was expanded to similar pipe in a different location in 2003. The results of the 2003 model refinement can be seen in Table 5**.**

Table 5 -- 2003 Excavation Results from NGPL SCC Model (25)

Location (joint ID)	Coating Condition (from CP data, excavation results)	Typical Pipe Surface Deposits	Number of Colonies	Depth Range of SCC Colonies	≈ Length of Inspection (ft)
1 (105280)	Intact, disbonded	Extensive $FeCO_3$, $CaCO_3$, Fe-Oxide/hydroxide	56	10-15%	31
2 (113560)	Intact, disbonded	Extensive $FeCO_3$, $CaCO_3$, Fe-Oxide/hydroxide	78	7-10%	40
3 (144300)	Intact, disbonded	Extensive $FeCO_3$, $CaCO_3$, Fe-Oxide/hydroxide	158	15-20%	45
4 (94190)	Intact, disbonded	Extensive $FeCO_3$, $CaCO_3$, Fe-Oxide/hydroxide	43	20-25%	40
4A (93480) (null excavation)	Intact, disbonded	$FeCO_3$, $CaCO_3$, Fe-Oxide/hydroxide	0	0	41

5 (63650)	Intact, disbonded	Extensive $FeCO_3$, $CaCO_3$, Fe-Oxide/hydroxide	38	10-15%	36
6 (47330)	Extensive variability -- low CP spikes, coating broken apart, damaged, missing	Extensive $CaCO_3$, Fe-Oxide/hydroxide	0	0	40

Although this model was applied to an asphalt coated pipeline, the methodology and use of several data sources can be applied to tape coated lines as well.

While empirical models have been developed by industry in an attempt to trend SCC information, there have also been attempts to model the phenomenon from a combination of empirical and theoretical perspectives as well. King et al. (26) developed a model designed to predict the occurrence of initiation and early-stage crack growth on operating pipelines. The work presented in this paper used results found in the lab to identify different factors affecting the probability of SCC occurrence on pipeline steels. From the lab work, five factors were identified which lead to the earliest stages of NNpHSCC initiation and crack growth: inclusions, aligned defects, pre-existing defects on the pipe surface, persistent slip bands produced by mechanical pre-treatment of the steel, and coating disbondment. There was also a mention of residual stress being a factor in early stage initiation; however, this study did not focus on that aspect.

A figure representing the various stages of SCC crack growth can be seen below.

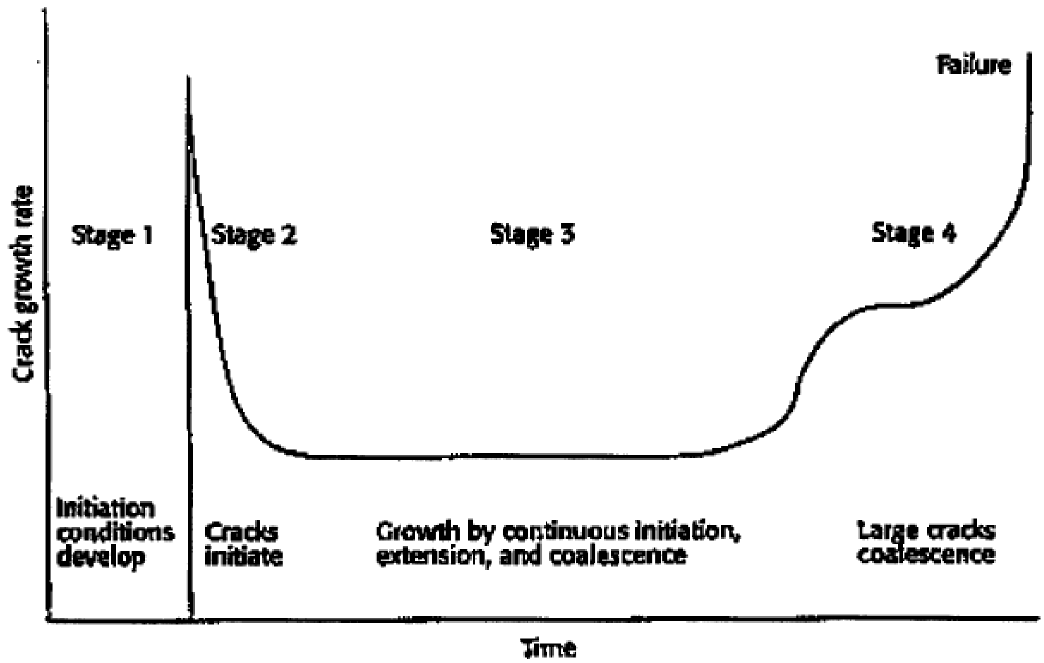

Figure 26 -- Various Stages in the Life of an SCC Crack (26)

The model format was approached from a probabilistic point of view; the overall probability of finding a viable crack (cracks which exist between stages 2 and 3) is as follows:

$$P_v(t) = P_I(t)P_{EG}(t)\big(1 - P_D(t)\big)$$

Where $P_I(t)$, $P_{EG}(t)$ and $P_D(t)$ are the time dependent probabilities of crack initiation, early growth, and dormancy, respectively.

The input data for the model can be seen in Figure 27**.**

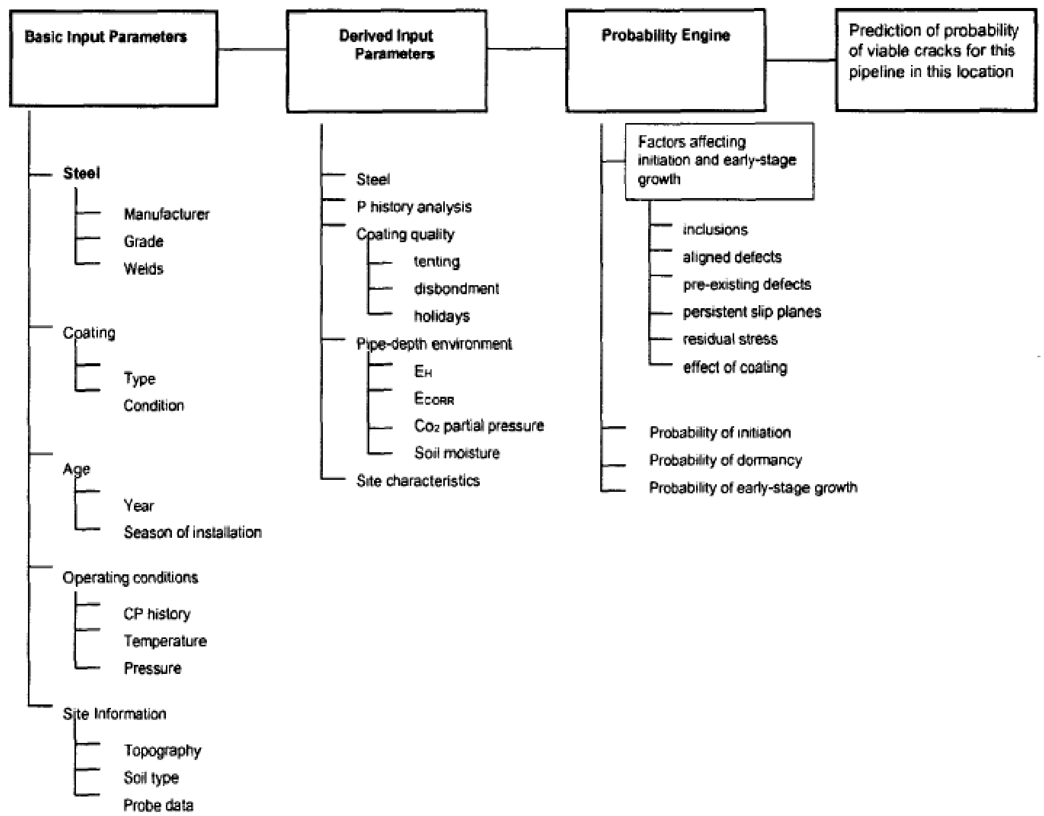

Figure 27 -- Outline of Near-Neutral pH SCC Viable Crack Probability Model (26)

Once the input parameters have been determined and the empirical data collected, a lab program was developed. The goal of the lab program was to be able to identify factors which affected NNpHSCC initiation and early crack growth. In an attempt to model field conditions, several different electrolytes were considered from a range of solutions which simulated trapped water taken from SCC digs in Northern Ontario and Alberta.

Once the environment had been selected, the mechanical loading conditions needed to be determined. Pressure-time SCADA data from gas lines which were known to have NNpHSCC issues were analyzed using ASTM techniques for fatigue cycle counting. One of the significant issues with attempting to model a complex field pheonomenon like SCC is dealing with the large time periods needed to necessitate the initiation and growth of the features. King et al. (26) mention that in determining the mechanical loading conditions associated with NNpHSCC the strain rates experienced by linepipe are in the range of 10^{-10}-10^{-6} s^{-1}, whereas lab studies are typically run at 10^{-5} s^{-1}. The difference in strain rate and its effect on overall crack initiation and growth is understood for studying High-pH SCC; however, the same cannot necessarily be said for NNpHSCC.

The model proposed by King et al. (26) also identified several different types of linepipe steel in their program. The steels also had polished and mill scale finishes, determining if the potential oxide on the exterior of the steel had a significant effect on the initiation of NNpHSCC.

As can be seen, models have been developed using both in-field environmental data, as well as attempting to develop a model from laboratory results. Both of these approaches have benefits and drawbacks. The field model requires a significant amount of data in order to capture the appropriate factors which may affect the actual initiation and growth of NNpHSCC. The term 'correlation does not mean causation' often applies to these types of field programs; however, it is extremely difficult for lab programs to reproduce the actual field conditions which are pertinent to the occurrence of NNpHSCC. On the other hand, the laboratory programs are often very reproducible, and the large amount of control to the investigators working on the program allows them to isolate specific factors and potentially hone in on the crucial conditions much quicker. The goal of the work contained within this Master's project was to develop a computer model which could be fed actual pressure data as well as preliminary environmental data in an attempt to generate an estimate of crack growth rate (and potentially remaining life) for a given NNpHSCC feature in a given valve segment of pipeline. The approach was to utilize first principles and approaches which were validated in the laboratory and apply them to the actual field data to merge the two approaches.

3.0 Model Approach

The predictive model being developed utilizes fundamental understandings of NNpHSCC and then attempts to use field data such as SCADA data (internal pressure history) and the associated inspection dig reports to curve fit the various factors contained in experimentally derived equations. This approach applies to areas of the pipe surface where the integrity of the coating has failed (e.g. disbondments and holidays).

Laboratory data and trends are also included, which are used to determine initial dissolution rates, as well as describe the feature behavior under various loading and environmental conditions (i.e. corrosion fatigue). Before the details of the model are presented, the assumed stages of NNpHSCC will be discussed.

3.1 Typical Stages of NNpHSCC and the Governing Mechanisms in Each Stage

NNpHSCC is a complex process involving different stages in which various factors, both environmental and loading, have different effects. The first stage of cracking is the initiation of an extremely shallow crack. In pipeline steels this often occurs from the base of a corrosion pit, a heterogeneous interface in the material's microstructure or a superficial scratch. All of these features may have a slightly anodic condition relative to the base material, which allows for preferential corrosion of the region. While this may cause the initiation of the crack; the depth of the feature is not sufficient to create a stress intensity factor which would overcome the material's resistance to fracture. As the corrosion feature becomes deeper, the geometric constraint of the 'crack' is such that it may impede the progress of the corrosive species to enter the feature tip, which essentially slows the corrosion down. This phenomenon is depicted in Figure 28**.**

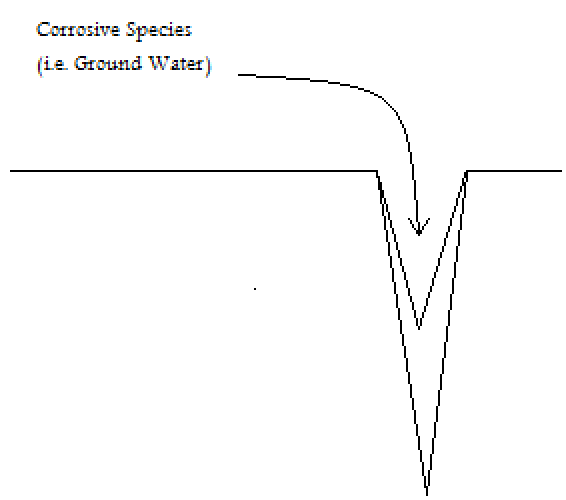

Figure 28 -- Geometric Constraint of Corrosive Species inside Corrosion Pit

The geometric constraint explained above can create a situation in which the initiated crack ends up not growing to a critical depth. If the critical depth is not reached, the crack essentially becomes dormant, unless loading conditions change to reactivate it (i.e. hydrostatic tests, operational upsets, etc.). This may explain why 95% of SCC in natural gas pipelines becomes dormant at a relatively shallow depth.

If the crack geometry reaches a critical state, the loading parameters will create a stress intensity at the crack tip which will then drive the crack growth. This phase of crack growth was titled the Mechanically Active phase. In the Mechanically Active phase, the crack growth rate due to the loading of the material significantly out-paces the growth rate attributed to dissolution. The growth rate of the crack during the Mechanically Active phase is dependent on not only the loading conditions, but also the amount of available atomic hydrogen, which will be explained in further detail in the following sections.

3.2 Growth Rate Governing Equations for Different Stages

In order to appropriately capture the different stages and their associated growth rates, different equations and approaches were required. For the Dissolution Controlled phase, both lab and field results were used to estimate a given dissolution behavior. The Mechanically Active stage was calculated using fundamental Fracture Mechanics equations, as well as work done by Chen and Sutherby (24). It should be noted that while the two stages of crack growth have been identified, the equations used to describe the Mechanically Active stage were applied to every cycle, regardless of the size of the crack. The reason for the differentiation of the two stages with regards to the calculation was that it took a significantly deeper crack for the fracture mechanics to have any meaningful contribution to the crack growth.

While it is nice to have a base dissolution rate for a given linepipe steel, the change in the dissolution rate as the aspect of the initial crack changes is just as important. In order to gather a starting point for this behavior, cracks found in the field were gathered and plotted as a function of their length vs. depth by Chen (27). The results of the work are shown below:

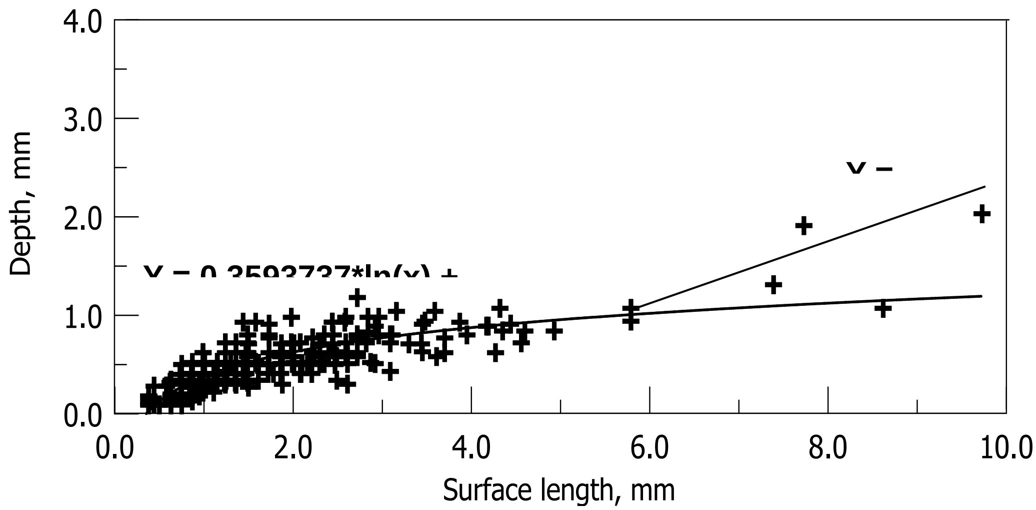

Figure 29 -- Plotted feature dimensions of field data (27)

The given aspect ratio determined from the field data presented by Chen (27) alludes to the dissolution behavior of the surface of the pipeline steel in service. It was proposed that the reason that the dissolution rate in the depth direction decreases due to the geometric constraint of the feature as mentioned previously. The discrepancy between the dissolution rates of the pit wall and tip being quantified, a dissolution function can now be applied to the early stages of feature growth. The inverse of the curve-fit equation above was used to describe a plausible dissolution behavior for corrosion pits which would lead to SCC initiation. The resulting dissolution rate behavior is shown below:

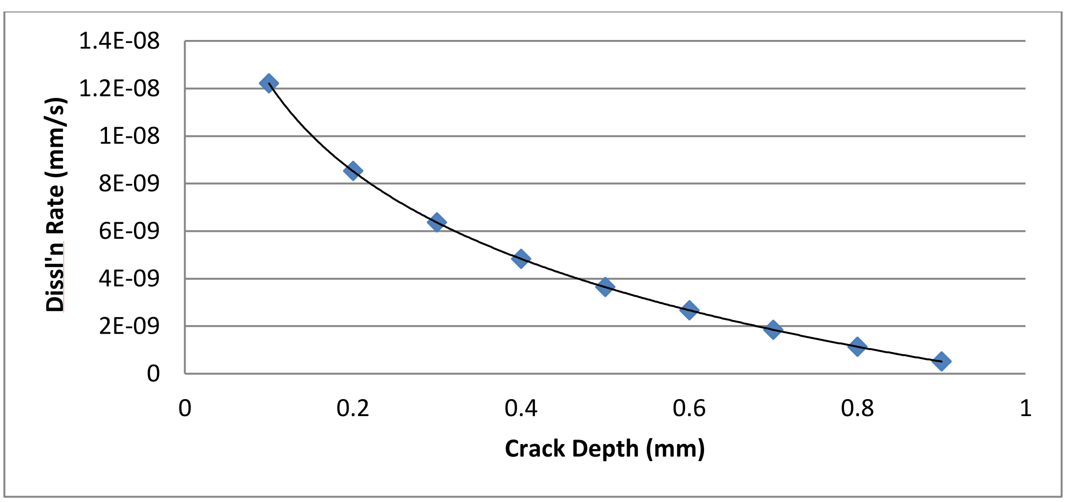

Figure 30 -- Dissolution Rate vs. Crack Depth

The behavior is simply the shape of the curve above; to converge on a quantified dissolution mechanism, two specific parameters can be varied to fit individual material / environmental combinations: the crack tip dissolution rate (i.e. the initial rate at which material is lost) and the threshold at which the dissolution rate drops off to zero. As was previously discussed a large percentage of Stress Corrosion Cracks become dormant at a depth around one (1) millimeter deep; therefore, the initial threshold which was chosen for crack dormancy was set to one millimeter. The initial dissolution rate which was picked as a starting point was given by the dissolution rate determined for typical line-pipe steel in a lab environment designed to simulate typical ground water (24). The overall severity of the dissolution controlled phase can be determined through further experimentation with different environments and materials, which will result in different threshold values and initial dissolution rates.

As mentioned before, once the initial crack depth exceeds the appropriate threshold depth it enters the Mechanically Active stage of growth. This stage is determined by a crack dimension such that the loading parameters act on the crack generating a Stress Intensity Factor which surpasses the material's resistance to crack growth. Whether this transition is generated by a specific environmental factor, such as seasonal wet and dry periods, or a change in loading parameters, such as a hydrostatic test or an operational upset, a very specific set of conditions are needed for the transition from the Dissolution Controlled stage to the Mechanically Active Stage. No specific equation was used to predict when or where this might happen, as the complexities involved with such a transition are too great to simulate in a lab.

Once the Mechanically Active stage begins, the fracture mechanics portion of the model begins to dominate the crack growth. Before discussing the effect of hydrogen embrittlement and its effect on NNpHSCC, the model's general approach to estimating the Stress Intensity Factor for a given crack morphology and load will be explained. The crack was modeled as a part-through crack in a flat plate. The equation for the geometric factor was taken from the Fracture Mechanics Textbook by T.L. Anderson (3). The geometric factor for the geometry used contained a function which was dependant on the crack depth, the aspect ratio, the width of the plate, as well as the position along the crack face. The equation used in the model can be seen in Figure 31**.**

TABLE A9.1

Stress-Intensity Solution for a Semielliptical Surface Flaw in a Flat Plate for $a \leq c$ [10].

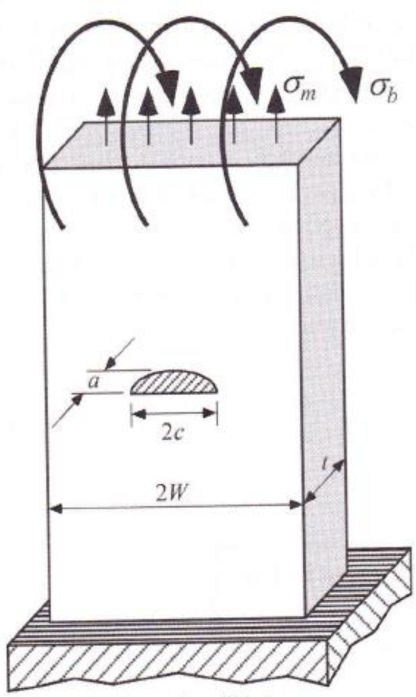

σ_m - Membrane (tensile) stress

σ_b - Bending stress

$$\sigma_b = \frac{Mt}{2I}$$

where

$$I = \frac{Wt^3}{6}$$

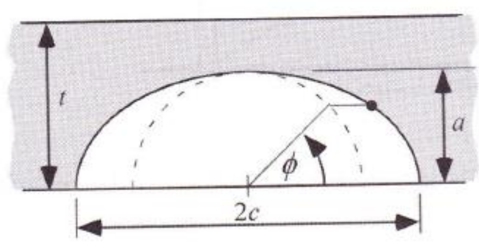

$$K_I = (\sigma_m + H\sigma_b)\sqrt{\frac{\pi a}{Q}}\,F\left(\frac{a}{t}, \frac{a}{c}, \frac{c}{W}, \phi\right)$$

where

$$Q = 1 + 1.464\left(\frac{a}{c}\right)^{1.65}$$

$$F = \left[M_1 + M_2\left(\frac{a}{t}\right)^2 + M_3\left(\frac{a}{t}\right)^4\right] f_\phi f_w g$$

$$M_1 = 1.13 - 0.09\left(\frac{a}{c}\right)$$

$$M_2 = -0.54 + \frac{0.89}{0.2 + \frac{a}{c}}$$

$$M_3 = 0.5 - \frac{1.0}{0.65 + \frac{a}{c}} + 14\left(1.0 - \frac{a}{c}\right)^{24}$$

$$f_\phi = \left[\left(\frac{a}{c}\right)^2 \cos^2\phi + \sin^2\phi\right]^{1/4}$$

$$f_w = \left[\sec\left(\frac{\pi c}{2W}\sqrt{\frac{a}{t}}\right)\right]^{1/2}$$

$$g = 1 + \left[0.1 + 0.35\left(\frac{a}{t}\right)^2\right](1 - \sin\phi)^2$$

$$H = H_1 + (H_2 - H_1)(\sin\phi)^p$$

$$p = 0.2 + \frac{a}{c} + 0.6\left(\frac{a}{t}\right)$$

$$H_1 = 1 - 0.34\frac{a}{t} - 0.11\frac{a}{c}\left(\frac{a}{t}\right)$$

$$H_2 = 1 + G_1\left(\frac{a}{t}\right) + G_2\left(\frac{a}{t}\right)^2$$

$$G_1 = -1.22 - 0.12\left(\frac{a}{c}\right)$$

$$G_2 = 0.55 - 1.05\left(\frac{a}{c}\right)^{0.75} + 0.47\left(\frac{a}{c}\right)^{1.5}$$

Figure 31 -- Geometric Factor for Crack Growth Model (3)

The SIF for both the maximum stress in the loading cycle and the minimum stress of the loading cycle was determined using the above equation. It should be noted that the SIF for only the maximum depth of the crack was calculated (Φ = 90°). The SIF for the surface of the pipe material was not considered, due to the fact that the aspect ratio was pre-determined along with the dissolution rates from data presented in Figure 29.

Once the maximum and minimum SIFs were determined, the Irwin approximation was used to get an effective crack depth and a subsequent effective SIF. The effective values were determined by using an iterative process as outlined when introducing the Irwin Approximation in Section 2 of the paper. Once the SIFs have been determined, the model logic is implemented.

The loading history is analyzed considering two competing mechanisms: hydrogen embrittlement and low-temperature creep. As previously discussed, while creep is normally seen at high temperatures, a low temperature variation of this phenomenon can be seen at the crack tip on the microscopic level. This low temperature creep can cause the crack tip to be blunted due to localized deformation under a constant stress level.

During unloading of the cracked material, the residual compressive stress at the crack tip pushes hydrogen out of the region. The chance of hydrogen embrittlement adversely affecting the steel decreases as the hydrogen is pushed out of the crack tip zone. The rate at which hydrogen is removed from the crack tip is dependent on the amount of stress reduction, and in turn, the amount of compressive stress produced in the plastic zone. The larger the unloading, the more hydrogen is removed from the crack tip. Low temperature creep is another on-going mechanism which affects the crack contribution of the various loading cycles. If the stress is high enough and held constant for a long enough time, the low temperature creep phenomenon can blunt the crack tip, as previously discussed. Taking these two effects into consideration, the loading history prior to each cycle is taken through the decision tree shown in Figure 32.

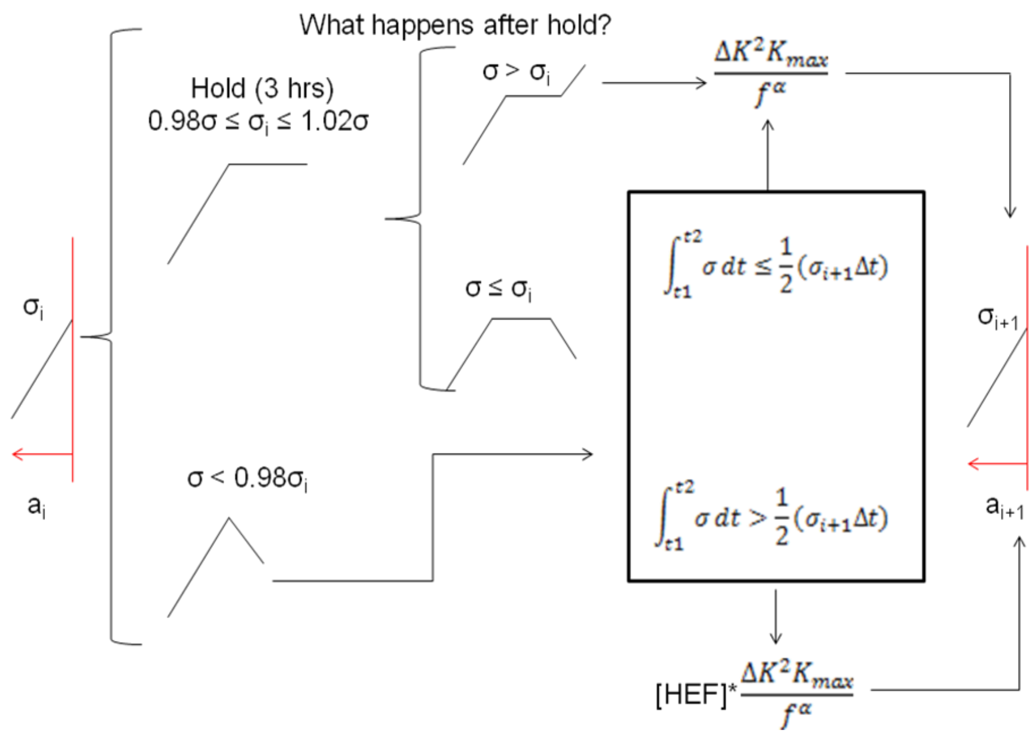

Figure 32 - Crack Model Decision Tree

The model takes a look at how the material has been prepared by the pipe's loading history. The state of the crack tip is estimated prior to calculating the crack growth contribution of the following cycle. The growth rate of the cycle on the right of Figure 32 will be calculated differently depending on the loading preceding it. Initially, the time in between loading cycles is considered, if the stress is held without any unloading, it is considered as one loading cycle and is not broken into individual cycles. Once the hold has been taken into consideration, a base rate equation provided by Chen and Sutherby (24) is used. The growth rate of a given loading pattern was determined using the following equation:

$$\frac{da}{dN} = A\left[\frac{\Delta K^{\alpha} K_{max}^{\beta}}{f^{\gamma}}\right]^{n}$$

Where *A*, *α*, *β*, *γ* and *n* were given constants, provided by an assumed curve fit based off of the work done by Chen and Sutherby **(24)**. These curve fits were done on a variety of materials in a series of different environments; however, these material / environment combinations do not span even close to the entirety of what is present in the field with the wide range of environmental and materials currently in service. For this specific work, the following values were assumed:

- *A:* 0.79 x 10^{-7}
- α: 0.667
- β: 0.333
- *γ:* 0.033
- *n:* 3.45

One component which affects the crack growth rate contribution is the Hydrogen Enhancement Factor (HEF). The HEF attempts to model the migration of atomic hydrogen in and out of the crack tip zone due the amount of loading and unloading between cycles. In order to determine the relative HEF for a give cycle, the area under the loading curve is compared to a reference area. A theoretical loading scenario and comparison can be seen in Figure 33.

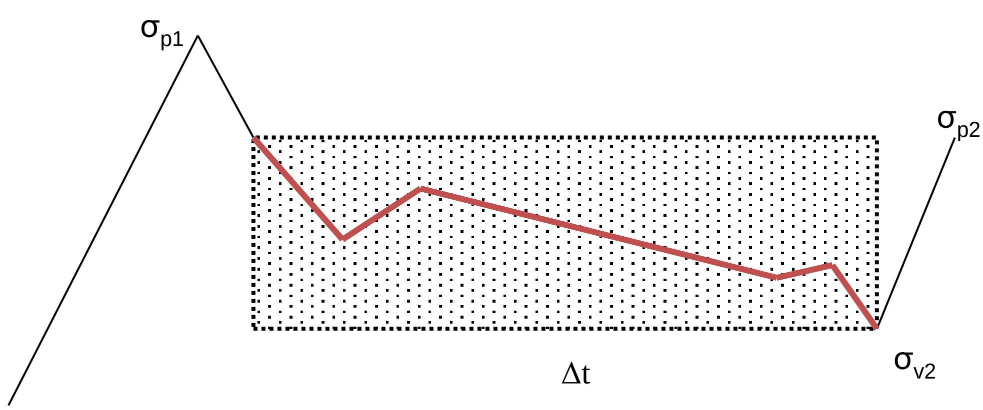

Figure 33 -- Area Under Highlighted Curve is Compared to the Reference Area (shaded box)

Initial criteria for the HEF's and their resulting value can be seen in Table 6**.**

Table 6 -- Initial HEF Criteria

Condition	HEF
$\int_{t1}^{t2} \sigma \, dt > 0.5(\sigma_{i+1}\Delta t)$	1.05
$\int_{t1}^{t2} \sigma \, dt > 0.6(\sigma_{i+1}\Delta t)$	1.10
$\int_{t1}^{t2} \sigma \, dt > 0.7(\sigma_{i+1}\Delta t)$	1.15
$\int_{t1}^{t2} \sigma \, dt > 0.8(\sigma_{i+1}\Delta t)$	1.20
$\int_{t1}^{t2} \sigma \, dt > 0.9(\sigma_{i+1}\Delta t)$	1.25

The values of relative comparison and given HEF's were initially chosen as place-holders. The act of comparing the actual loading condition to the reference area is attempting to capture how hydrogen may move in and out of the crack tip region. As the material is loaded, the material lattice is stretched, allowing for more hydrogen to enter the crack tip region. On the opposite side, unloading the material places the crack tip in relative compressive stress, which pushes the hydrogen out of the crack tip, allowing less hydrogen to be active in the HE process. To summarize, the larger the area under the actual loading profile is to the reference area, the more hydrogen is available to the crack tip for HE. More research is required to match the HEF with actual growth rates seen in the lab and in the field. The HEF can also be modified to generate a 'worst-case scenario' growth rate, which from discussion with various engineers in the industry would give a rate of 0.3 mm / year in the depth direction. A sensitivity analysis with the HEF will be shown in Section 5.3 in order to illustrate how vital this component is in future development of the model.

The incremental crack growth from the analyzed cycle is then determined and added to the total growth at that point. The new crack dimensions are taken and applied to the next loading cycle, and the model logic starts from the beginning again.

3.3 Considerations for Random Pressure Fluctuations

Due to the fact that real-life pressure data does not meet the typical pressure fluctuation pattern seen in a laboratory, the real-life fluctuations were categorized based upon different factors. All of the sets of data had a small amount of 'noise' or scatter associated with it, as seen in Figure 34. In order to analyze the data for fatigue cycles, this noise needs to be cleaned up somehow. In order to achieve this, a smoothing algorithm was applied. This algorithm measured the difference between data points and compared it to a threshold value. If the difference was less than the pre-determined threshold, then the local maxima/minima was smoothed out. If the difference was greater than the threshold, the maxima/minima was then included in the smoothed data. The value of this pre-determined threshold will also be analyzed in the Sensitivity Analysis in Section 5.3. The output of this algorithm was the absolute value of the smoothed maxima and minima, as well as the time at which they occurred. The relative smoothed data compared to actual data can also be seen in Figure 34**.** The circles in the figure represent local maxima values, whereas the squares represent local minima values.

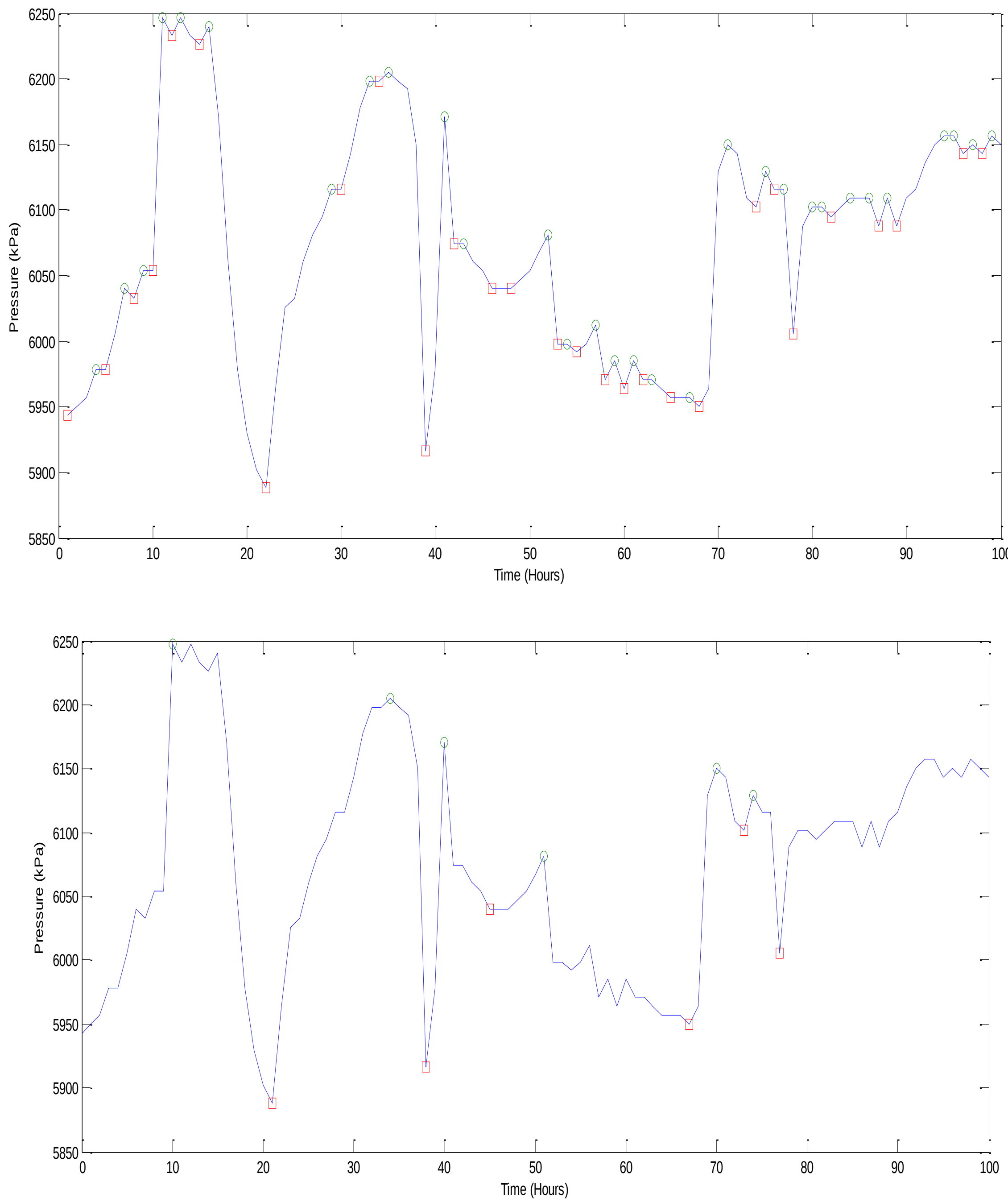

Figure 34 -- Absolute Maxima/Minima (top) vs. Smoothed Maxima/Minima (bottom)

The algorithm for removing the noise in the data was taken from Eli Billauer on a Matlab community site, and was explicitly not copyrighted. A copy of the code is included in Appenix A It should be noted that this method of smoothing only dealt with loading cycles which were insignificantly small. Some data sets may also have errors and irregular loading which may be an artifact of the collection system. These were not explicitly dealt with at the time of the work, and may perhaps affect the field result validation, as shown later.

Once the SCADA data has been smoothed, each maxima / minima pair is taken and used in the model logic described in the previous section.

3.4 Overall Predicted Crack Growth Curves

In order to illustrate the interaction of the two growth stages of NNpHSCC, initial runs of the model are shown in Figure 35. For the runs there was an assumed crack tip depth of 0.1 mm. For the plot, a wall thickness of 9.14 mm was used, as well as a NPS 36 size pipe (outside diameter of 914.4mm).

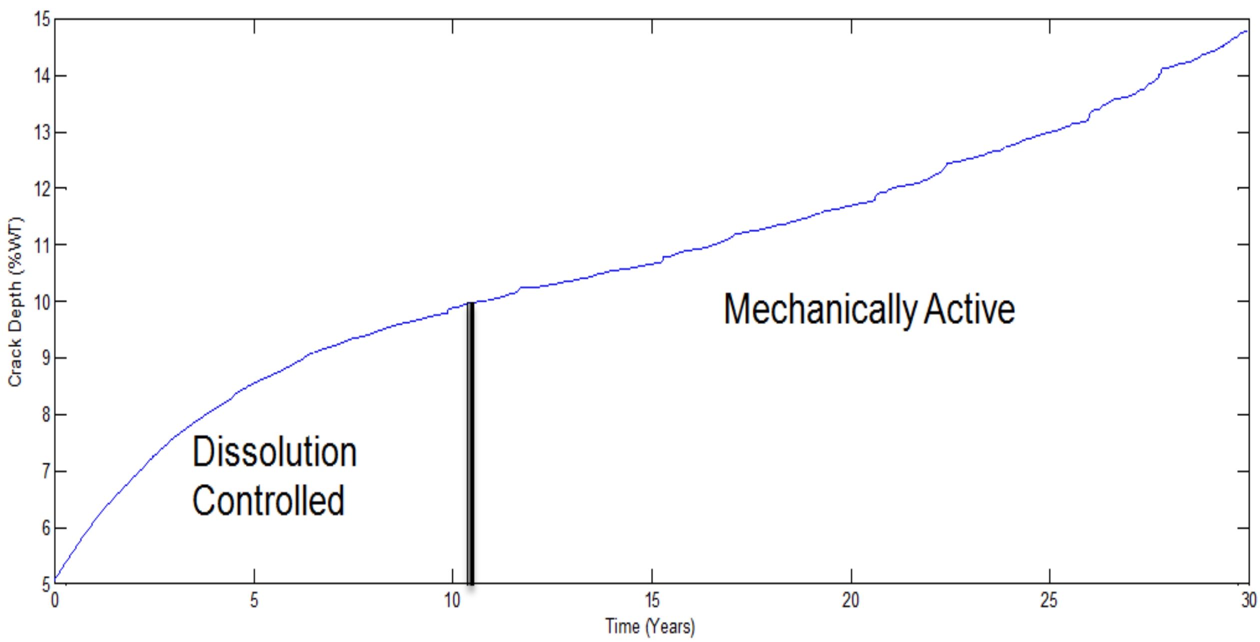

Figure 35 -- Typical Results of Program Run, a_0 = 0.1 mm

Another illustration of the mechanical contribution against the dissolution contribution can be seen in Figure 36.

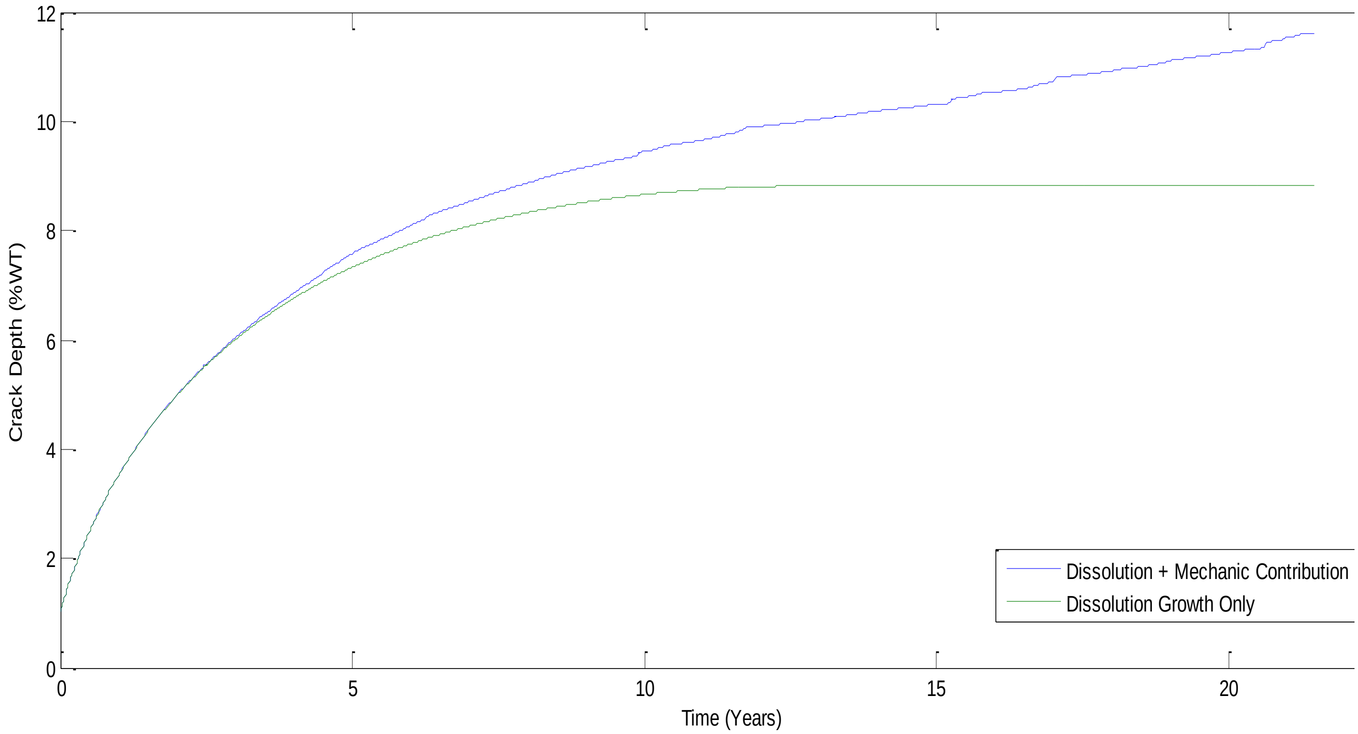

Figure 36 -- Dissolution and Mechanical Contribution Comparison

An important note regarding the typical data trend is that the initial crack / pit depth was 0.1 mm. Normally in the field these features are barely detectable, and do not cause problems with regard to pipe integrity. When a larger initial crack depth was assumed, there code generated an error in which the Irwin approximation for the plastic zone did not converge quickly enough, leading to the effective plastic zone becoming larger than the pipe wall thickness for cracks which would not typically cause any significant integrity concerns.

When the Irwin approximation iteration step in the model is removed, the following growth rates can be seen below:

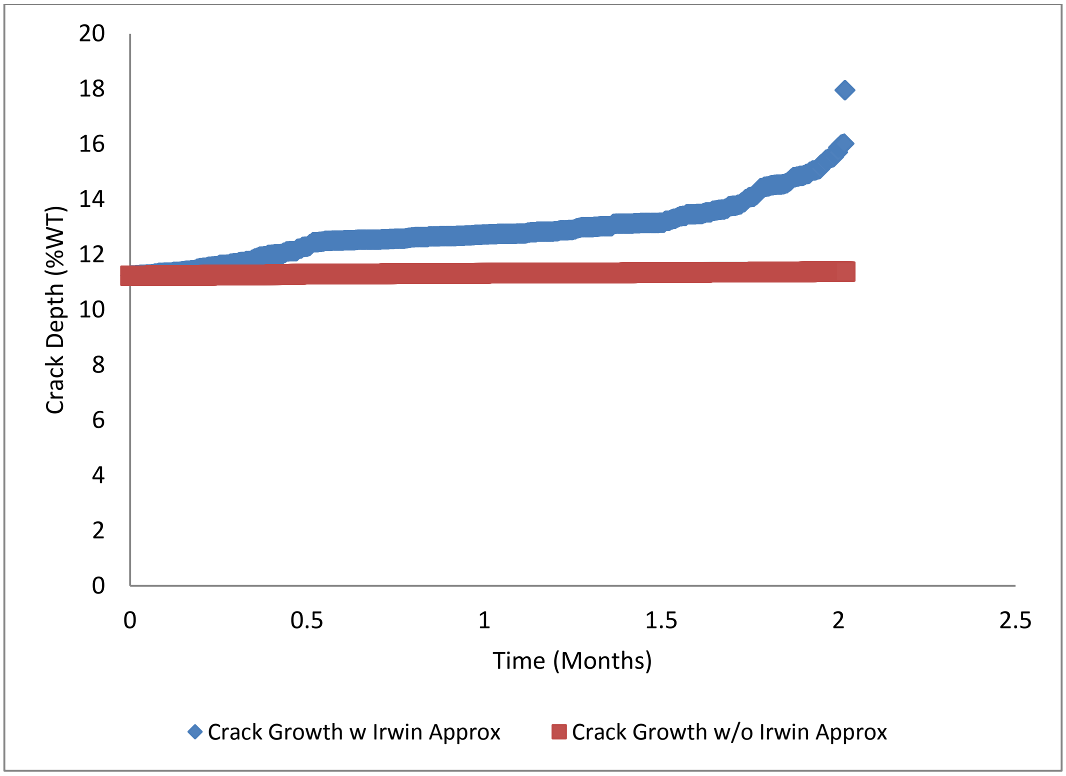

Figure 37 -- Effect of Irwin Approximation on Crack Growth

As can be seen, at the end of the growth with the Irwin Approximation applied, the crack depth nearly asymptotes directly vertical after only two months of growth. Without the approximation utilized, the crack depth remains virtually constant. For the remainder of the work, the Irwin Approximation was taken out of the program to ensure that all of the data and trending had the least amount of unexplained error as possible.

This run shown in Figure 35 displays the theoretical approach described previously. In order to gather twenty five years' worth of data, the loading histories were cut and pasted together. Unfortunately, this action creates an artificially high ΔK for a few loading cycles, which can be seen in the later stages of the mechanically active growth period. Even with the artificial 'jumps' in the growth rate, there still appears to be a significantly slow growth rate over the large time scale (until the Irwin Approximation error drives the growth rate vertical). This slow growth rate can be explained by either the Dissolution Controlled portion or the Mechanically Active portion. Due to the fact that the dissolution controlled portion is obtained from field data, there is more confidence in the parameters used to describe its behavior. In an attempt to explain the growth rate dependence on the mechanically active section, a series of sensitivity analyses were performed in Section 5.

4.0 Data Collection / SCADA Analysis

During this project, time was spent at the head offices of TransCanada Pipelines (TCPL) and Spectra Energy Limited (SEL). The focus of the time was to gather information regarding the field occurrences of SCC. This information included both failure information as well as integrity excavation reports. There were a total of 93 dig reports received from SEL, and a dig database from TCPL which contained a total of 31 digs. All of the information provided was for the lines and valve sections of which SCADA data (loading history) was provided. There was also a total of 40 additional failure records provided, which included in-service ruptures, leaks, and hydrostatic test failures.

4.1 Historical Information on the Pipelines

Before looking at the pressure fluctuations in each pipe segment, the history of each section was considered, looking at the historical dig findings and failures, if applicable. While SCADA data was collected for five different pipeline segments, the failure database covered all failures system wide, not just for the lines and valve segments where SCADA was provided. The theory behind the additional data collection was to attempt to curve fit any environmental conditions (e.g. topography, coating type, coating condition, etc.) to see if a specific set of conditions had a quantifiable effect on the presence and severity of NNpHSCC.

There were a total of five lines between TCPL and SEL which had both the SCADA and integrity dig data provided. They have been given representative letters in the table below and their generic static data provided. It should be noted that these values were taken to be the worst case scenario (i.e. highest operating pressure as a percentage of the SMYS under non-high performance coating, such as Fusion Bonded Epoxy).

Table 7-- Pipe Segment Static Information

Segment "Name"	Outer Diameter [mm]	Nominal Wall Thickness [mm]	Grade [MPa]	Maximum Operating Pressure [kPa]	% SMYS	Const. Year
A	914.4	9.9	414	6454	71.99%	1971
B	914.4	9.9	414	6454	71.99%	1970
C	914.4	9.9	414	6454	71.99%	1970
D	914.4	8.9	448	6280	72.01%	1980
E	762	8.35	448	7067	71.98%	1982

One key item to note from the data set above is that none of the data is from a vintage of pipe which is older than the 1970's. This could potentially be due to the fact that the highest susceptibility of SCC appears to come from segments poorly coated with polyethylene tape, which was the primary coating type during this time frame. Along with the vintage of pipe, there is no complete data from lower strength pipe, such as Grade 359, or from higher grade pipe, such as Grade 483. It was previously mentioned that hydrogen embrittlement has been shown to be more active in higher strength steels; however, the higher strength steels have been around for a much shorter time than other grades, and have been most often coated with high performance coating.

There was discussion during the data collection stage of the project as to gathering data from some different selections with an older vintage of pipe, as well as potentially slightly higher operating pressures with regards to % SMYS; however, these segments had many manual tie-overs between more than two lines, so the pressure within a given stretch of pipe could not be confidently estimated from the compressor station discharge pressure.

When looking at the failure database, there have been no in-service failures on the 5 segments due to SCC. There was 1 hydrostatic test failure due to SCC experienced on Segment C back in 2006. It should be noted that this SCC was found in the toe of the seam weld, which is not specifically what this model is looking at. The toe of the weld often has different metallurgical properties which affect crack initiation and propagation, not to mention the disposition to coating disbondment at this specific location. It is interesting to note that there have not been as many failures experienced as on other lines in different systems; this may be a function of the construction year being relatively recent.

With the history of the different pipeline segements considered from the failure database and static data, the pressure fluctuation information needs to be considered for input into the predictive model.

4.2 Pressure Fluctuation Characteristics of the Pipelines

The pressure fluctuations within the given pipeline segments is a key factor for the predictive model in determining a predicted overall crack growth rate. Each segment has unique loading spectrums, and this section will discuss these spectrums in further detail.

Before discussing the pressure fluctuation characteristics of the specific pipe segments, an assumption regarding the data collection must first be noted. Due to the fact that loading histories were obtained only from the discharge of upstream compressor stations, the specific pressure amplitude at a given site could not be determined unless elevation information was provided. While the exact amplitude of the stress experienced by the pipe at a certain level could not be ascertained, the relative loading waveforms could be which was the primary focus on the preliminary development of the model. For application to results found in the ditch, a hydraulic elevation calculation can be used to determine the magnitude of the stresses that a particular joint of pipe may see. Another comment regarding the loading histories is that the loading profile was assumed to be an accurate snapshot of the entire life of the pipeline, which may not be the case; however, there is no additional data which could be gathered to determine whether or not this was true. With this assumption in mind, the pressure fluctuation characteristics were attempted to be characterized from the SCADA data collected.

SCADA data was collected from two different companies for five different pipeline sections. Of the five sections, four were known to have SCC present and one did not have a history of SCC. Two of the data sets measured the internal pressure at the compressor station every hour; whereas the other three data sets were measured any time that the pressure changed. All of the data sets were pulled from “bullet lines” – that is, they were single lines that were not looped; therefore, the pressure read in the compressor station could not have been tied into other lines further down the system (such as 'looped' lines). A summary of the amount of data gathered can be seen in Table 8.

Table 8-- SCADA Data Collected

Company	# of Segments	Density	Amount of Data
TCPL	4	Hourly	5 & 10 years
SEL	3	3 minute	1 year
SEL		Hourly	3 years

The data came from two TCPL lines (one segment per line) and 1 line from SEL (three segments within this line). Initially, there was a discussion as to what value minute data provided concerning the loading condition. Loading and unloading of a natural gas pipeline takes a significant amount of time (in the magnitude of hours) due to the compressibility of the service fluid. This is why rupture sites may burn for several hours, even though the valve section has been isolated. The relative slow loading cycles can be captured by the hourly data; therefore, minute density data is not required for this modeling effort.

The pressure fluctuation characteristics of the five segments in question are shown in Table 9. These loading characteristics are captured from the predictive model, and are dependent on the threshold of the maxima / minima detection script. For the sake of this section, this threshold was given as 25 kPa.

Table 9 -- Pressure Fluctuation Characteristics of Given Pipeline Segments

Segment "Name"	σ_{max}		R-Ratio			Frequency (1/s)		
	[MPa]	[% SMYS]	Max	Min	Avg.	Max	Min	Avg.
A	408	98.6%	0.9969	0.823	0.9698	1.39E-04	2.17E-06	4.37E-05
B	Error							
C	393	94.9%	0.9966	0.7338	0.9835	1.39E-04	4.87E-07	3.96E-05
D	433	96.7%	0.9968	0.3975	0.9786	1.39E-04	3.46E-07	3.97E-05
E	Error							

The two errors found in determining these characteristics are due problems with the model handling some of the input data, which is further explained in the Results and Discussion section of this work.

From the data presented, it can be seen that the majority of these pressure fluctuations are relatively small in amplitude, as is the case for natural gas transmission operation. None of the loading parameters appear to meet 100% SMYS when assuming a residual stress of 110 MPa, as discussed in Van Boven et al.'s work (28), although it does come close.

Although minimum frequencies do range a significant amount, the average frequencies for the various segments appear to be close to 4 x 10^{-5}, which equates to about one cycle every seven (7) hours or so. This would mean that on average, the pipe segment experiences approximately 1250 cycles per year, and therefore it would take 799 years for the pipeline segment to experience a million small scale cycles. As discussed previously, these small scale cycles would not be enough to cause problems in the absence of an aggressive environment.

4.3 SCC Characteristics of Pipelines Being Considered

While the data collected during integrity digs is often very extensive, the indications of a specific growth rate can only be estimated from indirect methods, rather than studying an individual feature during its lifetime. Before looking at the field data collected, it should be noted that all of the segments where the inspections have occurred are coated with Polyethylene tape. A summary of the five segments and the pertinent SCC data is shown below:

Table 10 -- SCC Data from Digs on Each of the Five Pipeline Segments

Segment "Name"	Number of SCC Integrity Digs	Number of SCC Colonies Found	Number of Digs with Significant SCC Found	% of Digs with Significant SCC	Deepest Colony Found
A	61	5210	14	23	30.30%
B	1	80	0	0	< 5%
C	36	2154	7	19	38.40%
D	23	803	4	17	53.93%
E	7	388	1	14	43.26%

The number of SCC integrity digs and colonies found is important; they determine where environmental models have found SCC during the process of implementing investigative digs. It may also represent a relative level of SCC in one section compared to another. The model focuses on the crack growth due to varying loading conditions; therefore, the most severe SCC would exist in the mechanically active region, which poses a real integrity threat, as opposed to dormant cracks which are shallower than approximately 10% of the wall thickness. The presence of "significant" cracks represents a scenario in which more than the loading condition creates a susceptibility to SCC. The coating condition, topography, soil drainage, soil type, and many others must be present in order for cracks to grow to a significant state. To just have a single instance of the perfect storm does not necessarily make an entire segment susceptible to SCC. In order to compare the segments to each other, a certain percentage of digs should contain significant SCC colonies in order to be deemed susceptible. Based on the data presented in Table 10, the percentage of significant SCC found per integrity dig is fairly close for all segments except for Segment B. While this percentage may be relatively close, there may not have been enough digs performed on Segment E to validate the susceptibility. For this reason it was deemed that Segments A, C and D were the most susceptible out of the group of five.

At the time of the data collection, Electro-Magnetic Acoustic Transducer (EMAT) In-line Inspection (ILI) tools had not been used as extensively as they are today; therefore, the majority of the SCC digs were picked based off of environmental factors and known history of SCC on these specific valve segments. The focus of SCC digs can lend us to believe that some segments were given a higher susceptibility by the operators than others. This selection process was based off of many years of industry experience, and should not be discounted when talking about a segment's susceptibility.

5.0 Results and Discussion of the Predictions

The outputs of the predictive model were generated for the different loading conditions of the different pipeline segments. There was also work done to look at the model's sensitivity to various variables, such as the HEF, threshold for maxima / minima selection, the initial crack depth as well as others. This work is explained in the sections below.

5.1 Predicted Crack Growth Curves for Various Pipeline Segments

In order to compare the various loading conditions of the different pipeline segments, the predicted crack growth curves were plotted for each segment. The resulting plot can be seen in Figure 38. Due to the fact that each segment has a different overall time period, the crack growth rate per year is utilized as the comparative variable when looking at each segment's susceptibility.

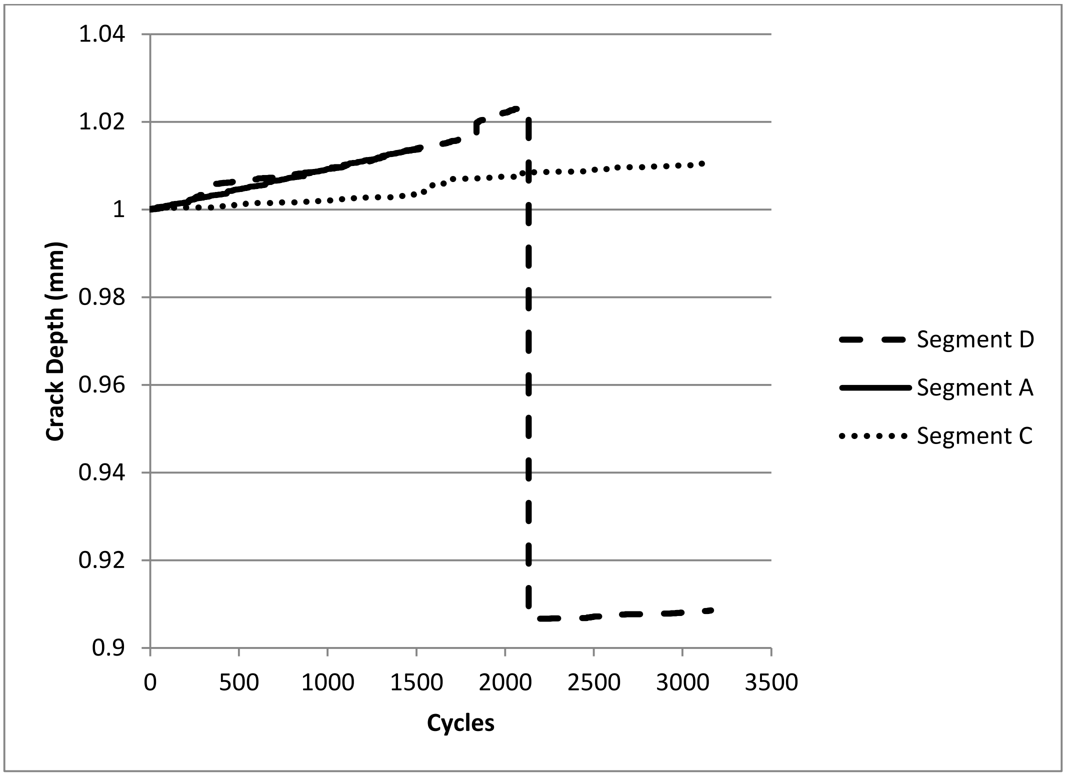

Figure 38 -- Predicted Crack Growth Curves for Various Segments

Only Segments A, C and D were plotted with the given predicted crack growth curves. This is due to the fact that both Segments B and E had errors in running the predictive model. These errors speak to the model's ability to take in various loading cycles which may have a series of odd data trends. An example of one of these trends which was found with the segments was a period over several months when the pressure did not vary by a single kilopascal. This lack of variation is not possible during operation; even with segments isolated there is slight variation due to temperature changes.

Looking at the data shown in Figure 38 also shows a negative crack growth rate in Segment D. This obviously is not an actual crack growth rate, but rather an artifact of the predictive model. While this artificial crack growth rate does exist, it appears to only occur over one specific loading cycle. In an attempt to decipher why this negative crack growth rate occurred, the loading profile of this segment was plotted.

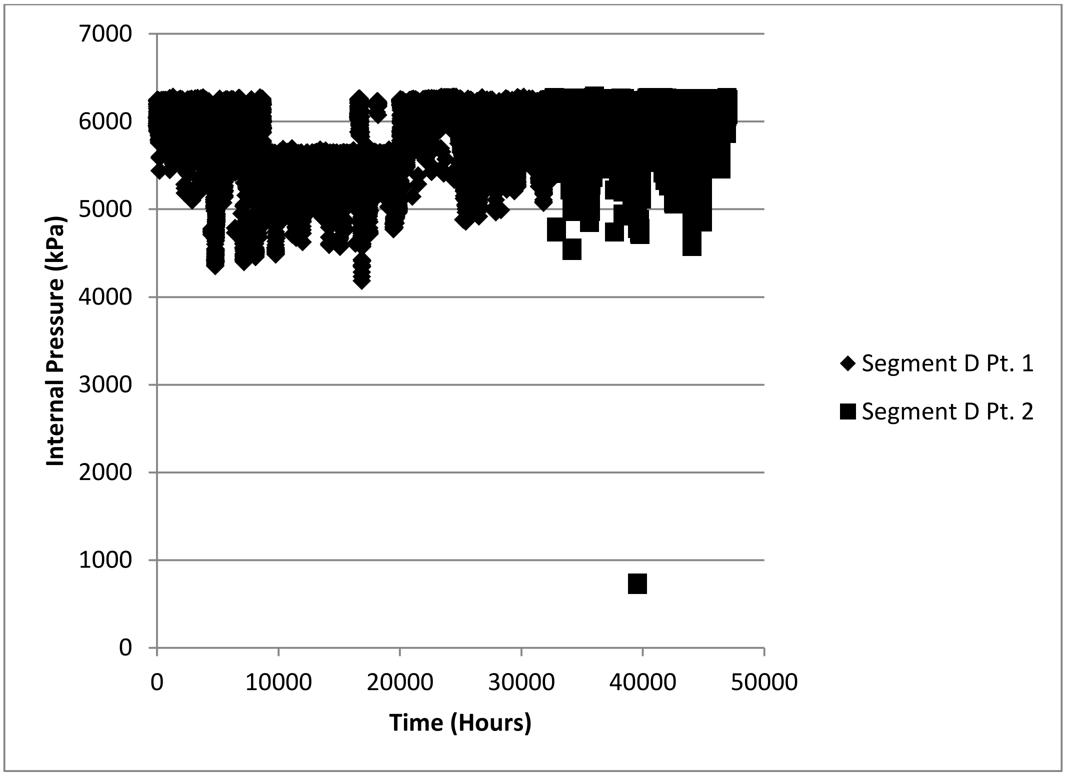

Figure 39 -- Loading History of Segment D

The loading history of Segment D was broken down into two sections in order to work past an Excel limitation of 32000 data points per a two dimensional plot. Although there does appear to be one low reading, it does not seem to make sense that this low reading would create a negative crack growth rate. The time data was also reviewed and all of the cumulative hours were successive with no reversals present; therefore, the frequency would never be negative. A line of code was added to the program to alert the user of a negative frequency via an error statement. While running Segment D's data through the predictive model, this error message did not appear. Further work is required in order to explain the single cycle anomaly present in the data.

The resulting amounts of crack growth for each segment were collected and tabulated in Table 11. The single negative growth cycle in Segment D was removed and the two periods of positive growth were taken and added together to get a comparative value.

Table 11 – Predicted Crack Growth Rates for Different Pipeline Segments

Segment 'Name'	Growth (mm)	Time (year)	Growth Rate (mm/yr)
A	0.0137	3.98	0.0034
C	0.0106	5.30	0.0020
D	0.13977	5.33	0.0262

Two main conclusions can be drawn from the data presented above: first, the crack growth rates are extremely slow. This discrepancy can be explained by adjust the HEF and other loading variables accordingly as outlined in Section 5.2. The second conclusion is that there is a wide variability between growth rates, as Segment D is an order of magnitude larger than the other two segments. The validity of this result will be discussed further during the correlation of field data in Section 5.3.

5.2 Sensitivity Study

A sensitivity study was done on several different variables being input into the model. This includes the Local Maxima / Minima Detection Threshold (the minimum required ΔP required for a cycle to be analyzed), different HEF values, different initial crack sizes and different loading conditions (the SCADA data input).

During the various sensitivity analyses, Segment D will be used as the base information (NPS 36 x 8.9 mm, Grade 448, as well as the associated loading profile). The rest of the inputs are shown in Table 12, unless otherwise specified.

Table 12 - Sensitivty Analysis Inputs

Assumed Initial Crack Depth (mm)	3
Initial Dissolution Rate (mm/s)	5.93E-09
Dissolution drops of to zero at:	1 mm depth
HEF Values	See Table 6 (reference HEF)
Assumed Residual Stress (MPa)	110
A	7.90E-08
n	3.45
Alpha	0.667
Beta	0.333
Gamma	0.033
Local Maxima Detection Threshold (kPa)	25
Length of SCADA profile (Years)	5.33

The first variable to be analyzed is the threshold change in pressure which determines whether a pressure cycle will be analyzed as a fatigue cycle in the model. The initial base assumption was 25 kPa; however, there was no significance to this reason. Different values of 25, 250, 500, 1000, and 3000kPa were used and the resulting crack growth plotted. The results of the sensitivity analysis can be seen in Figure 40.

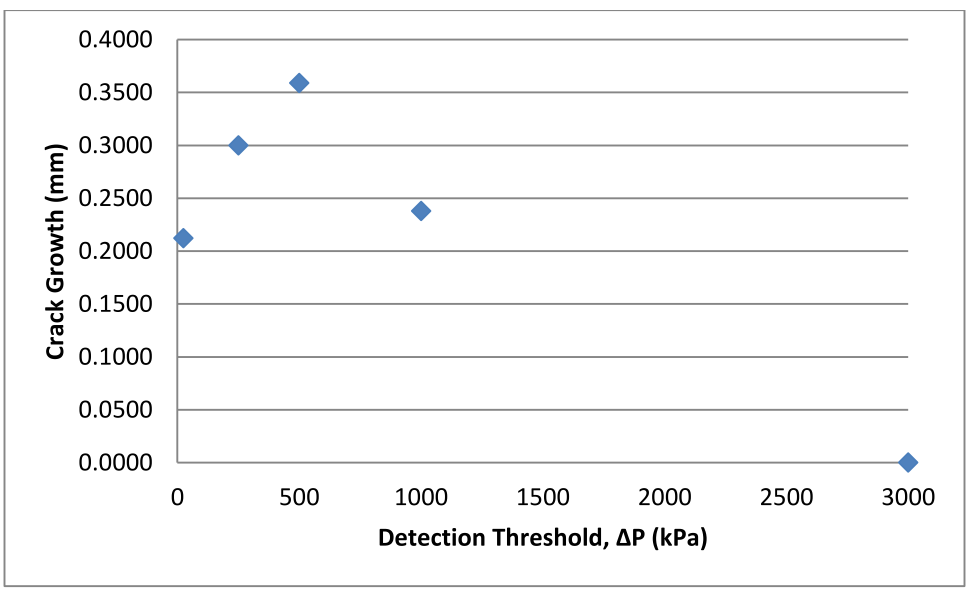

Figure 40 -- Crack Growth Sensitivity on Detection Threshold

As can be seen above, none of the calculated crack growth rates reach the field value of 0.3 mm / year. It appears that if the change in pressure is too small, the accumulated stress intensity change is not high enough to generate crack growth. On the other extreme, if the threshold value is too high (i.e. 3000kPa) there are not enough cycles present to have any growth at all. The threshold values may change slightly depending on which SCADA profile is analyzed, and this exercise will be repeated with the different loading profiles when the profiles themselves are looked at.

The second variable to be analyzed was the HEF. The HEF was varied by different factors and the resulting crack growth rate was plotted in Figure 41. It should be noted that although the most severe detection threshold was noted to be 500 kPa in the previous analysis, the threshold was kept at 25 kPa just to remain consistent. The most severe case will be presented at the end of the section once the rest of the sensitivity analyses are completed.

Table 13 -- HEF Sensitivity Input and Results

Condition (% reference Area)	HEF 1	HEF 2	HEF 3	HEF 4	HEF 5
50-60	1.25	5.00	12.50	25.00	62.50
60-70	1.50	6.00	15.00	30.00	75.00
70-80	1.75	7.00	17.50	35.00	87.50
80-90	2.00	8.00	20.00	40.00	100.00
90-100	2.25	9.00	22.50	45.00	112.50
Factor of Base Level	1.00	4.00	10.00	20.00	50.00
Growth (mm)	**0.2159**	**0.2881**	**0.4447**	**0.7514**	**2.3958**

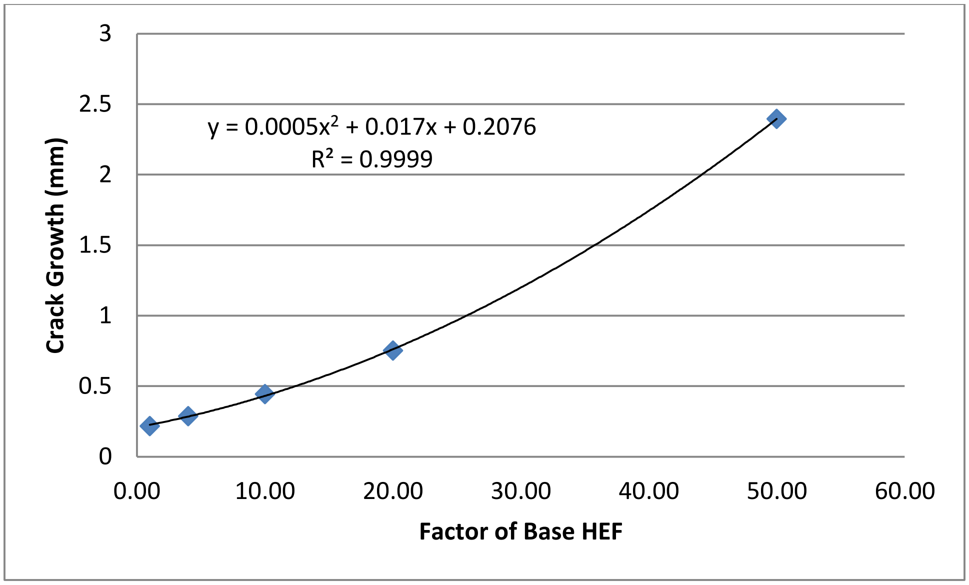

Figure 41 -- HEF Sensitivity Analysis

The sensitivity was fit with a second order polynomial, which yielded the best fit of the regression lines applied. The growth rate does not scale linearly with the HEF, which makes sense. The increasing crack size creates a larger delta K, which in turn increases the effect of the HEF. With the last set of HEF values, the predicted growth exceeded the worst case scenario as seen in the field, so in order for the model to be somewhat realistic, the values would have to be reduced somewhere between HEF 4 and HEF 5 in Table 13.

From talking with various engineers in the industry the most severe SCC growth rates average 0.3 mm / year in the depth dimension. The growth in the length direction is not as heavily weighted, due to the fact that the predicted rupture pressure of a given Stress Corrosion Crack is more heavily dependent on its depth, rather than its length. Considering that a loading profile over five years was given, it was assumed that this was a significant 'snap shot' of time which a growth rate of 0.3 mm / year could be used as a target to fine tune a general HEF for a loading parameter.

When the initial crack depth is changed, the following growth rates are observed:

Table 14 -- Initial Crack Depth Sensitivity

a_0 (mm)	Growth (mm)
1	0.0215
2	0.0830
3	0.2121
4	0.4782
5	1.0383
6	2.2382

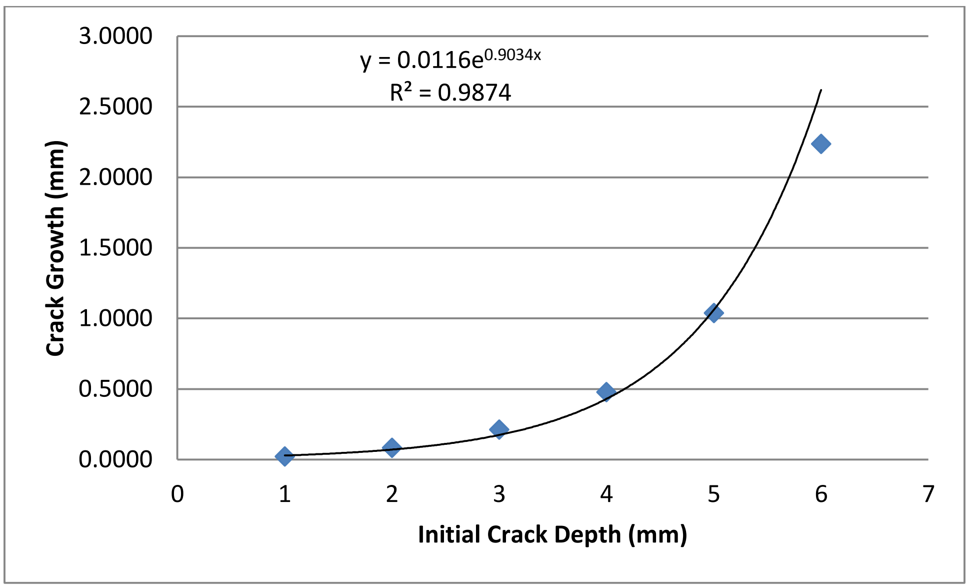

Figure 42 -- Initial Crack Depth Sensitivity

As the initial crack depth increases, so does the growth rate. This trend appears to follow a near exponential regression. The trend makes sense, seeing as when the crack is larger, the SIFs associated with it increase significantly; thereby increasing crack growth and making the resulting crack for the next iteration that much larger. As the crack reaches near through-wall, the model may become less accurate, due to the fact that the boundary conditions of the inner surface of the plate are not explicitly considered.

When the different loading profiles are compared to each other, their respective static data (i.e. wall thickness, pipe diameter, grade of steel) will change to suit the appropriate loading parameters. Each data set was run through the model and their respective crack growths are plotted against each other. Due to the fact that the various loading histories vary in time, the shorter timelines were stitched together to get the appropriate length of time. The alternative to this would be to attempt to normalize the data and derive a growth rate in millimeters per year. The issue with the attempted normalization is that as previously shown; an increase in initial crack depth exponentially increases the relative growth. The stitching of the SCADA histories may create a relatively large artificial cycle; however, the growth attributed to that cycle will most likely have less of an effect than comparing the results of the crack growth over different time periods.

Table 15-- SCADA Input Sensitivity

Segment "Name"	Predicted Growth (mm)
A	0.1254
B	ERROR
C	0.0965
D	0.2121
E	ERROR

As can be seen from the table above, there is an issue in the program depending on the input data itself. Both errors appear to come from an array not writing in a logical form into a logic equation for these two SCADA sets. The error message for both of these runs is ‘Subscript indices must either be real positive integers or logicals’. If we take out the error runs for the time being and look at the remaining data sets, none of the sets create a crack growth which comes close to the worst case scenario as seen in the field (i.e. 0.3 mm / year). In an attempt to look further into the sensitivity of the varying loading histories, the worst case scenario maxima detection threshold and an HEF generating a growth similar to 0.3 mm / year (20 times the base factor used in the original HEF sensitivity analysis) was used and applied to the remaining three loading histories. The results of the analysis can be seen in Table 16.

Table 16 -- Loading Profile Sensitivity with Various Delta P and HEF

Segment "Name"	Outer Diameter [mm]	Nominal Wall Thickness (mm) [mm]	Grade [MPa]	Maximum Operating Pressure [kPa]	% SMYS	Const. Year	Growth for Base Scenario (mm) [mm]	Growth with Delta P = 500kPa, no change to HEF [mm]	Growth with Delta P = 500 kPa, HEF 3 [mm]
A	914.4	9.9	414	6454	71.99%	1971	0.1254	0.2283	2.8518
B	914.4	9.9	414	6454	71.99%	1970	ERROR	ERROR	ERROR
C	914.4	9.9	414	6454	71.99%	1970	0.0965	0.1160	0.1338
D	914.4	8.9	448	6280	72.01%	1980	0.2121	0.3588	1.8060
E	762	8.35	448	7067	71.98%	1982	ERROR	ERROR	ERROR

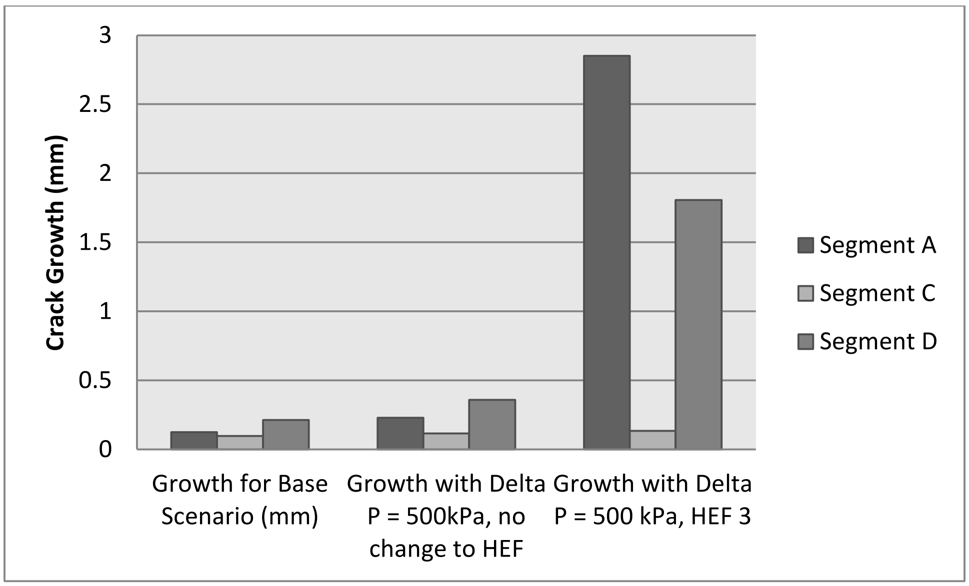

Figure 43 -- Loading Profile Sensitivity with Various Delta P and HEF

As can be seen above, the change in the local maxima detection threshold (delta P) does not change the order of severity in growth between the three data sets; however, when the HEF is increased, the SCC growth severity ranking does change. Depending on the loading history, it may be possible to have the severity ranking change with a change in Delta P; however, it did not occur with the given data sets. What can be hypothesized about the loading histories for Segments A and D is that Segment A had more severe cycling, which caused the change in HEF to have a greater influence on the overall crack growth compared to Segment D's loading history. It should also be noted that due to the fact that the HEF may vary from not only segment to segment, but even from location to location within a given segment, that a different HEF for each segment may be required to obtain realistic results.

Another sensitivity analysis was performed regarding the Delta P variable on a different loading history. The results are shown in Figure 44.

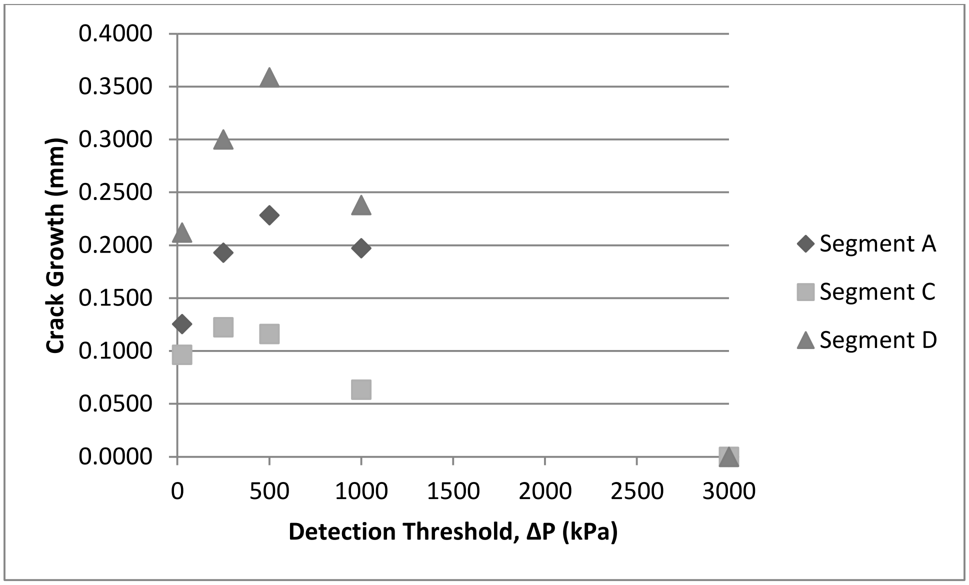

Figure 44 -- Detection Threshold Sensitivity by Loading History

The above sensitivity analysis demonstrates that the peak detection threshold for the most crack growth is not the same value for all loading profiles. Segment C generates the most crack growth with a detection threshold of 250 kPa, whereas the other two segments see the highest growth for a detection threshold of 500 kPa. Further research or consultation with field engineers will be required to get an idea of which type of cycles are significant in terms of natural gas transmission line operation.

From the above analyses, there are several variables which all have a varying affect on the predicted crack growth for a given pipeline segment. Until EMAT data can be provided to give a specific feature's actual growth rate, an exercise similar to the one performed above will be needed in order to curve fit the predicted data to simulate the real-world situation.

5.3 Correlation of the Predicted Crack Growth with the Field Ranking

In order to determine the effectiveness of the predictive model, the results must be compared to the data found in the field. Before correlating the field data, it should be noted that in order to have any SCC initiate in the first place, there must be some sort of coating disbondment. The model did not take into account a probabilistic mechanic which would rank different coating types on their affinity for disbonding, which may be something to consider in future work with the model. This lack of consideration may explain some discrepancies seen in Section 5.2.

Another phenomenon seen in the field is the presence of ‘Toe Cracks’ – these cracks exist in the toe of the seam weld, which has different material properties than the base metal. These cracks can also run into weld defects, which will artificially increase the length of the cracks and show the field data to have longer cracks than what the model is predicting. Coalescence of cracks within a colony is also not considered, as the crack coalescence mechanism will also provide a similar artificially increased effective crack growth rate.

Finally, the last point of discussion when discussing field data correlation is determining which field variable accurately describes a segment’s susceptibility to SCC. All field data comments not only on a given segment’s susceptibility to SCC, but also the operator’s ability to select sites for investigation. As previously mentioned, this is especially true for when the data was collected which was before the further development of the EMAT crack detection tool. Even deciding which segments need to have the EMAT tool run is dependent on the operator’s risk assessment. The three variables considered for field data correlation are ‘Number of SCC Digs’, ’Percentage of Digs Containing Significant SCC’ and ‘Deepest SCC Found’. Rather than trying to separate out the segments susceptibility and the operators ability to select a representative dig sample, this work focused on a known ‘worst case scenario’. Taking the deepest SCC found would ensure that the worst growth rate known to have occurred on the segment would be compared to the model which was developed to take into account the worst possible conditions present.

Once the comparative variable was selected, the data presented in Table 10 was used to get a growth rate for each of the segments analyzed. The deepest feature in each segment was taken and its growth per year was tabulated.

Table 17-- Initial Calculated Field Growth Rates

Segment "Name"	Const. Year	Inspection Year	Deepest Colony Found	Growth Rate [mm/year]
A	1971	1999	30.30%	0.1071321
B	1970	2004	<5%	N/A
C	1970	2006	38.40%	0.1056
D	1980	2008	53.93%	0.1714204
E	1982	2009	43.26%	0.1337856

As previously discussed, the greatest growth rate seen in the field by industry engineers is 0.3 mm / year. In order to reach that level of growth, some period of time regarding initiation must be taken into account. This initiation period is not only mechanical initiation previously discussed in fracture mechanics, but also the time it takes for the soil to apply enough stress to the coating in order to disbond it and allow for the corrosive environment to interact with the steel. The worst growth rate was assumed to be 0.3 mm / year, and each segment was given the same initiation time, due to the fact that all of the segments were tape coated. For the purpose of this data, the initiation time was given to be twelve (12) years. The resulting adjusted growth rates were then calculated for and compared to get a given field ranking. The field rankings can be seen below, as well as the models predicted ranking using the base calculation variables discussed in Section 5.1.

Table 18 –Actual Field and Predicted Ranking of Pipeline Segments Based on Deepest Feature Found

Segment "Name"	Const. Year	Inspection Year	Deepest Colony Found	Growth Rate [mm/year]	Adjusted Growth Rate [mm/year]	Ranking (Most Susceptible:1, Least Susceptible: 5)	
						Field	Predicted
A	1971	1999	30.30%	0.11	0.19	3	2
B	1970	2004	<5%	N/A	N/A	5	Error
C	1970	2006	38.40%	0.11	0.16	4	3
D	1980	2008	53.93%	0.17	0.30	1	1
E	1982	2009	43.26%	0.13	0.24	2	Error

When the field susceptibility rankings were compared to the growth rates generated from the various sensitivity analyses performed with the model, some discussion points arise. Using only the deepest feature does show a good correlation with the initial input variables explained in the sensitivity analysis, regardless of the errors present model output for Segments B and E. The second observation is that the growth rates and predicted rankings can vary significantly depending on the input data as seen in the sensitivity analysis. In fact, the growth rates produced in the third sensitivity analysis test are the closest to the worst case expected field analysis, and these have the worst correlation. The fact that the predicted order of susceptibility can change requires further research with additional data sets in order to determine a statistically valid correlation.

6.0 Conclusions / Future Work

This work has focused on developing a predictive model of the crack growth mechanism of Near Neutral pH SCC in underground natural gas transmission pipelines. Field data was collected in the form of integrity excavation reports and SCADA data from compressor stations. The SCADA loading histories were broken down and a logic flow chart was applied using a Corrosion Fatigue model with aspects of hydrogen embrittlement being included. The following is a list of conclusions from this work, as well as some recommendations for future work with the modeling effort:

1. The model illustrated a crack growth behavior with two distinct phases: a Dissolution Controlled phase and a Mechanically Activated phase. The interaction of these two phases was developed in an attempt to explain the crack dormancy phenomenon seen in the majority of SCC features in the field.
2. A development of a Hydrogen Enhancement Factor (HEF) was utilized to help curve fit the results of the model in an attempt to match field conditions. The HEF can be changed for different locations in order to describe the complex situations which may exist at a specific location. Further field research and curve fitting would allow for a matrix of HEFs to be utilized depending on various environmental conditions (i.e. CP, Soil Type, Drainage, etc.)

3. An increase in the HEF results in an increase in the resulting crack growth; however, the amount of crack growth increase does not vary linearly, and also varies with the different loading histories.
4. A change in the localized maxima / minima detection threshold causes an increase in the crack growth rate to a certain value before dropping off again. This maximum value is dependent on the different loading histories.
5. Attempts to compare the predicted NNpHSCC growth results to the field findings did show an adequate correlation with a majority of the sensitivity scenarios. The validation of the model results will require additional data to ensure that the validation is statistically significant.
6. The inclusion of the Irwin Approximation for a plastic zone size correction did not converge as crack depths exceeded one (1) millimeter; future work will have to investigate further as to why this error was experienced.
7. Inputting various loading histories did highlight an issue with the model to handle various profiles; more data will be required to narrow down the specific issue with reading the cycles from the input data.

Bibliography

1. *Developing a Predictive Model of Near Neutral pH Stress Corrosion Cracking of Underground Pipelines.* **Conrad, Brett, et al.** Calgary : American Society of Mechanical Engineers, 2012. International Pipeline Conference.

2. **Jones, Denny A.** *Principles and Prevention of Corrosion.* Upper Saddle River, NJ : Prentice Hall, 1996.

3. **Anderson, T.L.** *Fracture Mechanics.* 3rd. Boca Raton : Taylor & Francis Group, 2005.

4. **Reed-Hill, Robert E. and Abbaschian, Reza.** *Physical Metallurgy Principles.* 3rd Edition. Boston : PWS Publishing Company, 1994.

5. **Callister Jr., W.** *Materials Science and Engineering: An Introduction.* New York : John Wiley & Sons, Inc., 2007.

6. **Paris, P.C., Gomez, M.P and Anderson, W.P.** A Rational Analytic Theory of Fatigue. *The Trend in Engineering.* 1961, Vol. 13, pp. 9-14.

7. *A Critical Analysis of Crack Propagation Laws.* **Paris, P.C. and Erdogan, F.** 1960, Journal of Basic Engineering, Vol. 85, pp. 528-534.

8. **American Society of Testing and Materials (ASTM) International.** *Standard Practices for Cycle Counting in Fatigue Analysis.* West Conshohocken, PA : ASTM, 2011. E1049-85 .

9. **National Energy Board.** *Stress Corrosion Cracking on Canadian Oil and Gas Pipelines.* Calgary, AB : National Energy Board, 1996.

10. **Delanty, B and O'Beirne, J.** Major Field Study Compares Pipeline SCC with Coatings. *Oil & Gas Journal.* June 15, 1992, Vol. 90, 24, pp. 39-44.

11. *Transgranular Crack Growth in Pipeline Steels Exposed to Near-neutral pH Soil Aqueous Solutions - Role of Hydrogen.* **Chen, W., et al.** s.l. : Acta Materialia. Manuscript Number: A-09-1037R1.

12. **Transportation Safety Board of Canada.** *Pipeline Investigation Report -- TransCanada Pipelines Limited 914.4 mm Diameter Pipeline Line 100-2 MLV 76-2 Near Beardmore, Ontario.* 21 March 2012. P11H0011.

13. **Parkins, R.N., Blanchard, W.K. and Delanty, B.S.** Transgranular Stress Corrosion Cracking of High Pressure Pipelines in Contact with Solutions of Near Neutral pH. *Corrosion.* 1994, Vol. 50, 5, pp. 394-408.

14. *The Role of Soil Data in Pipeline Integrity.* **Marr, J., et al.** Calgary, AB : American Society of Mechanical Engineers (ASME), 2004. International Pipeline Conference 2004. IPC2004-508.

15. *Concepts of Underground Corrosion.* **Escalante, E.** [ed.] V Chaker and J.D. Palmer. Philidelphia : American Society for Testing and Materials, 1989, Effects of Soil Characteristics on Corrosion, pp. pp. 81-94. ASTM STP 1013.

16. *Testing Soil for Corrosiveness.* **Robinson, W.** 1993, Materials Performance, Vol. 32, pp. pp. 56-58.

17. *Factors Influencing Stress Corrosion Cracking of Gas Transmission Pipelines: Detialed Studies Following a Pipeline Falure. Part 1: Environmental Considerations.* **Wilmott, Martyn J. and Diakow, David A.** New York : ASME, 1996. International Pipeline Conference. Vol. 1, pp. 507-524.

18. **Eslami, A., et al.** Stress corrosion cracking initiation under the disbonded coating of pipeline steel in near-neutral pH environment. *Corrosion Science.* 2010, Vol. 52.

19. **Payer, Dr. Joe H.** Methods to Control Corrosion: Protective Coatings and Potential Modification. *Course 0131: Corrosion.* s.l. : ASM International, 1994.

20. *Effect of Cathodic Protection on Corrosion of Pipeline Steel Under Disbonded Coating.* **Chen, X., et al.** s.l. : Corrosion Science, 2009, Vol. 51.

21. **Chu, R., et al.** Microstructure Dependence of Stress Corrosion Cracking Initiation in X-65 Pipeline Steel Exposed to a Near-Neutral pH Soil Environment. *Corrosion.* 2004, Vol. 60, 3.

22. **Hibbeler, R.C.** *Mechanics of Materials.* Singapore : Pearson Prentice Hall, 2005.

23. **NACE International Technical Committee.** *External Stress Corrosion Cracking of Underground Pipelines.* Calgary, AB : NACE International, 2003. NACE International Publication 35103.

24. *Crack Growth Behavior of Pipeline Steel in Near-Neutral pH Soil Environments.* **Chen, W. and Sutherby, R.** s.l. : The Minerals, Metals & Materials Society and ASM International, 2007, Metallurgical and Materials Transactions A, Vol. 38A.

25. *SCC Integrity Management Case Study Kinder Morgan Natural Gas Pipeline of America.* **Davis, J.D., Marr, J.E. and Venance, D.** Calgary, Alberta : American Society of Mechanical Engineers, 2004. Proceedings of IPC 2004. IPC2004-586.

26. *Development of a Predictive Model for the Initiation and Early-Stage Growth of Near-Neutral p SCC of Pipeline Steels.* **King, F., et al.** Houston, Texas : NACE International, 2001. Corrosion 2001. Paper No. 01214.

27. *Characteristics of Low pH SCC Cracks.* **Chen, W.** 2003.

28. **Van Boven, G., Chen, W. and Rogge, R.** The Role of Residual Stress in Near Neutral pH Stress Corrosion Cracking of Pipeline Steels Part 1: Pitting and Cracking Occurence. *Acta Materialia.* 2007, 55, pp. 29-42.

Appendix A: Crack Growth Modeling Program with Irwin Approximation

```
%Fatigue cycle counting program
%Loading portions (positive derivatives) account for crack growth
rate
%Unloading portions (negative derivative) have no affect on crack
growth
%rate, just have the time factor involved and determine whether
creep or
%hydrogen effects dominate crack growth.

%Initialize crack contribution to 0. Also initialize crack growth
due to
%dissolution only (presentation purposes).
da_total = 0;
da_dissolution_total = 0;
%Only want stress intensity factor at crack depth tip; therefore,
phi will
%be pi/2
phi = pi/2;
%Define what length of crack you want to assume.
a=input('What crack depth are you assuming (in mm)?: ');
a = a/1000;
if a<0.001
    c = (exp(((a*1000)-0.3769922693)/0.3593737257))/2;
    c = c/1000;
else
    c = 3.3*a;
end
%Define pipe dimensions.
t = input('What is the wall thickness of the pipe (in mm)? ');
t = t/1000;
d = input('What is the diameter of the pipe (in mm)?: ');
d = d/1000;
sigmayield = input('What is the SMYS (in MPa)?: ');
%Define dissolution rate parameters.
drate = input('What is the dissolution rate of the material (mm/s)?:
');
tdepth = input('What depth will the dissolution rate drop off to
zero (mm)?: ');
if a<0.001
    ctdrate = (drate*2.5)*((0.3593737257*log(tdepth)+0.3769922698)-
(0.3593737257*log(a*1000)+0.3769922698));
    ctdrate = ctdrate*3600;
    else ctdrate = 0;
end
a0=a;
%Define HEF array.
HEF50 = input('What will be the HEF between 50-60%?: ');
HEF60 = input('What will be the HEF between 60-70%?: ');
HEF70 = input('What will be the HEF between 70-80%?: ');
HEF80 = input('What will be the HEF between 80-90%?: ');
HEF90 = input('What will be the HEF between 90-100%?: ');
%Define residual stress assumed.
```

```
sigmaR = input('What is the assumed residual stress in the line (in
MPa)?: ');
if sigmaR < 0 || sigmaR > 200;
    disp('Error: Residual Stress must be between 0 and 200 MPa');
end
%Define exponents for rate equation.
A = input ('What is the rate equation coefficient?(A): ');
n = input ('What is the rate equation exponent?(n): ');
alpha = input('What is the delta K exponent?(alpha): ');
beta = input('What is the Kmax exponent?(beta): ');
gamma = input('What is the frequency exponent?(gamma): ');
%Import hourly SCADA data, only pressure values
SCADA = input('Import hourly SCADA data (kPa) using xlsread function:
');
%Define threshold value for peak detection.
delta = input('What is the assumed threshold value (in kPa) for the
peak detection?: ');
%Identify local maximas.
%Finds maximum stresses and assigns reference stresses.
    %PEAKDET Detect peaks in a vector
%        [MAXTAB, MINTAB] = PEAKDET(V, DELTA) finds the local
%        maxima and minima ("peaks") in the vector V.
%        MAXTAB and MINTAB consists of two columns. Column 1
%        contains indices in V, and column 2 the found values.
%
%        With [MAXTAB, MINTAB] = PEAKDET(V, DELTA, X) the indices
%        in MAXTAB and MINTAB are replaced with the corresponding
%        X-values.
%
%        A point is considered a maximum peak if it has the maximal
%        value, and was preceded (to the left) by a value lower by
%        DELTA.
[maxtab,mintab] = peakdet(SCADA(:,2),delta,SCADA(:,1));
% Deconstruct maxtab and mintab into single columns.
maximas = maxtab(:,2);
maximaLoc = maxtab(:,1);
minimas = mintab(:,2);
minimaLoc = mintab(:,1);
   for j=1:((length(maximas))-3)
        if minimaLoc(j) < maximaLoc(j+1)
            p1 = maximas(j);
            p1Loc = maximaLoc(j);
            p2 = maximas(j+1);
            p2Loc = maximaLoc(j+1);
            p3 = minimas(j);
            p3Loc = minimaLoc(j);
        elseif minimaLoc(j)< maximaLoc(j+2)
            p1 = maximas(j+1);
            p1Loc = maximaLoc(j+1);
            p2 = maximas(j+2);
            p2Loc = maximaLoc(j+2);
            p3 = minimas(j);
            p3Loc = minimaLoc(j);
        elseif minimaLoc(j)<maximaLoc(j+3)
            p1 = maximas(j+2);
            p1Loc = maximaLoc(j+2);
            p2 = maximas(j+3);
```

```
            p2Loc = maximaLoc(j+3);
            p3 = minimas(j);
            p3Loc = minimaLoc(j);
        end
        sigma1 = (((p1/1000)*(d)/(2*t))+(sigmaR));
        sigma2 = (((p2/1000)*(d)/(2*t))+(sigmaR));
        sigma3 = (((p3/1000)*(d)/(2*t))+(sigmaR));
        if sigma3>=sigma2
            disp('Error: Minimum stress cannot be larger than
maximum stress.')
        end
        %Before going through decision, determine HEF array.
        if (sum(SCADA((maximaLoc(j)):(maximaLoc(j+1))<=
(0.6*p2*(maximaLoc(j+1)-maximaLoc(j))))))
            HEF = HEF50;
        elseif (sum(SCADA((maximaLoc(j)):(maximaLoc(j+1)))<=
(0.7*p2*(maximaLoc(j+1)-maximaLoc(j)))))
            HEF = HEF60;
        elseif (sum(SCADA((maximaLoc(j)):(maximaLoc(j+1)))<=
(0.8*p2*(maximaLoc(j+1)-maximaLoc(j)))))
            HEF = HEF70;
        elseif (sum(SCADA((maximaLoc(j)):(maximaLoc(j+1)))<=
(0.9*p2*(maximaLoc(j+1)-maximaLoc(j)))))
            HEF = HEF80;
        else
            HEF = HEF90;
        end
        %Fracture Mechanics (delta K and Kmax)
        %Use Irwin Correction Method for Plasticity.
        %First, determine K in absence of Plasticity correction.
          Q = 1+1.464*((a/c)^(1.65));
          M1 = 1.13-0.09*(a/c);
          M2 = -0.54+(0.89/(0.2+(a/c)));
          M3 = 0.5-(1/(0.65+(a/c)))+(14*(1-(a/c))^24);
          fphi = (((a/c)^2)*cos(phi)^2+sin(phi)^2)^(1/4);
          g = 1+(0.1+(0.35*(a/t)^2))*((1-sin(phi))^2);
          F = (M1+(M2*((a/t)^2))+(M3*((a/t)^4)))*(fphi)*g;
          Kmax = (sigma2)*(sqrt((pi*a)/Q))*F;
          Kmin = (sigma3)*(sqrt((pi*a)/Q))*F;
          f = (1/2)*(1/3600)/(p2Loc-p3Loc);
          if f<0;
              disp('Error: Frequency cannot be less than zero.')
          elseif f==0
              disp('Error: Frequency cannot be equal to zero.')
          end
        %Now obtain first order estimate for aeffmin and aeffmax.
        rymax = (1/(2*pi))*((Kmax/sigmayield)^2);
        aeffmax = a+rymax;
        if aeffmax < 0.001
        ceffmax = (exp(((aeffmax*1000)-
0.3769922693)/0.3593737257))/2;
        ceffmax = ceffmax/1000;
        else
        ceffmax = 3.3*aeffmax;
        end
        rymin = (1/(2*pi))*((Kmin/sigmayield)^2);
        aeffmin = a+rymin;
```

```
        if aeffmin < 0.001
        ceffmin = (exp(((aeffmin*1000)-
0.3769922693)/0.3593737257))/2;
        ceffmin = ceffmin/1000;
        else
        ceffmin = 3.3*aeffmin;
        end
        %Use aeffmax to calculate Kmaxeff
          Qmax = 1+1.464*((aeffmax/ceffmax)^(1.65));
          M1max = 1.13-0.09*(aeffmax/ceffmax);
          M2max = -0.54+(0.89/(0.2+(aeffmax/ceffmax)));
          M3max = 0.5-(1/(0.65+(aeffmax/ceffmax)))+(14*(1-
(aeffmax/ceffmax))^24);
          fphimax =
(((aeffmax/ceffmax)^2)*cos(phi)^2+sin(phi)^2)^(1/4);
          gmax = 1+(0.1+(0.35*(aeffmax/t)^2))*((1-sin(phi))^2);
          Fmax =
(M1max+(M2max*((aeffmax/t)^2))+(M3max*((aeffmax/t)^4)))*(fphimax)*gm
ax;
          Kmaxeff = (sigma2)*(sqrt((pi*aeffmax)/Qmax))*Fmax;
          f = (1/2)*(1/3600)/(p2Loc-p3Loc);
          if f<0;
              disp('Error: Frequency cannot be less than zero.')
          elseif f==0
              disp('Error: Frequency cannot be equal to zero.')
          end
          %Initialize plastic zone sizes for maximum stress.
          ry1max = rymax;
          ry2max = 1.2*rymax;
          while (ry2max-ry1max) >= (0.05*ry2max)
            %Use Kmaxeff to re-estimate aeffmax.
            ry1max = (1/(2*pi))*((Kmaxeff/sigmayield)^2);
            aeffmax = a+ry1max;
            if aeffmax < 0.001
            ceffmax = (exp(((aeffmax*1000)-
0.3769922693)/0.3593737257))/2;
            ceffmax = ceffmax/1000;
            else
            ceffmax = 3.3*aeffmax;
            end
            %Repeat process until the change in successive plastic
zone sizes
            %is less than 5%.
            Qmax = 1+1.464*((aeffmax/ceffmax)^(1.65));
            M1max = 1.13-0.09*(aeffmax/ceffmax);
            M2max = -0.54+(0.89/(0.2+(aeffmax/ceffmax)));
            M3max = 0.5-(1/(0.65+(aeffmax/ceffmax)))+(14*(1-
(aeffmax/ceffmax))^24);
            fphimax =
(((aeffmax/ceffmax)^2)*cos(phi)^2+sin(phi)^2)^(1/4);
            gmax = 1+(0.1+(0.35*(aeffmax/t)^2))*((1-sin(phi))^2);
            Fmax =
(M1max+(M2max*((aeffmax/t)^2))+(M3max*((aeffmax/t)^4)))*(fphimax)*gm
ax;
            Kmaxeff = (sigma2)*(sqrt((pi*aeffmax)/Qmax))*Fmax;
            f = (1/2)*(1/3600)/(p2Loc-p3Loc);
            if f<0;
```

```
              disp('Error: Frequency cannot be less than zero.')
            elseif f==0
              disp('Error: Frequency cannot be equal to zero.')
            end
            ry2max = (1/(2*pi))*((Kmaxeff/sigmayield)^2);
            aeffmax = a+ry2max;
            if aeffmax < 0.001
            ceffmax = (exp(((aeffmax*1000)-
0.3769922693)/0.3593737257))/2;
            ceffmax = ceffmax/1000;
            else
            ceffmax = 3.3*aeffmax;
            end
         end
        %THIS IS WHERE THE MINIMUM IRWIN CORRECTION GOES
          %Use aeffmin to calculate Kmineff
          Qmin = 1+1.464*((aeffmin/ceffmin)^(1.65));
          M1min = 1.13-0.09*(aeffmin/ceffmin);
          M2min = -0.54+(0.89/(0.2+(aeffmin/ceffmin)));
          M3min = 0.5-(1/(0.65+(aeffmin/ceffmin)))+(14*(1-
(aeffmin/ceffmin))^24);
          fphimin =
(((aeffmin/ceffmin)^2)*cos(phi)^2+sin(phi)^2)^(1/4);
          gmin = 1+(0.1+(0.35*(aeffmin/t)^2))*((1-sin(phi))^2);
          Fmin =
(M1min+(M2min*((aeffmin/t)^2))+(M3min*((aeffmin/t)^4)))*(fphimin)*gm
in;
          Kmineff = (sigma3)*(sqrt((pi*aeffmin)/Qmin))*Fmin;
          f = (1/2)*(1/3600)/(p2Loc-p3Loc);
          if f<0;
              disp('Error: Frequency cannot be less than zero.')
          elseif f==0
              disp('Error: Frequency cannot be equal to zero.')
          end
          %Initialize plastic zone sizes for minimum stress.
          ry1min = rymin;
          ry2min = 1.2*rymin;
          while (ry2min-ry1min) >= (0.05*ry2min)
            %Use Kmineff to re-estimate aeffmin.
            ry1min = (1/(2*pi))*((Kmineff/sigmayield)^2);
            aeffmin = a+ry1min;
            if aeffmin < 0.001
            ceffmin = (exp(((aeffmin*1000)-
0.3769922693)/0.3593737257))/2;
            ceffmin = ceffmin/1000;
            else
            ceffmin = 3.3*aeffmin;
            end
            %Repeat process until the change in successive plastic
zone sizes
            %is less than 5%.
            Qmin = 1+1.464*((aeffmin/ceffmin)^(1.65));
            M1min = 1.13-0.09*(aeffmin/ceffmin);
            M2min = -0.54+(0.89/(0.2+(aeffmin/ceffmin)));
            M3min = 0.5-(1/(0.65+(aeffmin/ceffmin)))+(14*(1-
(aeffmin/ceffmin))^24);
```

```
            fphimin =
(((aeffmin/ceffmin)^2)*cos(phi)^2+sin(phi)^2)^(1/4);
            gmin = 1+(0.1+(0.35*(aeffmin/t)^2))*((1-sin(phi))^2);
            Fmin =
(M1min+(M2min*((aeffmin/t)^2))+(M3min*((aeffmin/t)^4)))*(fphimin)*gm
in;
            Kmineff = (sigma3)*(sqrt((pi*aeffmin)/Qmin))*Fmin;
            f = (1/2)*(1/3600)/(p2Loc-p3Loc);
            if f<0;
              disp('Error: Frequency cannot be less than zero.')
            elseif f==0
              disp('Error: Frequency cannot be equal to zero.')
            end
            ry2min = (1/(2*pi))*((Kmineff/sigmayield)^2);
            aeffmin = a+ry2min;
            if aeffmin < 0.001
            ceffmin = (exp(((aeffmin*1000)-
0.3769922693)/0.3593737257))/2;
            ceffmin = ceffmin/1000;
            else
            ceffmin = 3.3*aeffmin;
            end
          end
         deltaK = (Kmaxeff - Kmineff);
        %Now go through program flow, using switch cases.

if(((0.98*p1)<(SCADA((maximaLoc(j))+1)))&&((0.98*p1)<(SCADA((maximaL
oc(j))+2)))&&((0.98*p1)<(SCADA((maximaLoc(j))+3)))&&((SCADA((maximaL
oc(j))+1))<(1.02*p1))&&((SCADA((maximaLoc(j))+2))<(1.02*p1))&&((SCAD
A((maximaLoc(j))+3))<(1.02*p1))&&((p3)>(0.98*p1))&&((p2)>(1.02*p1))&
&((p3)<(1.02*p1))&&(((minimaLoc(j))-(maximaLoc(j)))>3));
          %Rate Equation goes here.
          da = A*(((deltaK^alpha)*(Kmaxeff^beta))/(f^gamma))^n;
        elseif
(((0.98*p1)<(SCADA((maximaLoc(j))+1)))&&((0.98*p1)<(SCADA((maximaLoc
(j))+2)))&&((0.98*p1)<(SCADA((maximaLoc(j))+3)))&&((SCADA((maximaLoc
(j))+1))<(1.02*p1))&&((SCADA((maximaLoc(j))+2))<(1.02*p1))&&((SCADA(
(maximaLoc(j))+3))<(1.02*p1))&&((p3)<(0.98*p1))&&((sum(SCADA((maxima
Loc(j)):(maximaLoc(j+1)))))<  (0.5*p2*((maximaLoc(j+1))-
(maximaLoc(j))))));
          %Rate Equation*HEF
          da =
(A*((((deltaK^(alpha))*(Kmaxeff^beta))/(f^gamma)))^n)*(HEF);
        elseif
(((0.98*p1)<(SCADA((maximaLoc(j))+1))&&((0.98*p1)<(SCADA((maximaLoc(
j))+2)))&&((0.98*p1)<(SCADA((maximaLoc(j))+3)))&&((sum(SCADA((maxima
Loc(j)):(maximaLoc(j+1)))))>(0.5*p2*((maximaLoc(j+1))-
(maximaLoc(j)))))));
          %Rate Equation*HEF
          da =
(A*((((deltaK^alpha)*(Kmaxeff^beta))/(f^gamma)))^n)*(HEF);
        else
          %Rate Equation goes here.
          da = A*(((deltaK^alpha)*(Kmaxeff^beta))/(f^gamma))^n;
        end
        if (aeffmax >=t) || (aeffmin >= t);
```

```
            disp ('Plastic Zone exceeds plate dimensions (i.e. pipe
wall thickness).')
            plot(maximaLoc(1:(length(percentWT)))/(24*365),percentWT);
            return
        elseif a >= t
            disp('Failure: Pipe ruptured via crack propagation.')
            return
        elseif(isnan(da)~=1)&&(isreal(da)==1)&&(isinf(da)~=1)
      %Addition of crack growth due to just dissolution, only for
      presentation purposes.
            da_dissolution = (ctdrate*(maximaLoc(j+1)-maximaLoc(j)));
            da_dissolution_total = da_dissolution +
da_dissolution_total;
            da_dissolution_depth = (da_dissolution_total/1000)+ a0;
            %Total crack growth.
            da_total = da+da_total+(ctdrate*(maximaLoc(j+1)-
maximaLoc(j)));
            a = (da/1000)+((ctdrate*(maximaLoc(j+1)-
maximaLoc(j)))/1000)+a;
            if a<0.001
                 c = (exp(((a*1000)-0.3769922693)/0.3593737257))/2;
                 c = c/1000;
            else c = 3.3*a;
            end
            if a<0.001
             ctdrate =
2.5*drate*((0.3593737257*log(tdepth)+0.3769922698)-
(0.3593737257*log(a*1000)+0.3769922698));
             ctdrate = ctdrate*3600;
             else ctdrate = 0;
            end
        else
             disp('Error: Crack growth is not a real number.')
        end
        %Store changing variables to understand the
loading %conditions in comparison with other compressor stations.
        crackdepth(j,:)=(a);
        cracklength(j,:)=c;
        percentWT(j,:)=((a/t)*100);
        crackgrowth(j,:)=da;
        frequency(j,:)=(f);
        maxstress(j,:)=(sigma2-(sigmaR/1000));
        Rratio(j,:)=((sigma3-(sigmaR/1000))/(sigma2-(sigmaR/1000)));
        dissolutiongrowth(j,:)=((da_dissolution_depth/t)*100);
   end
  da_total
  maxf = max(frequency);
  minf = min(frequency);
  avgf = mean(frequency);
  maxR = max(Rratio);
  minR = min(Rratio);
  avgR = mean(Rratio);
  Maxsigma = max(maxstress);
  plot(maximaLoc(1:(length(maximaLoc)-
3))/(24*365),percentWT,maximaLoc(1:(length(maximaLoc)-
3))/(24*365),dissolutiongrowth);
```

Appendix B: Crack Growth Modeling Program without Irwin Approximation

```
 %Fatigue cycle counting program no irwin approximation
%Loading portions (positive derivatives) account for crack growth
rate
%Unloading portions (negative derivative) have no affect on crack
growth
%rate, just have the time factor involved and determine whether
creep or
%hydrogen effects dominate crack growth.

%Initialize crack contribution to 0. Also initialize crack growth
due to
%dissolution only (presentation purposes).
da_total = 0;
da_dissolution_total = 0;
%Only want stress intensity factor at crack depth tip; therefore,
phi will
%be pi/2
phi = pi/2;
%Define what depth of crack you want to assume.
a=input('What crack depth are you assuming (in mm)?: ');
a = a/1000;
if a<0.001
    c = (exp(((a*1000)-0.3769922693)/0.3593737257))/2;
    c = c/1000;
else
    c = 3.3*a;
end
%Define pipe dimensions.
t = input('What is the wall thickness of the pipe (in mm)? ');
t = t/1000;
d = input('What is the diameter of the pipe (in mm)?: ');
d = d/1000;
sigmayield = input('What is the SMYS (in MPa)?: ');
%Define dissolution rate parameters.
drate = input('What is the dissolution rate of the material
(mm/s)?: ');
tdepth = input('What depth will the dissolution rate drop off to
zero (mm)?: ');
tdepth = tdepth/1000;
if a<tdepth
    ctdrate =
(drate*2.5)*((0.3593737257*log(tdepth*1000)+0.3769922698)-
(0.3593737257*log(a*1000)+0.3769922698));
    ctdrate = ctdrate*3600;
    else ctdrate = 0;
end
a0=a;
%Define HEF array.
HEF50 = input('What will be the HEF between 50-60%?: ');
HEF60 = input('What will be the HEF between 60-70%?: ');
HEF70 = input('What will be the HEF between 70-80%?: ');
HEF80 = input('What will be the HEF between 80-90%?: ');
```

```
HEF90 = input('What will be the HEF between 90-100%?: ');
%Define residual stress assumed.
sigmaR = input('What is the assumed residual stress in the line
(in MPa)?: ');
if sigmaR < 0 || sigmaR > 200;
    disp('Error: Residual Stress must be between 0 and 200 MPa');
end
%Define exponents for rate equation.
A = input ('What is the rate equation coefficient?(A): ');
n = input ('What is the rate equation exponent?(n): ');
alpha = input('What is the delta K exponent?(alpha): ');
beta = input('What is the Kmax exponent?(beta): ');
gamma = input('What is the frequency exponent?(gamma): ');
%Import hourly SCADA data, only pressure values
SCADA = input('Import hourly SCADA data (kPa) using xlsread
function: ');
%Define threshold value for peak detection.
delta = input('What is the assumed threshold value (in kPa) for
the peak detection?: ');
%Identify local maximas.
%Finds maximum stresses and assigns reference stresses.
    %PEAKDET Detect peaks in a vector
%        [MAXTAB, MINTAB] = PEAKDET(V, DELTA) finds the local
%        maxima and minima ("peaks") in the vector V.
%        MAXTAB and MINTAB consists of two columns. Column 1
%        contains indices in V, and column 2 the found values.
%
%        With [MAXTAB, MINTAB] = PEAKDET(V, DELTA, X) the indices
%        in MAXTAB and MINTAB are replaced with the corresponding
%        X-values.
%
%        A point is considered a maximum peak if it has the
maximal
%        value, and was preceded (to the left) by a value lower by
%        DELTA.
[maxtab,mintab] = peakdet(SCADA(:,2),delta,SCADA(:,1));
% Deconstruct maxtab and mintab into single columns.
maximas = maxtab(:,2);
maximaLoc = maxtab(:,1);
minimas = mintab(:,2);
minimaLoc = mintab(:,1);
   for j=1:((length(maximas))-3)
       %Check to make sure that the proper peaks are being
compared.  Makes
       %program more robust to dealing with different SCADA data
sets.
        if minimaLoc(j) < maximaLoc(j+1)
            p1 = maximas(j);
            p1Loc = maximaLoc(j);
            p2 = maximas(j+1);
            p2Loc = maximaLoc(j+1);
            p3 = minimas(j);
            p3Loc = minimaLoc(j);
        elseif minimaLoc(j)< maximaLoc(j+2)
            p1 = maximas(j+1);
            p1Loc = maximaLoc(j+1);
            p2 = maximas(j+2);
```

```
            p2Loc = maximaLoc(j+2);
            p3 = minimas(j);
            p3Loc = minimaLoc(j);
        elseif minimaLoc(j)<maximaLoc(j+3)
            p1 = maximas(j+2);
            p1Loc = maximaLoc(j+2);
            p2 = maximas(j+3);
            p2Loc = maximaLoc(j+3);
            p3 = minimas(j);
            p3Loc = minimaLoc(j);
        end
        sigma1 = (((p1/1000)*(d)/(2*t))+(sigmaR));
        sigma2 = (((p2/1000)*(d)/(2*t))+(sigmaR));
        sigma3 = (((p3/1000)*(d)/(2*t))+(sigmaR));
        if sigma3>=sigma2
            disp('Error: Minimum stress cannot be larger than
maximum stress.')
        end
        %Before going through decision, determine HEF array.
        if (sum(SCADA((maximaLoc(j)):(maximaLoc(j+1))<=
(0.6*p2*(maximaLoc(j+1)-maximaLoc(j))))))
            HEF = HEF50;
        elseif (sum(SCADA((maximaLoc(j)):(maximaLoc(j+1)))<=
(0.7*p2*(maximaLoc(j+1)-maximaLoc(j)))))
            HEF = HEF60;
        elseif (sum(SCADA((maximaLoc(j)):(maximaLoc(j+1)))<=
(0.8*p2*(maximaLoc(j+1)-maximaLoc(j)))))
            HEF = HEF70;
        elseif (sum(SCADA((maximaLoc(j)):(maximaLoc(j+1)))<=
(0.9*p2*(maximaLoc(j+1)-maximaLoc(j)))))
            HEF = HEF80;
        else
            HEF = HEF90;
        end

        %Fracture Mechanics (delta K and Kmax)
        %Use Irwin Correction Method for Plasticity.
        %First, determine K in absence of Plasticity correction.
          Q = 1+1.464*((a/c)^(1.65));
          M1 = 1.13-0.09*(a/c);
          M2 = -0.54+(0.89/(0.2+(a/c)));
          M3 = 0.5-(1/(0.65+(a/c))+(14*(1-(a/c))^24);
          fphi = (((a/c)^2)*cos(phi)^2+sin(phi)^2)^(1/4);
          g = 1+(0.1+(0.35*(a/t)^2))*((1-sin(phi))^2);
          F = (M1+(M2*((a/t)^2))+(M3*((a/t)^4)))*(fphi)*g;
          Kmax = (sigma2)*(sqrt((pi*a)/Q))*F;
          Kmin = (sigma3)*(sqrt((pi*a)/Q))*F;
          deltaK = Kmax - Kmin;

          f = (1/2)*(1/3600)/(p2Loc-p3Loc);
          if f<0;
              disp('Error: Frequency cannot be less than zero.')
          elseif f==0
              disp('Error: Frequency cannot be equal to zero.')
          end
```

```
        %Now go through program flow.
        %First case: Hold at least three hours, followed by
increase of
        %stress where sigma2>sigma1.

if(((0.98*p1)<(SCADA((maximaLoc(j))+1)))&&((0.98*p1)<(SCADA((maxim
aLoc(j))+2)))&&((0.98*p1)<(SCADA((maximaLoc(j))+3)))&&((SCADA((max
imaLoc(j))+1))<(1.02*p1))&&((SCADA((maximaLoc(j))+2))<(1.02*p1))&&
((SCADA((maximaLoc(j))+3))<(1.02*p1))&&((p3)>(0.98*p1))&&((p2)>(1.
02*p1))&&((p3)<(1.02*p1))&&(((minimaLoc(j))-(maximaLoc(j)))>3));
          %Rate Equation goes here.
          da = A*(((deltaK^alpha)*(Kmax^beta))/(f^gamma))^n;
        %Second case: Hold at least three hours, followed by
decrease of
        %stress and area under curve is greater than 50% reference
state area.
        elseif
(((0.98*p1)<(SCADA((maximaLoc(j))+1)))&&((0.98*p1)<(SCADA((maximaL
oc(j))+2)))&&((0.98*p1)<(SCADA((maximaLoc(j))+3)))&&((SCADA((maxim
aLoc(j))+1))<(1.02*p1))&&((SCADA((maximaLoc(j))+2))<(1.02*p1))&&((
SCADA((maximaLoc(j))+3))<(1.02*p1))&&((p3)<(0.98*p1))&&((sum(SCADA
((maximaLoc(j)):(maximaLoc(j+1)))))>(0.5*p2*((maximaLoc(j+1))-
(maximaLoc(j))))));
          %Rate Equation*HEF
          da =
(A*((((deltaK^(alpha))*(Kmax^beta))/(f^gamma)))^n)*(HEF);
        %Third case: No hold, stress is immediately decreased and
area
        %under curve is greater than 50% reference state.
        elseif
(((0.98*p1)>(SCADA((maximaLoc(j))+1))&&((0.98*p1)>(SCADA((maximaLo
c(j))+2)))&&((0.98*p1)>(SCADA((maximaLoc(j))+3)))&&((sum(SCADA((ma
ximaLoc(j)):(maximaLoc(j+1)))))>(0.5*p2*((maximaLoc(j+1))-
(maximaLoc(j)))))));
          %Rate Equation*HEF
          da =
(A*((((deltaK^alpha)*(Kmax^beta))/(f^gamma)))^n)*(HEF);
        else
          %Rate Equation goes here.
          da = A*(((deltaK^alpha)*(Kmax^beta))/(f^gamma))^n;
        end
        if a >= t
           disp('Failure: Pipe ruptured via crack propagation.')
           return
        elseif(isnan(da)~=1)&&(isreal(da)==1)&&(isinf(da)~=1)


           %Addition of crack growth due to just dissolution, only
for
           %presentation purposes.
           da_dissolution = (ctdrate*(maximaLoc(j+1)-
maximaLoc(j)));
           da_dissolution_total = da_dissolution +
da_dissolution_total;
           da_dissolution_depth = (da_dissolution_total/1000)+ a0;
           %Total crack growth.
           da_total = da+da_total+(ctdrate*(maximaLoc(j+1)-
maximaLoc(j)));
```

```
            a = (da/1000)+((ctdrate*(maximaLoc(j+1)-
maximaLoc(j)))/1000)+a;
            if a<0.001
                 c = (exp(((a*1000)-0.3769922693)/0.3593737257))/2;
                 c = c/1000;
            else c = 3.3*a;
            end
            if a<tdepth
             ctdrate =
2.5*drate*((0.3593737257*log(tdepth*1000)+0.3769922698)-
(0.3593737257*log(a*1000)+0.3769922698));
             ctdrate = ctdrate*3600;
             else ctdrate = 0;
            end
        else
            disp('Error: Crack growth is not a real number.')
        end

        %Store changing variables to understand the loading
conditions in
        %comparisons with other compressor stations.
        crackdepth(j,:)=(a);
        cracklength(j,:)=c;
        percentWT(j,:)=((a/t)*100);
        crackgrowth(j,:)=da;
        frequency(j,:)=(f);
        maxstress(j,:)=(sigma2-(sigmaR/1000));
        Rratio(j,:)=((sigma3-(sigmaR/1000))/(sigma2-
(sigmaR/1000)));
        dissolutiongrowth(j,:)=((da_dissolution_depth/t)*100);
   end
  da_total
  maxf = max(frequency);
  minf = min(frequency);
  avgf = mean(frequency);
  maxR = max(Rratio);
  minR = min(Rratio);
  avgR = mean(Rratio);
  Maxsigma = max(maxstress);
  plot(maximaLoc(1:(length(maximaLoc)-
3))/(24*365),percentWT,maximaLoc(1:(length(maximaLoc)-
3))/(24*365),dissolutiongrowth);
```